SYNTHESIS CHARACTERIZATION AND MODIFICATION OF α-TRICALCIUM PHOSPHATE BASED BONE SUPPORTING SYSTEMS

A THESIS SUBMITTED TO
THE GRADUATE SCHOOL OF NATURAL AND APPLIED SCIENCES
OF
MIDDLE EAST TECHNICAL UNIVERSITY

BY

GÜLÇİN ÇİÇEK

IN PARTIAL FULFILLMENT OF THE REQUIREMENTS
FOR
THE DEGREE OF MASTER OF SCIENCE
IN
BIOMEDICAL ENGINEERING

FEBRUARY 2012

Approval of the thesis:

SYNTHESIS CHARACTERIZATION AND MODIFICATION OF α-TRICALCIUM PHOSPHATE BASED BONE SUPPORTING SYSTEMS

Submitted by **GÜLÇİN ÇİÇEK** in partial fulfillment of the requirements for the degree of **Master of Science in Biomedical Engineering Department, Middle East Technical University** by,

Prof. Dr. Canan Özgen ——————
Dean; Graduate School of **Natural and Applied Sciences**

Prof. Dr. Semra Kocabıyık ——————
Head of Department, **Biomedical Engineering**

Prof. Dr. Nesrin Hasırcı ——————
Supervisor, **Chemistry Dept., METU**

Dr. Eda Ayşe Aksoy ——————
Co-Supervisor, **Central Laboratory, METU**

Examining Committee Members:

Prof. Dr. Menemşe Gümüşderelioğlu ——————
Chemical Engineering Dept., Hacettepe University

Prof. Dr. Nesrin Hasırcı ——————
Chemistry Dept., METU

Prof. Dr. Zülfü Aşık ——————
Engineering Sciences Dept., METU

Assoc. Prof. Dr. Caner Durucan ——————
Metallurgical and Materials Engineering Dept., METU

Assist. Prof. Dr. İrem Erel ——————
Chemistry Dept., METU

Date: 09/02/2012

I hereby declare that all information in this document has been obtained and presented in accordance with academic rules and ethical conduct. I also declare that, as required by these rules and conduct, I have fully cited and referenced all material and results that are not original to this work.

Name, Last name: Gülçin ÇİÇEK

Signature:

ABSTRACT

SYNTHESIS CHARACTERIZATION AND MODIFICATION OF
α-TRICALCIM PHOSPHATE BASED BONE SUPPORTING SYSTEMS

Çiçek, Gülçin
M.Sc., Department of Biomedical Engineering
Supervisor: Prof. Dr. Nesrin Hasırcı
Co-Supervisor: Dr. Eda Ayşe Aksoy

February 2012\99 pages

The constitutive studies of this thesis were achieved and presented in three parts. In the first part, the effects of solid state synthesis process parameters and the impurity content of primary calcium precursor on the cement-type hydration efficiency for the conversion of α-tricalcium phosphate ($Ca_3(PO_4)_2$ or α-TCP) into hydroxyapatite ($Ca_{10-x}HPO_4(PO_4)_{6-x}(OH)_{2-x}$ x = 0–1, or HAp) have been investigated (at 37°C). α-TCP was synthesized by thermal processing of stoichiometric amounts of calcium carbonate ($CaCO_3$) and monetite ($CaHPO_4$) at 1150–1350°C for 2 h. Three commercial grade $CaCO_3$ powders of different purity were used as starting materials for the synthesis process and the resultant α-TCP products for all synthesis routes were compared in terms of the material properties and their reactivities.

In the second part of the studies, α-TCP and chitosan fiber (CF) composites were prepared as injectable bone cement systems which have a potential to degrade in time to be replaced by the natural bone tissue. α-TCP/CF composites were prepared in different compositions and the effect of CF addition on cement properties were

examined by mechanical and injectability tests as well as microstructural and phase analysis studies.

In the third part of the studies, metal chelating property of CFs was used on development of controlled zinc release systems that can be applied in local zinc deficiency therapies of bone tissue. For this purpose, CF scaffolds were prepared by wet-spinning technique and appropriate amount of zinc was loaded to these scaffolds in regard to the zinc content of a healthy human bone tissue. Zinc release studies were performed on calcium phosphate (CaP) covered and non-covered CF scaffolds and zinc ion concentrations of the release solutions were determined by ICP-MS.

Keywords: Calcium Phosphate**,** α-Tricalcium Phosphate, Chitosan, Composite, Zinc Chelating.

ÖZ

α-TRİKALSİYUM FOSFAT BAZLI KEMİK DESTEK SİSTEMLERİNİN SENTEZLENMESİ, KARAKTERİZASYONU VE MODİFİKASYONU

Çiçek, Gülçin
Yüksek Lisans, Biyomedikal Mühendisliği Bölümü
Tez Yöneticisi: Prof. Dr. Nesrin Hasırcı
Ortak Tez Yöneticisi: Dr. Eda Ayşe Aksoy

Şubat 2012\99 sayfa

Bu tezi oluşturan çalışmalar üç aşamada gerçekleştirilmiş ve üç bölümde sunulmuştur. İlk bölümde, α-trikalsium fosfatın ($Ca_3(PO_4)_2$, α-TCP) hidroksiapatite ($Ca_{10-x}HPO_4(PO_4)_{6-x}(OH)_{2-x}$ x = 0–1, HAp) dönüşmesindeki hidrasyon etkinliği üzerine katı hal sentez parametreleri ve başlangıç kalsiyum kaynağındaki safsızlık miktarılarının etkisi (37°C'de) incelenmiştir. α-TCP, sitokiyometrik miktarlarda kalsiyum karbonat ($CaCO_3$) ve monetitin ($CaHPO_4$), 1150-1350°C'de 2 saat ısıl işleme tabi tutulmasıyla sentezlenmiştir. Sentez işleminde başlangıç maddesi olarak farklı saflıklardaki üç ticari $CaCO_3$ tozu kullanılmış ve tüm sentez yöntemleriyle elde edilen α-TCP ürünleri, malzeme özellikleri ve reaktivite açısından karşılaştırılmıştır.

Çalışmaların ikinci bölümünde, zamanla bozunarak doğal kemik dokusuyla yer değiştirme potansiyeline sahip olan, enjekte edilebilir kemik çimento sistemleri olarak α-TCP ve kitosan fiber (CF) kompozitleri hazırlanmıştır. α-TCP/CF kompozitleri farklı kompozisyonlarda hazırlanmış ve CF ilavesinin çimento

özellikleri üzerindeki etkisi, mekanik ve enjekte edilebilirlik testlerinin yanısıra mikroyapısal ve faz analizi çalışmalarıyla incelenmiştir.

Çalışmaların üçüncü bölümünde, kemik dokusundaki bölgesel çinko eksikliği tedavilerinde uygulanabilir olan kontrollü çinko salım sistemleri geliştirmek amacıyla CF'lerin metal şelatlama özelliği kullanılmıştır. Bu amaçla, yaş eğirme tekniği ile CF iskeleleri hazırlanmış ve bu iskelelere, sağlıklı insan kemik dokusunun çinko içeriği göz önüne alınarak çinko yüklemesi yapılmıştır. Kalsiyum fosfat (CaP) kaplanmış ve kaplanmamış CF iskeleleri ile çinko salım çalışmaları gerçekleştirilmiş ve salım çözeltilerindeki çinko iyon konsantrasyonları ICP-MS ile belirlenmiştir.

Anahtar Kelimeler: Kalsiyum Fosfat**,** α-Trikalsiyum Fosfat, Kitosan, Kompozit, Çinko Şelatlama.

To my sweet little petunia...

ACKNOWLEDGEMENTS

I sincerely acknowledge Prof. Dr. Nesrin Hasırcı for her support and unique guidance and giving me a chance to be a part of her highly qualified laboratory throughout my study.

I would like to express my special thanks to Dr. Eda Ayşe Aksoy for strengthening my motivation when I needed, her support and help in crisis management moments.

I also would like to show my gratitude to Assoc. Prof. Dr. Caner Durucan for his authentic support and the time he has spent to improve my experience in research during my graduate studies.

I would like to thank to my teammates; Özge Özgen, Shahla Bagherifam, Ümran Aydemir, Aysun Güney, Seniz Uçar, Filiz Kara, Aysel Kızıltay and Tuğba Endoğan. I will never forget chats, laughs, discussions and their precious help during this period of my life.

This study was supported by METU-BAP and I would like to thank METU Central Laboratory for SEM, ICP-MS, and surface area analyses performed on this thesis.

Finally, I owe my deepest gratitude to my family for the love and guidance they have shown throughout my life.

TABLE OF CONTENTS

LIST OF TABLES

TABLES

LIST OF FIGURES

FIGURES

ABBREVIATIONS

ACP	Amorphous Calcium Phosphate
ALP	Alkaline Phosphatase
CaP	Calcium Phosphate
CDHAp	Calcium Deficient Hydroxyapatite
CF	Chitosan Fiber
CPC	Calcium Phosphate Cement
ECM	Extracellular Matrix
DCPA	Dicalcium Phosphate Anhydrous
DCPD	Dicalcium Phosphate Dehydrate
HAp	Hydroxyapatite
ICP-MS	Inductively Coupled Mass Spectrometer
MCPM	Monocalcium Phosphate Monohydrate
PBS	Phosphate Buffered Saline
SEM	Scanning Electron Microscope
TCP	Tricalcium Phosphate
TTCP	Tetracalcium Phosphate
OCP	Octacalcium Phosphate
XRD	X-Ray Diffraction

CHAPTER 1

INTRODUCTION

1.1 Biological, Chemical and Structural Properties of Bone

Bone is calcified and semi-rigid type of connective tissue forming the skeleton of the human body. The hierarchical complex structure of bone comprise of calcium phosphate mineral (69 wt%), collagen (20 wt%), water (9 wt%) and cellular elements such as proteins, polysaccharides and lipids (2 wt%) [1]. The variation of proportions of these components results in creation of different bone types with diverse porosity and mechanical strength.

The organic matrix of bone is made up of a dense fibrillar structure of type-1 collagen as illustrated in Figure 1.1. Each fibril consists of 1000 amino acids long three polypeptide chains. The chains come together to create a triple helix structure called tropocollagen, which is cylindrically shaped with the dimensions of 300/1.5 nm (length/diameter) [2]. These helical structures are parallelly organized with respect to each other but their ends are separated by 40 nm hole regions which behave like a matrix for accumulation of hydroxyapatite (HAp) crystals [3]. HAp crystals act as a crosslinking agent and the crosslinking between two individual fibers leads to an increase in resistance to deformation of collagen [4]. This is the basic phenomena behind the strong mechanical characteristic of bone. The parallelly aligned associated fibers form a bundle structure called collagen fiber.

The mineral phase of bone, poorly crystalline carbonated apatite, is predominantly existing as embedded in collagen fibrils [5, 6]. The average dimentions of plate-like

crystals are about 50 nm x 25 nm (length/widths) [2]. Carbonate ions can incorporate into the HAp structure via two different sites: The substitution can take place in OH^- ion position or PO_4^{3-} position in the lattice structure [7]. Crystal size, chemical composition and stability of biological apatites display an important role on normal and pathological characteristic of calcified tissues [8].

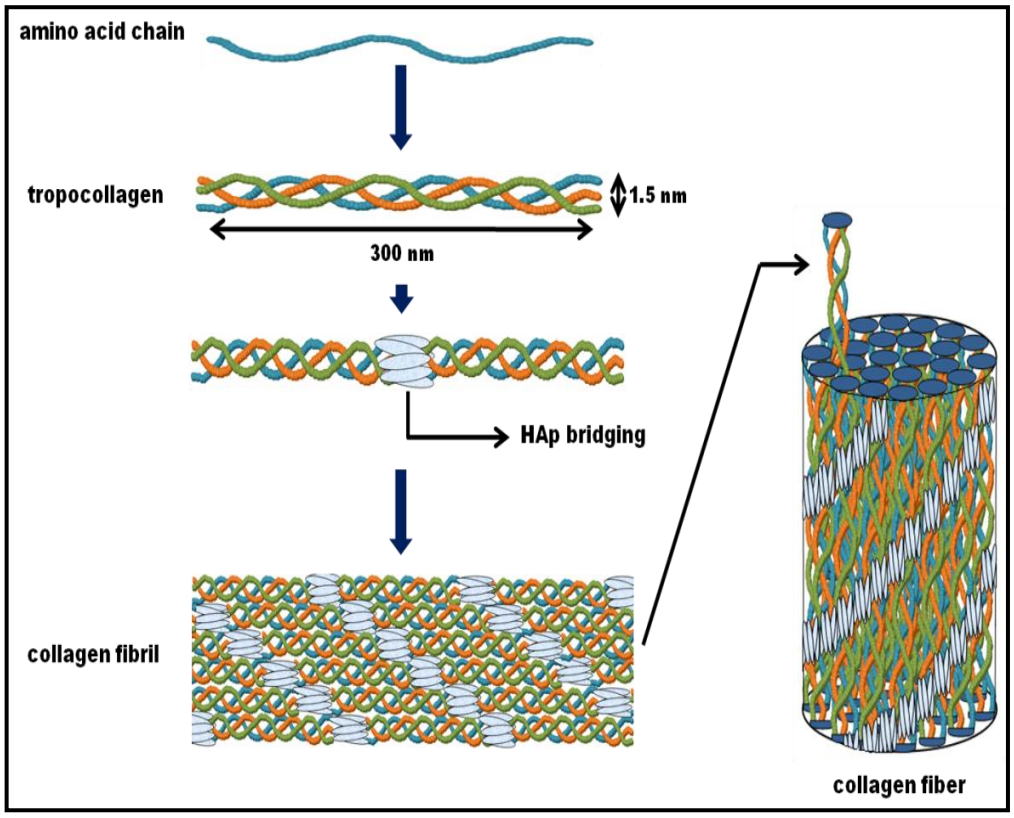

Figure 1.1 Systemic illustration of the structural organization of collagen fiber.

The major function of mineral constituent is converting organic soft tissues into a rigid material to provide resistance against internal and external forces applied on bone to protect vital organs and preserve the shape of the organism [9]. As a minor function, the mineral phase acts as an ion reservoir which can rapidly maintain

appropriate concentrations of calcium, sodium, carbonate, phosphate and magnesium ions in extracellular fluid.

Another important major component, water, has a primary importance on maintaining the mechanical properties of natural bone structure. It is demonstrated that, water loss results in a remarkable decrease in toughness and elasticity of bone [10]. Different types of water are present in bone structure such as free water (existing in the gaps of micropores), crystal water (bonded to apatite surfaces) and the structural water which is in charge of forming hydrogen bonds within triple helix of collagen molecules [11].

At the macrostructural hierarchical organization level, human bone is classified into two groups as cortical (compact) and cancellous (trabecular) bone. The significant distinction between these two structures is mainly arising from their degree of porosity. Cancellous bone has a highly porous structure, i.e. 50 - 90 vol%, while cortical bone is much denser with porosity between 5 - 10 vol%. The mechanical properties of these two types of bone differ due to variation in porosity, the amount of mineralization and organization of collagen fibers. Generally, bone macrostructure is a heterogeneous combination of strong cortical bone with a functional, low modulus cancellous core.

Three groups of bone cells named osteoblasts, osteoclasts and osteocytes have specific roles on bone regulation processes. Osteoblasts secrete bone matrix proteins and they are responsible for formation of new bone tissue while the other group, osteoclasts are in charge of absorption and removal of bone. The other type of cells entrapped within the bone matrix, osteocytes, which have a function on secreting osseous growth factors promote osteoblastic differentiation [12].

Bone formation is mainly performed by a two step mechanism [13]. Firstly, bone marker genes are expressed (mainly by bone-specific transcription factor Runx2) and induce osteoprogenitor cells to differentiate into osteoblasts that are in charge of

encoding bone-spesific extracellular matrix (ECM) proteins like collagen type-I, alkaline phosphatase (ALP), bone sialoprotein, osteocalcin and ostepontin. Subsequently, the synthesized matrix proteins are secreted from osteoblast cells and accumulate in the ECM to build mature bone matrix. The accumulated protein layer in the ECM lead to Ca^{2+} and $PO4^{3-}$ deposition in the matrix and eventually, bone minerilization occurs.

1.2 Biomaterials to Fill Bone Defects: Bone Grafts

When bone is subjected to an extensive damage and if the damaged area is too large for self repair, the defective gap must be supported by using alternative materials such as autografts, allografts or synthetic materials. Autografts, which are transferred from healthy bones from a different part of the body, are still the first choice on account of superior osteogenic, osteoconductive and osteoinductive properties. However, there are problems related to limited supply of tissue due to lack of availability and there is additional damage to the body since the bone tissue is extracted from the patient. Although allografts (tissue from other people) and xenogafts (tissue from other species) are also used, they have some disadvantages like limited availability or problems related probable foreign body reactions and infections. Therefore, ideal synthetic materials which are free from these limitations are needed to achieve riskless and more effective treatment of bone defects.

There are some main characteristics that an ideal bone graft material should exhibit, and these can be given as follows;

i) The ability to chemically bond to the surface of bone tissue without causing fibrous tissue formation (osteointegration)

ii) The potential to act as a scaffold for new bone tissue formation and support adhesion and proliferation of osteoblasts (osteoconduction)

iii) The ability to induce differentiation of stem cells present in surrounding tissues to osteoblastic cell types (osteoinduction)

iv) Similar mechanical characteristics with the target bone tissue

v) Adequate porosity for cell penetration and tissue ingrowth

vi) Capability of perfectly fit into irregular defects in bone

Many synthetic materials including ceramics, polymers and metals are used to repair the bone defects. Among them, ceramics and ceramic-composite materials remarkably offer a great clinical potential as bone graft substitutes.

1.3 Bioceramics as Bone Graft Materials

Bioceramics are ceramic products especially developed for medical and dental applications as implant materials. They are needed particularly to restore the function and to diminish pain of diseased or damaged calcified tissues in the body. These ceramics might be prepared from elements such as alumina, zirconia, carbon, silica or calcium phosphate containing compounds and as composites of other chemicals [14, 15]. All of them might be produced in block forms with certain geometry or as powders according to the desired medical application [16]. Additionally, there are injectable forms of bioceramics which spontaneously solidify and take the geometrical shape of the bone defect area during a surgical operation [17]. At present, bioceramics are commonly used in bone defect treatments for non-load bearing areas, periodontal applications, total joint replacement, cranio maxillofacial reconstruction and spinal surgeries [17-20].

In the design of bioceramic based implant systems, surface reactivity is an important property. Surface has the leading role on bone bonding ability of bioceramics hence it determines the characteristic of the bone-tissue interface [21, 22]. After implantation, time-dependent changes on the surface of the implanted materials are observed due to interactions at the tissue-implant interface [23]. Clinical success requires the

achievement of a stable implant-bone tissue interface. Preferably, a synthetic bone graft substitute should lead to a minimal fibrotic reaction and the material itself should undergo remodeling and induce new bone tissue formation.

Bioresorbable ceramics are ideally designed to degrade gradually in time to be replaced by the natural bone tissue. Calcium phosphate/calcium sulphate ceramics, resorbable bioactive glasses have been successfully used as resorbable bone graft materials [24, 25]. However, ceramics inherently have sub-micron size pores and lack of macro porosity is a limiting factor on biodegradation of ceramic materials. This slow degradation characteristic of ceramic implants might lead to impair bone healing. Therefore, introducing meso/macro pores into ceramic structures is a key point in order to shorten the degradation time, enhance the bone tissue in growth and accelerate the bone replacement process [26, 27]. However, increasing the porosity of the material also results in a decrease on the mechanical strength of the ceramic [28]. The ideal ceramic material should balance these two features by preserving optimal biointegration with strength maintenance over a convenient time for bone tissue healing.

Bone substitutes should have a similar mechanical strength and modulus of elasticity to that of the target bone tissue in order to prevent stress shielding. In addition, a bone graft is expected to provide appropriate toughness and prevent fatique failure of the implant in the case of cyclic loading. From a mechanical point of view, the brittle characteristic of ceramics is the major concern for hard tissue applications. For this reason, there have been many studies with the object of increasing the mechanical strength of bioceramic systems. Common methods that are used in these studies are addition of other ceramic phases [29, 30], introducing metallic dopants to the crystal structure [31, 32] and composite preparation with biocompatible polymers [33-35].

1.3.1 Calcium Phosphate (CaP) Materials as Bone Grafts

The main driving force behind the use of CaPs as bone substitute materials is their chemical similarity to the mineral component of human bone [36]. Because of this chemical structure match, they are unrecognized by immune system and treated like a native hard tissue member by the body in the case of implantation. As a result, they are non-toxic, biocompatible materials and they can integrate into living tissue by the natural active process in bone resorption and remodeling [37, 38]. By this way, a direct physicochemical bond between implant and bone is created (osteointegration) and a thin layer of HAp is formed shortly after implantation [38]. Calcium phosphate materials act as a scaffold for new bone tissue formation and support adhesion and proliferation of osteoblasts (osteoconductivity) [39]. Besides, they provide additional Ca and PO_4 ions for bone mineralization and induce new bone formation in surrounding tissues. However, their brittleness, insufficient mechanical strength, fracture prone on shock loading, low degradation potential of sintered phases and the difficulty in predicting the resorption time for highly porous CaPs in vivo conditions are limiting factors in their clinical usage.

There are various CaPs such as hydroxyapatite, octacalcium phosphate, tetracalcium phosphate, tricalcium phosphates, mono and dicalcium phosphates as shown in Table 1.1 The major distinguishing parameters for these compounds are their solubility and the molar Ca/P ratio. Depending on Ca/P ratio, as a function of pH value and calcium concentration, the solubility of each compound differs in aqueous environment [40]. These different characteristics determine the medical significance of calcium phosphate compounds [36].

Table 1.1 CaP-compounds with corresponding Ca/P ratio.

Name	Abbreviation	Formula	Ca/P ratio
Amorphous calcium phosphate	ACP	–	1.25-1.55
Hydroxyapatite	HAp	$Ca_{10}(PO_4)_6(OH)_2$	1.67
Dicalcium phosphate anhydrous, Monetite	DCPA	$CaHPO_4$	1.00
Dicalcium phosphate dehydrate, Brushite	DCPD	$CaHPO_4.H_2O$	1.00
Monocalcium phosphate monohydrate	MCPM	$Ca(H_2PO_4)_2.H_2O$	0.50
Octacalcium phosphate	OCP	$Ca_8H_2(PO_4)_6.5H_2O$	1.33
α-Tricalcium phosphate	α-TCP	α-$Ca_3(PO_4)_2$	1.50
β-Tricalcium phosphate, Whitlockite	β –TCP	β –$Ca_3(PO_4)_2$	1.50
Tetracalcium phosphate, Hilgenstockite	TTCP	$Ca_4(PO_4)_2$	2.00

1.3.1.1 Hydroxyapatite (HAp)

HAp has chemical formula of $Ca_{10}(PO_4)_6(OH)_2$ and known as bone mineral since it constitutes the mineral component of bone tissue. As a synthetic bone graft material, it has a wide range of applications and a significant place in medical research area for more than 60 years. In 1951 Ray and Ward revealed the medical efficacy of synthetic HAp on bone healing by the placement of synthetic granular HAp into the surgically created defects on cats and dogs [41]. It was concluded that, HAp can be partially resorbed and replaced by the new bone tissue.

Although, HAp is a highly osteointegrative material, sintered ceramic HAp products are resistant to resorption in vivo environment (1–2% per year) [42]. Since the degradation time of non-porous and highly crystalline HAp products is evaluated in decades, they might be regarded as non degradable. In consequence, attempts have been done to increase biointegration capability of HAp by introducing porosity to the implant material [43-45].

HAp, which is the most stable calcium phosphate phase at room temperature at pH between 4 and 12, can be obtained by solid state synthesis, wet chemical precipitation methods, hydrothermal synthesis and cement-type formation from other CaP phases [46-49]. Hydration of calcium phosphate cements (CPCs) is a common technique to obtain HAp in vivo conditions. The capability of CPCs to set and turn into monolithic HAp via a cementitious reaction with water was first discovered in 1980's [50]. CPC systems are injectable paste-like materials which are formed by mixing a powder of CaP phase with a liquid (water or appropriate aqueous solutions). After the injection of this paste into the body, hardening and formation of HAp occurs in physiological environment. When considered from this point of view, the formation of HAp through a cement-type reaction is a biomimetic process and indeed, the formed HAp is much more similar to biologic apatites than sintered ceramic ones [51]. Moreover, it has a lower crystallinity and higher specific surface than sintered HAps which enables its biodegradation and osteoconductive properties [52].

1.3.1.2 Beta-Tricalcium Phosphate (β-TCP)

Tricalcium phosphate ceramics [$Ca_3(PO_4)_2$,TCP] have four polymorphs as α, β, γ and super α. The γ and super α polymorphs are obtained at extreme pressure and temperature conditions and they do not survive quenching to room temperature [53, 54]. Therefore, the most frequently used calcium phosphate forms are α-TCP and β-TCP in medical area. Although, α and β-TCP have the same chemical composition, the difference in their crystallographic structure bring forth distinctive physiochemical characteristics.

Beta tricalcium phosphate (β-TCP) is the earliest CaP form which is used as bone graft material. According to available literature, in 1920's, Albee and Morrison used β-TCP as a bone graft substitute to repair surgically created defects in rabbits [55]. In the study, the β-TCP termed 'triple calcium phosphate' was used to stimulate bone growth. The results revealed more rapid bone growth in the fracture areas which are filled with β-TCP than the control groups.

β-TCP is commonly used as porous granules or blocks. From a mechanical point of view, β-TCP has a compressive strength comparable to cancellous bone although, like other CaP phases, it is brittle and weak under tension and shear forces [56]. β-TCP undergoes resorption and replacement by bone tissue over a 6-18 month period, the extent of this time depends on the porosity of the implant material and the metabolic activity of the host tissue environment.

Although there are various probable routes to obtain β-TCP, it is generally synthesized in a solid state process by the calcination of stochiometric amount of Ca and P sources at temperatures in the range of 650°C and 1125°C [57].

1.3.1.3 α-Tricalcium Phosphate (α-TCP)

The main advantage of α-TCP is its ability to hydrate and set into monolithic calcium deficient hydroxyapatite (CDHAp, $Ca_{10-x}(HPO)_x(PO_4)_{6-x}(OH)_{2-x}$, x=0-1) at near physiological pH and temperature from a single solid reactant. Majority of the other CaP systems require mixing of various calcium phosphate salts, such as tetracalcium phosphate (TTCP, $Ca_4(PO_4)_2O$) and dicalcium phosphate dihydrate (DCPD, $CaHPO_4{\cdot}2H_2O$) [58] or TTCP and dicalcium phosphate anhydrous (DCPA or monetite, $CaHPO_4$) [59] at fixed molar proportions to achieve stoichiometry for the HAp products. Bioactivity of α-TCP, as well as the microstructural and chemical resemblance of its hydration product to the mineral component of natural bone, makes it a good candidate for hard tissue applications [60-63]. Moreover, the setting reaction is potentially not destructive for the surrounding tissue due to minimal heat release and pH change, which stays almost constant at neutral values during the hydration [49]. However, there are still some limitations for the use of cement-type HAp products obtained from α-TCP due to their poor strength and lack of interconnected macroporosity.

The cement-type setting reaction of α-TCP upon reaction with aqueous solutions initially proceeds by surface area controlled dissolution which generates supersaturation of Ca^{2+} and PO_4^{3-} ions in the reactant solution. Then, the nucleation of HAp occurs followed by growth of entangled plate-like crystal precipitates of fully calcium deficient hydroxyapatite (CDHAp) [64, 65]. The kinetics and the control of the setting reaction of α-TCP are critical for the efficiency of the cement in clinical applications. There are many researches reporting the effect of different factors on the setting reaction of α-TCP. The effects of morphology [66], crystallinity [67, 68] and particle size of α-TCP [65, 68-70] on the kinetics of setting reaction have been reported. A number of researchers investigated the optimization of the injectability and setting time of α-TCP cements by forming hybrids with the addition of organic components such as gelatin [71], chitosan [72, 73], polylactic acid and glycerol [73].

Among all of these factors, it is well known that chemical composition of α-TCP dominantly affects its cement-type setting as well as its final physical properties. Since the natural bone mineral contains trace amount of cation/anion substitutions, synthetic analogs such as bone cements should be also chemically adaptable for substitution of ions of elements such as Mg, Na, Sr, Ba, Al, Cd, Pb, Cr, and Si for bone regeneration. In this respect, many researchers have investigated the effect ionic doping on the structural, physical, and chemical properties of HAp products of cement-type reactions. In recent years Sr-substituted [74-76], Ba-doped [77], Fe-modified α-TCPs [78] as well as Mg- [79-82] and Na-doped CaPs [83, 84] have been reported.

The synthesis of α-TCP is generally realized by solid state reactions. This is achieved by open air firing of homogenously mixed stoichiometric amount of calcium and phosphorus precursors at temperatures higher than 1125°C. This is followed by quenching to avoid formation of equilibrium polymorph of TCP, i.e. β-TCP. By this way, phase pure α-TCP can be obtained as shown by many studies [49, 67, 85]. However, direct assessment on the hydraulic reactivity of the α-TCP products of these studies is not possible, as the precursors and firing temperatures usually differ. In addition, despite the large body of previous work, due to inadequate information on chemical composition and physical properties of the starting materials, synthesis of reactive α-TCP becomes a problematic task for those trying to reproduce an available synthesis protocol. Similar to intentional ionic substitutions, a variety of intrinsic impurities present in the starting materials can affect the cement-type hydraulic reactivity, i.e. conversion of α-TCP to HAp accompanied by hardening.

1.3.1.3.1 α-TCP/Polymer Composite Systems

Polymers are incorporated into α-TCP structures in an effort to decrease the cement setting time, enhance the injectability and anti-wash out property of the cement paste and to increase the mechanical strength of the hardened form of the ceramic. In 2000, Durucan et al. prepared α-TCP based composite structures containing various copolymers of polylactic-co-glycolic acid (PLGA) [86]. In the study, the effect of the polymers on the hydration behaviour of α-TCP was investigated in accordance with TCP-CDHAp transformation amount. The results indicated that, copolymer with L-lactic acid:glycolic acid ratio of 85:15 exhibited the highest degree of CDHAp formation due to improvement of the interaction between TCP and water molecules with the help of PGA as an hydrophilic component. The study demonstrated the importance of the hydrophilic nature of the polymeric component on setting of a self-hardening α-TCP bone cement composite. In the following year, the group investigated the mechanical properties of the same composite system and reported an enhancement on tensile strength in the presence of PLGA [87].

A considerable amount of literature has been published on composite systems consisting of CPC and gelatin. The main reason of gelatin to gain such an attention on bone cement research area relies on its chemical relation with main organic constituent of natural bone; it is the thermal denaturation product of the collagen. Bigi et al. (2004) have developed an α-TCP/gelatin composite cement powder [88]. The results suggested that addition of gelatin accelerated the setting reaction of α-TCP and the presence of gelatin improved the compressive strength of cement material with regard to reduced total porosity and the more compact structure of the end product. In addition, the group investigated the biologic properties of the same system and pointed out the favorable effect of gelatin enriched α-TCP on osteoblast proliferation and differentiation [89]. Touny et al. investigated the effect of cross-linked gelatin fibers on CDHAp formation and mechanical strength of α-TCP cement based composites [90]. It was found that, gelatin fibers act as nucleation sites for CDHAp

crystallization and speed up CDHAp formation whereas mechanical strength of the composites decreases with fiber addition.

The injection of α-TCP offers a great advantage of using minimal invasive operation techniques for orthopedists but still, there are some limitations such as filter-pressing effect (the separation between solid and liquid phases). Besides, the disintegration of CPC upon early contact with blood and other body fluids could also be a risk for implantation of α-TCP as a single phasic paste. To overcome these problems, Khairon and coworkers (1999) introduced 1 wt% sodium alginate into the mixing liquid of α-TCP to prepare a cement with enhanced cohesion and injectability [91]. A good cohesion and injectability is reported when 1 wt% aqueous solution of sodium alginate was used as the cement liquid with a ratio of liquid to powder (L/P) 0.4, however, a decrease in compressive strength is also observed. Dos Santos et.al. (1999) repeated the use of sodium alginate as an additive in the cement liquid of α-TCP with a higher concentration (3.12 wt%) and demonstrated that addition of sodium alginate prolongs the initial cement setting time from 22 min to 1 h [33]. Alves et al. (2008) incorporated sodium alginate into the α-TCP in different concentrations and concluded 0.8 wt% alginate addition was the optimum concentration regarding homogeneity and injectability [92].

1.4 A Natural Biodegradable Polymer: Chitosan

Chitosan is a polysaccharide consisting of glucosamine and N-acetylglucosamine units linked by 1-4 glucosidic bonds (Figure 1.2). It is obtained by partial deacetylation of the second most naturally abundant polysaccharide, chitin, which can be derived from crab and shrimp shells, some fungis and microorganisms. It is worth to emphasize that, there are various series of chitosan polymers with different viscosity, crystallinity, molecular weight (50 kDa - 2000 kDa), degree of deacetylation (40 - 98%) and all these parameters have appreciable influence on physico-chemical properties of chitosan [93].

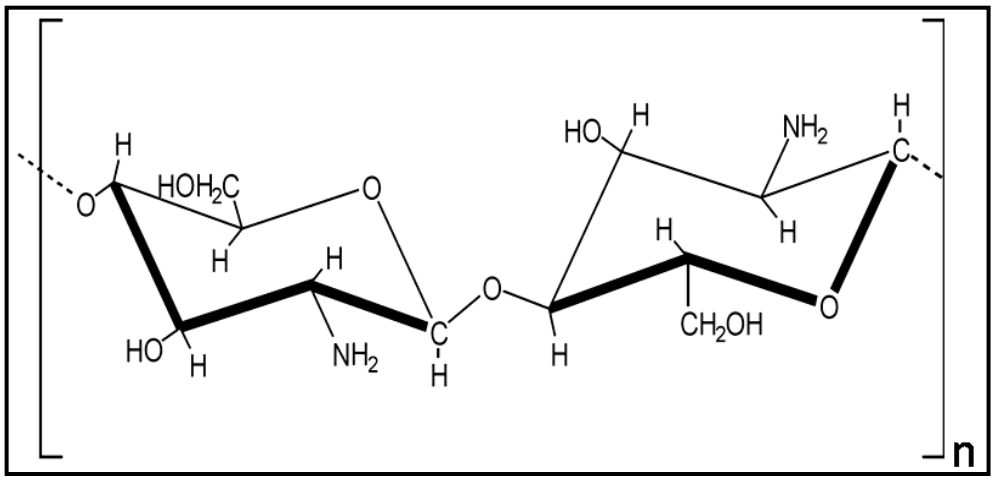

Figure 1.2 Chemical structure of chitosan.

Chitosans with high degree of deacetylation are not soluble in neutral and alkaline pH values. Since, chitosan have a number of amino groups that are available for chemical reaction, in dilute acid environments (pH<6), amine groups are protonated by turning the chitosan into a positively charged soluble polysaccharide form and dissolution of the polymer occurs [93, 94]. In vivo degradation of chitosan is performed by lysosyme enzyme and the degradation time is inversely proportional to degree of deacetylation and crystallinity. The final degradation products are biocompatible chitosan oligosaccharides of variable length [94].

Chitosan is chemically similar to glycosaminoglycan analogs that are present in cartilage and bone, hence, the same biodegradability and biocompatibility is observed in tissue substitutes made of chitosan [95]. Besides, owing to its cationic nature, chitosan attracts the negatively charged species like glycosaminoglycans, proteoglycans in body environment and accumulation of these molecules within a chitosan scaffold occurs [96]. As a result of this electrostatic interaction, a large group of growth factors and cytokines from surrounding tissue fluids, which are known to be bound and modulated by glycosaminoglycans, retain and concentrate around chitosan

implant [96]. This bioactive nature of chitosan have a stimulatory effect on colonizing cells and accelerates the tissue healing process [94]. Consequently, chitosan is a good candidate for various potential medical applications and products such as burn dressing materials [97], artificial skin grafts [98], bandages [99], medical sponges [100] and graft materials for hard tissues [35] are being developed.

Additionally, bone tissue studies on chitosan as a biomaterial, revealed its osteoconductive [101, 102] and osteoinductive [103, 104] characteristics. Seol et al, seeded freeze-dried chitosan scaffolds with rat osteoblasts and observed enhanced histological results compare to the control group in vitro [105]. An interesting study by Fakhry et al. displayed the preferential support of chitosan for initial attachment and spreading of osteoblasts over fibroblasts on tissue culture experiments. The study confirmed that, chitosan has a favorable affect in repairing bone deficiencies by promoting the early attachment and proliferation of osteoblasts over fibroblasts, which is important for the elimination fibrous encapsulation risk when using chitosan as a bone implant material [104]. In this context, chitosan has been found a very good candidate as a bone implant material.

From all of reasons above, one can conclude that chitosan is an excellent biomaterial for bone tissue applications however, there are some limitations of this polymer like its brittleness and low degradation rate (highly deacetylated forms may last several months in vivo). To overcome these restrictions, chitosan is generally used as a constituent of composite systems with ceramics [106] or it is blended with other polymers like gelatin [107] and collagen [108]. To adjust cell seeding efficiency, tissue ingrowth, degradation properties and mechanical strength of the implant system it is also possible to prepare and use chitosan in gel [109], sponge [110] and fiber [111] form by regeneration of chitosan or its derivatives from solutions.

1.4.1 Chitosan Fibers and Hard Tissue Applications

After the entire understanding of the collagen fiber-CaP composite nature of the bone structure, in order to mimic the natural architecture of the bone, CaP-fiber composite materials have gained a great attention in hard tissue applications. In addition, the capability of providing sufficient porosity for cell penetration, tissue ingrowth and nutrient exchange makes biodegradable fiber containing implant materials advantageous. Moreover, a composite structure of CaP and chitosan fiber (CF) is expected to enhance the biocompatibility and adequate biodegradation together with mechanical strength.

Different preparation methods have been reported to process chitosan in fiber form. Melt spinning, dry spinning and wet spinning are three basic techniques that are used. Among them, wet spinning is the most practical and common procedure which is successfully used in producing fibrous scaffolds from many natural and synthetic polymers [112-114]. To prepare CFs by wet spinning method, a solution named ‘dope’ is prepared by dissolving of the polymer in a solvent such as acetic acid and afterwards, the dope is pumped by an injection syringe into a high pH solution known as coagulation bath [114]. In this high pH bath, chitosan precipitates and forms fibers. Later on the coagulation, the resulting CFs might be washed to remove excess coagulant molecules and dried [115]. It is worthy of note that, in this method, fiber thickness depends on the needle diameter of the syringe and the radius of fiber is directly depend on the radius of the discharge end.

Wet-spinned CFs are started to attract attention to be used in hard tissue applications with the research of Tuzlakoglu et al. [111]. The team produced high tensile strength CFs by a wet spinning technique and demonstrated the bioactive behavior of the fiber scaffolds. In vitro studies were carried out with osteoblast cells and good osteoblast proliferation with appropriate cell morphology was observed over chitosan scaffold surfaces.

In 2004, Matsuda et al. prepared core-shell type chitosan/CaP composite fibers with shell of CaP and core of chitosan and observed an increase in mechanical strength of the fibers in direct proportion to the chitosan concentration in the composite [116]. In a number of following studies, CFs are incorporated into CPCs with intent to increase the early strength of the system and to prevent disintegration or fail of the cement in the early postoperative period of time. In 2007, Lian et al. prepared a CF reinforced CPC system with a 3D scaffolding method [117]. As a result of mechanical characterizations, it was concluded that, although the fiber structures made of pure chitosan did not cause a significant difference in compressive strength of the cement system, the existence of fibers markedly prevented the disintegration of CPC even if the CPC matrix had cracked. Zhaohui et al. covered CFs with gelatin and investigated the influence of these fiber structures as reinforcement agents on of the TTCP/DCPA cement [118]. The results exhibited the flexural strength of the composite can be enhanced by increasing the amount of chitosan fibers up to a certain limit.

It is well known that, as a result of submicron pore size of the CPCs, new bone tissue formation towards the material is very slow and restricted. It is possible to accelerate the resorption and induce new bone tissue replacement of the CPC materials by providing sufficient porosity for cell penetration, tissue ingrowth and nutrient exchange. In some studies CFs were used to create macropores in CPC structures. In vivo studies by Lian et al. demonstrated the advanced new bone tissue growth towards inside the CPC-fiber implant with the help of macrochannel formation in CPC material [117]. After the fiber resorption, the cylindrical pores are left behind which enable osteoblast generation towards the inside of the CPC and promote bone ingrowth. In another study, CF/CPC scaffolds were prepared and the results from in vitro studies revealed the rapid formation of patterned macropore structures related to morphology of fibers inside the CF/CPC system [119].

1.4.2 The Chelating Capacity of Chitosan

Chitosan has been demonstrated to be an effective chelating agent through its amino (-NH_2) and hydroxyl (-OH) groups which act as coordination sites to form complexes with metal ions [120, 121]. A number of studies on chitosan have been reported on its absorption and complex formation capacity with heavy metal ions such as Cu^{2+}, Zn^{2+}, Ni^{2+}, Cd^{2+}, Hg^{2+}, Pb^{2+} and Cr^{3+} [120]. Chitosan could take the proper configuration for complexation with each metal ion through its flexible chains. Metal ion absorption is a solid state action of chitosan and a large specific surface area is advantageous due to higher metal ion interaction capability. A previous study indicated that wet-spun CFs can efficiently used in metal chelating and fibers are able to chelate up to 6.2% zinc of their own weight [122].

Owing to this metal-complexation potential, chitosan and its derivatives are now widely used in removal of metal ions from waste waters, absorption of anionic/cationic dyes, and some other industrial applications [123-125]. However, far too little attention has been paid to chitosan-metal complexes in biomedical area. There are just a few studies focused on this subject; The chelating ability of chitosan was suggested to apply in the treatment of thalassemia or iron overload therapies [126, 127], metal-chitosan complexes were used to serve as contrast agents for magnetic resonance imaging purposes [128] and metal containing chitosan magnetic nanoparticles were developed to be used in targeted delivery for tumor therapies [129].

Despite of being an important and conventional biopolymer, non-usage of chitosan in essential trace metal delivery for tissue healing purposes is a gap in the field of biomaterial research. It is quite apparent that the metal chelating property of chitosan could potentially be used on the development of controlled metal release systems and applied in local metal deficiency therapies of different tissues to avoid systemic side effects.

1.5 The Physiological Role of Zinc on Bone Tissue

Metal ions have vital importance on preserving homeostasis and they participate in most of the biochemical processes in the body. For instance, metals play crucial roles on the specific structure and function of nucleic acids and take part in the catalytic activity of many proteins.

As the second most abundant essential trace metal ion after iron, zinc is in charge of determining tertiary or quaternary structure of as many as 3000 proteins in the human body [130]. In addition to be a functional trace metal on gene expression process, it acts in enzymatic reactions as cofactors [131].

The physiological role of zinc on bone homeostasis and growth was discovered more than 70 years ago and this subject is still widely studied [132, 133]. It is previously reported that zinc deficiency result in bone growth retardation on rats and the zinc can stimulate bone mineralization process [134-136].

Several studies demonstrated the essential effects of zinc on regulation of the bone metabolism. A report published in 1986 revealed that nutritional zinc supplementation led to an increase in total number of DNA and accordingly stimulate bone growth in femoral diaphysis of rats [137]. In following years, the stimulatory effect of zinc was reported by zinc administration on rat calvaria tissue culture system [138]. The results revealed the elevation of calcium and collagen amount as a result of zinc uptake by bone tissues. Moreover, in the presence of zinc, an enhancement in alkaline phosphatase activity was detected which is an indicator of osteoblastic cell function and new bone tissue formation [138].

Zinc specifically effects anabolic metabolism of osteoblasts by inducing bone protein synthesis at the translational level and a remarkable increase on protein content was observed in osteoblastic cells [139, 140]. Bone endogenous zinc has a stimulative

effect on proliferation and differentiation of osteoblasts [140, 141]. In 2007, the effect of zinc on the differentiation of human osteoblast-like cells (Saos-2) and the formation of mineralized bone nodules in tissue culture were investigated [142]. Cells were treated with tissue culture mediums involving varius concentrations of zinc (0, 1, 10, 25, and 50 μM) for 9 days. The effect of zinc on human osteoblast-like cells was shown to be concentration dependent, zinc significantly increased the number and area of mineralized bone nodules at low concentrations (1 and 10 μM) where as at higher concentrations (25 and 50 μM), the presence of zinc decreased both bone mineralization and alkaline phosphatase activity. This study demonstrated the inductive effect of zinc on osteoblast differentiation and bone mineralization is only possible in a certain concentration range. On this basis, it is required to have site specific administration and controlled release of zinc for bone treatment to observe a positive effect on bone mineralization and to avoid toxic effects in surrounding tissues

Despite the large body of previous works on the effect of zinc on animal and human bone studies, there is still very limited information about zinc regulation on bone formation at a biomoleculer level, and cellular mechanisms of zinc action in osteoblastic cells has not been fully clarified. In 1994, the effect of a zinc compound (β-alanyl-histidinato-zinc) on protein content of MC3T3-E1 osteoblastic cells were investigated in tissue culture and an increase was detected in concentrations of osteocalcin, insulin like growth factor-I and transforming growth factor β in cell culture medium [143]. The results indicated the enhancer effect of zinc on the synthesis of proteins which are responsible for the stimulation of bone formation in osteoblastic cells. Yamaguchi et al. (2008) demonstrated the role of zinc sulphate in the regulation of gene expression in osteoblastic cells; the presence of zinc improved Runx-2, osteoprotegerin and regucalcin mRNA expressions in vitro [144]. In 2010, Kwun and colleagues suggested that, zinc deficiency caused an attenuated ECM mineralization and new bone tissue formation due to inhibited or delayed expression of Runx-2 and bone marker gene transcription in osteoblasts [13].

In addition to all of these positive effects on new bone tissue formation, zinc has an repressive role on bone resorption by inhibiting osteoclast proliferation and osteoclastic activity [145-147]. In 1994, the inhibitory effect of zinc on mause marrow cell differentiation and osteoclast formation was reported [148]. Following that, Moonga and co workers investigated the effect of zinc on isolated rat osteoclasts and observed a noteworthy reduction in bone resorption because of the osteoclast activity inhibition [146]. Besides, zinc has been demonstrated to have a negative effect on osteoclast proliferaton by suppressing the expression of regucalcin, a stimulator protein of osteoclastogenesis in bone [144]. Recently, Yamaguchi et al. (2010) published a review including the cellular mechanisms of zinc action in osteoclastic cells and bone resorption [133].

1.6 Objective of the Study

There are various CPCs which have different Ca/P ratios and demonstrate different bioactivity and bioresorbability characteristics. Among other calcium phosphate phases, α-TCP based bone cements are getting increasing attention to be used in bone repair and reconstruction due to their capability to set into monolithic calcium deficient hydroxyapatite (CDHAp, $Ca_{10-x}(HPO)_4(PO_4)_{6-x}(OH)_{2-x}$, x=0–1) from a single solid reactant at conditions near to physiological pH and temperature. In addition, the injectability of α-TCP has a crucial importance on the placement of the cement into a bone defect area with limited accessibility and the injection of α-TCP offers a great advantage of using minimal invasive operation techniques for orthopedists. However, the relatively long degradation time of the hydration product (CDHAp) in vivo conditions and the drawbacks in the injection of the cement are limiting factors in clinical usage of α-TCP.

Despite the large amount of literature on characterization and possible applications of α-TCP, there is no detailed information on the optimum solid-state synthesis

parameters to produce a highly reactive α-TCP. Besides, due to inadequate information on chemical composition of the starting materials, synthesis of reactive α-TCP becomes a problematic task for those trying to reproduce an available synthesis protocol.

The first main objective of this thesis was to investigate the effects of α-TCP synthesis parameters, such as firing temperature and time, and the impurity content of the starting calcium sources on hydration reactivity of the end product. For this purpose, the samples of α-TCPs were synthesized by using different firing temperatures between 1150-1350°C for 2 h or 24 h. In order to investigate the effect of the metallic impurity content to the reactivity of α-TCP, three commercial calcium carbonate ($CaCO_3$) sources were used as primary calcium precursors and their impurity contents were determined by inductively coupled plasma mass spectrometry. The resultant α-TCP products for all synthesis routes were compared in terms of the material properties and the hydration reactivity.

The second main objective of this study is to prepare an injectable α-TCP and CF composite bone cement system which is designed to degrade gradually in time to be replaced by the natural bone tissue. It is well known that, CDHAp is the hydration product of α-TCP and as a result of its submicron pore size, new bone tissue formation towards the material is very slow and restricted in comparison with bone healing process. Providing porosity to CDHAp structure, which enables cell penetration and tissue ingrowth towards the material, is necessary to accelerate the resorption and induce bone tissue replacement of the implant. Therefore, a biocompatible and biodegradable natural polymer, chitosan, was chosen and blended with α-TCP to prepare novel cement composites. The main driving force behind the selection of chitosan is osteoinductive characteristics of the polymer that is known to promote osteogenesis. Fiber form of the polymer was preferred to be used in order to provide sufficient porosity to CDHAp structure and enable tissue in growth towards the composite graft while preventing the hampering effect of free chitosan molecules

on α-TCP hydration. After the fiber degradation, macropores are expected to be formed and filled by natural bone tissue that potentially accelerates the bone replacement process by increasing the surface area of tissue implant interface. As a minor objective, the injectability of the cement paste is intended to be increased by the fiber addition. With these objects, α-TCP/CF composites were prepared in different compositions and the effect of CF addition on cement properties were examined by mechanical and injectability tests as well as microstructural and phase analysis studies.

The third main objective of this thesis is to prepare a biodegradable bone supporting material to achieve site specific administration and controlled release of zinc. For this purpose, zinc containing chitosan scaffolds were prepared and treated with α-TCP. Zinc release studies were performed on CaP covered and non-covered CF scaffolds and zinc concentrations of the release solutions were analyzed by Inductively Coupled Plasma Mass Spectrometer (ICP-MS).

CHAPTER 2

ALPHA-TRICALCIUM PHOSPHATE (α-TCP): SOLID STATE SYNTHESIS FROM DIFFERENT CALCIUM PRECURSORS AND THE HYDRAULIC REACTIVITY

The synthesis of α-TCP is generally realized by solid state reactions. This is achieved by open air firing of homogenously mixed stoichiometric amount of calcium and phosphorus precursors at temperatures between than 1125°C-1430°C. By this way, phase pure α-TCP can be obtained as shown by many studies [49, 67, 85]. However, direct assessment on the hydraulic reactivity of the α-TCP products of these studies is not possible, as the precursors and firing temperatures usually differ. It is well known that chemical composition of the precursors ($CaCO_3$) and the firing procedure dominantly affects the cement-type setting as well as the final physical properties of α-TCP. In order to provide a reproducible and well-detailed α-TCP powder synthesis protocol, α-TCP production was attempted using three commercially available $CaCO_3$ sources with different chemical grades, i.e. different amounts of impurities. The chemical phases and hydraulic properties of the resultant products are examined and compared. Other critical synthesis parameters related with the reactivity and setting behavior of α-TCP are the firing time and temperature, which was also optimized systematically by employing different firing temperature of 1150°C, 1200°C and 1350°C for 2 h and 24 h. The resultant α-TCP products for all synthesis routes were compared in terms of the material properties and the hydration reactivity. The findings of the present work are a useful guideline for synthesis of highly reactive α-TCP.

2.1 Experimental

2.1.1 Materials for Synthesis and Hydration of α-TCP

Three different $CaCO_3$ precursors were used to prepare α-TCP. They were the commercial-grade products of Merck (Germany, Catalog no. 102066), Sigma Aldrich (Germany, Catalog no. C4830) and Carlo Erba (Italy, Catalog no. 327059), which will be referred as *CC-M, CC-S* and *CC-C,* respectively hereafter. H_3PO_4 (85 wt%) was received from Merck (Germany, Catalog no.100573). The hydration solution was obtained from $Na_2HPO_4{\cdot}2H_2O$ (Germany, Riedel-de Haen, Catalog no. 04272) and used as setting medium in cement-type reactions, i.e. in hydraulic property assessments.

2.1.2 Procedure for α-TCP Synthesis

α-TCP was synthesized by solid state reaction between $CaCO_3$ and pre-synthesized $CaHPO_4$ according to the following reaction.

$$CaCO_3\ (s) + 2CaHPO_4\ (s) \rightarrow Ca_3(PO_4)_2\ (s) + CO_2\ (g) + H_2O\ (g)$$

In the preparation of $CaHPO_4$, first $Ca(OH)_2$ was produced by a two-step process; calcination (1150°C for 3 h) of $CaCO_3$ to obtain CaO, followed by hydrolysis of CaO with deionized (DI) water. In these steps the same $CaCO_3$ source employed in the above given reaction, was used. Then, the resultant $Ca(OH)_2$ slurry was used in the production of $CaHPO_4$. For this purpose, $Ca(OH)_2$ was mixed with H_3PO_4 solution at 1:1 molar ratio in presence of excess DI-water at 60-65°C for 30 min. The final slurry was vacuum filtered and dried at 80°C for overnight to obtain $CaHPO_4$ powder. For the preparation of α-TCP, this pre-synthesized $CaHPO_4$ was mixed with $CaCO_3$ in 2:1 molar ratio using Turbula T2F mixer (WAB, Switzerland). After 1 h mixing, the solid

powder blend was fired in an alumina crucible in an open atmosphere furnace at 1200°C for 2 h (or 24 h). At the end of the firing period, the chunky product was discharged on a borosilicate glass plate and air quenched to room temperature. After hand grinding with an agate mortar and pestle, and sieving through –200 mesh, the obtained powder products were stored in a vacuum desiccator until further use. This synthesis protocol was repeated for all $CaCO_3$ sources of *CC-M, CC-S, CC-C.* In addition, for the experiments with *CC-M*, 2 h firing operations of $CaHPO_4$:*CC-M* blends were also performed at 1150°C and 1350°C to examine the effect of firing temperature, and then the same quenching treatment was applied.

2.1.3 Cement-type Setting of α-TCP

The cement-type setting of α-TCP products was performed by exposing the α-TCP powders to 2 wt% aqueous solution of $Na_2HPO_4{\cdot}2H_2O$. The hydration was achieved at 37°C for 24 h, at a solid to liquid weight ratio of 1:2. At the end of 24 h, the solid reaction products were washed with acetone and dried by air blowing to finalize hydration.

2.1.4 Material Characterization

The chemical composition of $CaCO_3$ sources were investigated by Inductively Coupled Plasma – Mass Spectrometer (ICP-MS, Perkin Elmer DRC II model). X-Ray diffraction (XRD) analyses were performed for phase analysis of the α-TCP products and their hydration products. XRD analyses were performed using Rigaku X-ray diffractometer (Ultima D/MAX 2200/PC). CuKα radiation was used at 40 kV voltage and 40 mA current. The scanning range of the samples was 20-40° and the scanning speed was 2°/min. The morphologies of all $CaCO_3$ precursors, α-TCP products and resultant HAp were examined with a FEI Quanta 400F Scanning Electron Microscope (SEM). The samples were coated by Au-Pd thin film by a Hummle VII sputter prior

to SEM investigations. The surface area of selected α-TCP powders were determined by nitrogen gas adsorption using Autosorb-1-C/Ms analyzer. The powders used in the analyses were approximately 0.40 g and were degassed using high purity N_2 at 80°C for 16 h prior to measurements.

2.2 Results and Discussion

Effects of solid state synthesis parameters (temperature and time) on cement-type hydration efficiency of α-TCP were investigated. α-TCP powders synthesized from three different sources of $CaCO_3$ and their hydration products were examined and compared. The obtained results and discussions are given in different sections below:

2.2.1 Temperature Effect on Hydraulic Reactivity

XRD diffractograms of the α-TCP powders synthesized from *CC-M* by firing at 1150°C, 1200°C and 1350°C, and the hydration products of these α-TCP powders are given in Figure 2.1a and 2.1b, respectively. The XRD patterns of the samples fired at 1200°C and 1350°C exhibited the characteristic peaks of α-TCP (JCPDS card no. 9-348). These products contained negligible amount of HAp as evidenced by very low intensity set of peaks at around 2θ≈31-33° matching with the characteristic peak positions of HAp (JCPDS card no. 9-432), and for practical purpose they were considered as phase pure α-TCP. No other crystalline phase was observed. So, after firing at these relatively high temperatures, α-TCP was obtained by the solid state reaction between $CaCO_3$ and $CaHPO_4$. The XRD pattern of the sample fired at 1150°C, on the other hand, reveals formation of some β-TCP (JCPDS card no. 9-169) as a second phase besides the main α-TCP product. The β–polymorph, the room temperature equilibrium phase of TCP, does not illustrate any cement-type setting as observed for α-polymorph. For TCP β-polymorph is the stable phase up to 1125°C

and at this critical temperature transformation of β to α-phase occurs [57, 149]. However, regardless of firing temperature, conservation of the metastable α-TCP phase at room temperature requires effective quenching. So, for the sample fired at 1150°C, the presence of β-polymorph is a combined result of various factors. A firing temperature around 1150°C is at close proximity of the equilibrium phase transformation temperature for β-to-α transition (1125°C), and this is thermodynamically more tolerant condition for the presence of β-TCP compared to its existence during firing at relatively higher temperatures. In addition, this situation also requires much more aggressive supercooling to avoid formation of the equilibrium phase (β-polymorph) upon cooling down to room temperature, which was most likely not accomplished by moderately effective air quenching for the samples fired at 1150°C. Therefore, some β-TCP together with α-TCP was formed in the end product.

The XRD pattern of the hydration products of the α-TCP powders synthesized from *CC-M* and fired at 1150°C suggests almost a complete transformation of α-TCP to HAp and small amount of β-TCP remained in the end product (Figure 2.1b). Similarly, for the sample fired at 1350°C, again formation of HAp was observed, but some α-TCP remained unreacted. On the other hand, the α-TCP synthesized at 1200°C showed the best hydraulic property and was almost completely transformed to HAp. Firing at higher temperatures leads to dead-burning associated with microstructural coarsening, which is known to occur in high temperature solid-state reactions [150, 151].

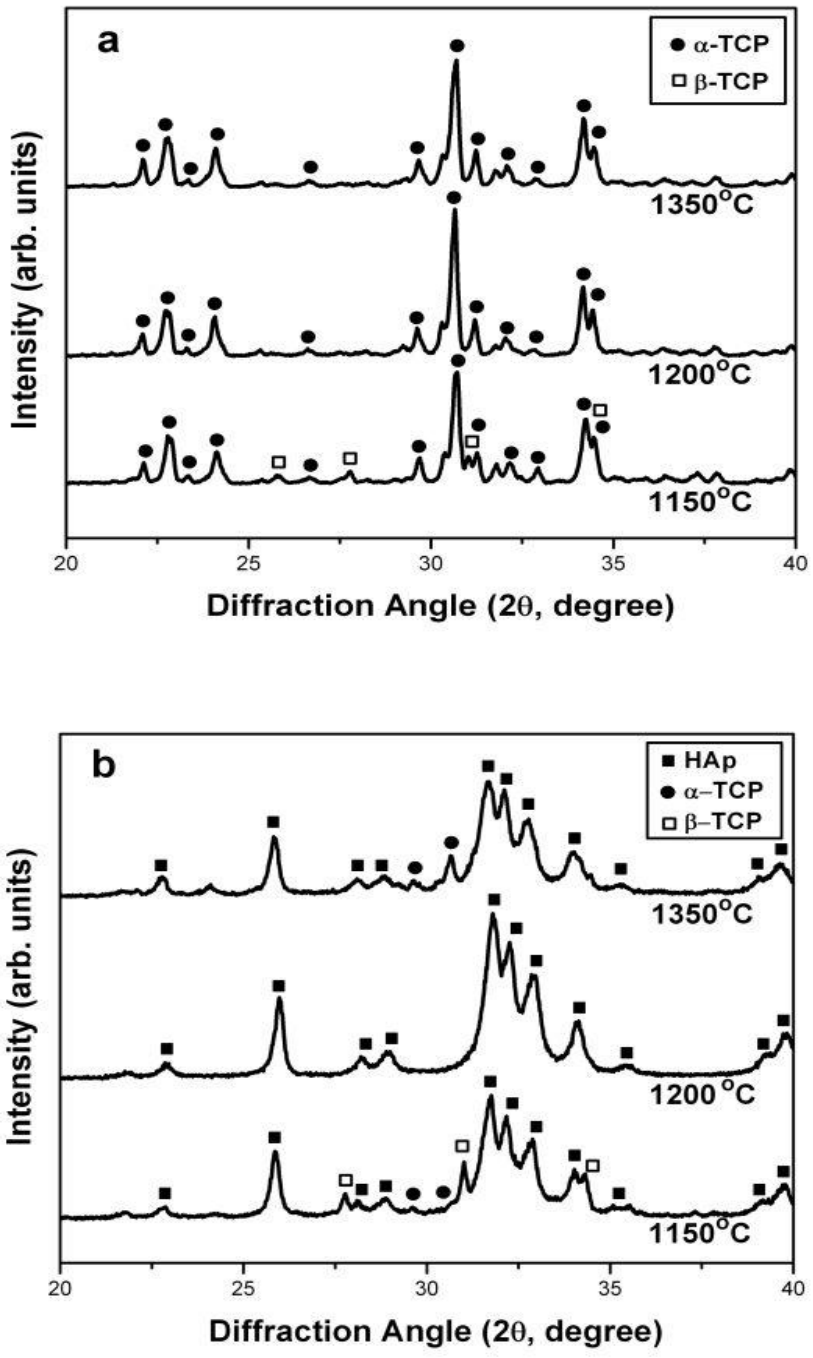

Figure 2.1 XRD diffractograms of α-TCP powders and their hydration products. **(a)** α-TCP powders synthesized from *CC-M* by firing at 1150, 1200 and 1350°C for 2 h, and **(b)** hydration products of the respective α-TCPs.

It is worth to emphasize that the surface area of α-TCP powders synthesized from *CC-M* fired at 1150, 1200 and 1350°C was determined as 1.47, 0.99 and 0.69 m^2/g, respectively. These results were also supported by SEM micrographs of the same powders which reveal an increase in the average particle size at higher firing temperatures (Figure 2.2); the average sizes of the α-TCP's fired at 1150, 1200 and 1350°C were at around 2, 5, and 8 μm, respectively.

A decrease in the surface area for the powders fired at 1350°C due to coarsening hampers the initial dissolution of α-TCP, therefore limiting the overall hydraulic reactivity and transformation to HAp. Thus, the XRD analyses and preliminary hydraulic reactivity evaluations illustrated that the firing temperature of 1200°C to be high enough to avoid the formation of β-TCP, while producing highly reactive α-TCP powder. Therefore, this temperature was chosen as the optimum firing condition and all other firing operations for the remainder of the experimental work were carried out at 1200°C.

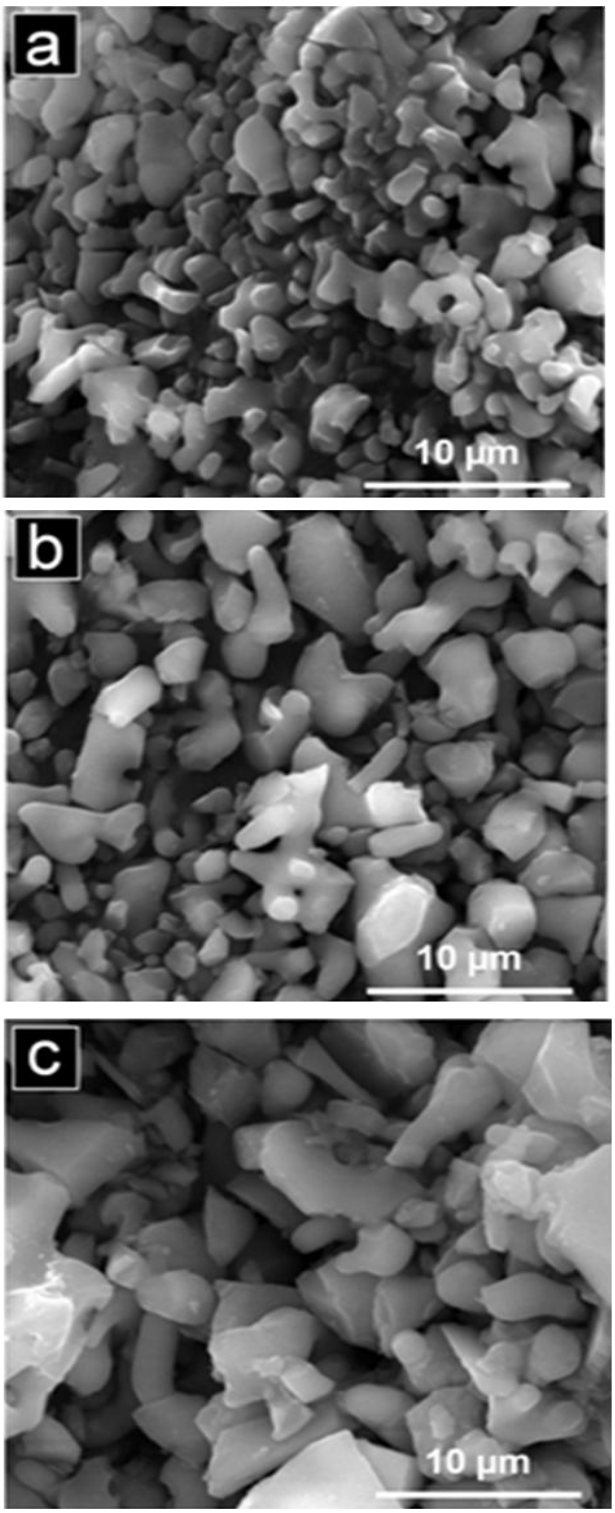

Figure 2.2 SEM micrographs of α-TCP powders synthesized from *CC-M* by firing for 2 h at different temperatures. **(a)** 1150°C, **(b)** 1200°C and **(c)** 1350°C.

2.2.2 α-TCP Synthesis from Different Calcium Precursors

XRD diffractograms for the α-TCP powders synthesized from three different $CaCO_3$ sources; *CC-M, CC-S* and *CC-C;* all fired at 1200°C for 2 h, and for the hydration products obtained from these α-TCP powders are given in Figure 2.3a and 2.3b, respectively. All the α-TCP products were almost identical in terms of the phase identity and crystallinity. They were all phase pure α-TCP (Figure 2.3a), except the one obtained from *CC-C* which had negligible amount of β-TCP. The possible reason for the formation of this additional phase might be the impurities present in the structure, and this effect will be discussed later (in section 2.2.4). Despite the similar chemical and phase characteristic of the three α-TCP products, their hydraulic reactivities were distinctly different as revealed by the XRD data shown in Figure 2.3b. Upon 24 h hydration with sodium phosphate solution, they all converted to HAp to some extent, but at different completion efficiencies. The α-TCP synthesized from *CC-M* source exhibited the highest reactivity among three products and was completely set to HAp after hydration. The α-TCP of *CC-S* again hydrated to HAp, however, the hydraulic reactivity was relatively poor compared to the α-TCP obtained from *CC-M* and some α-TCP remained as it is. On the other hand, α-TCP obtained from *CC-C* source showed almost no hydraulic reactivity and the majority of α-TCP stayed unreacted after hydration. The observations in regard to hydraulic reactivity are promising for the α-TCP of *CC-M* source, compared with α-TCPs of other $CaCO_3$ sources. It is considered that the observed differences in hydraulic reactivities are arising from the different quantities of impurities in $CaCO_3$ sources, therefore this point was searched in detail.

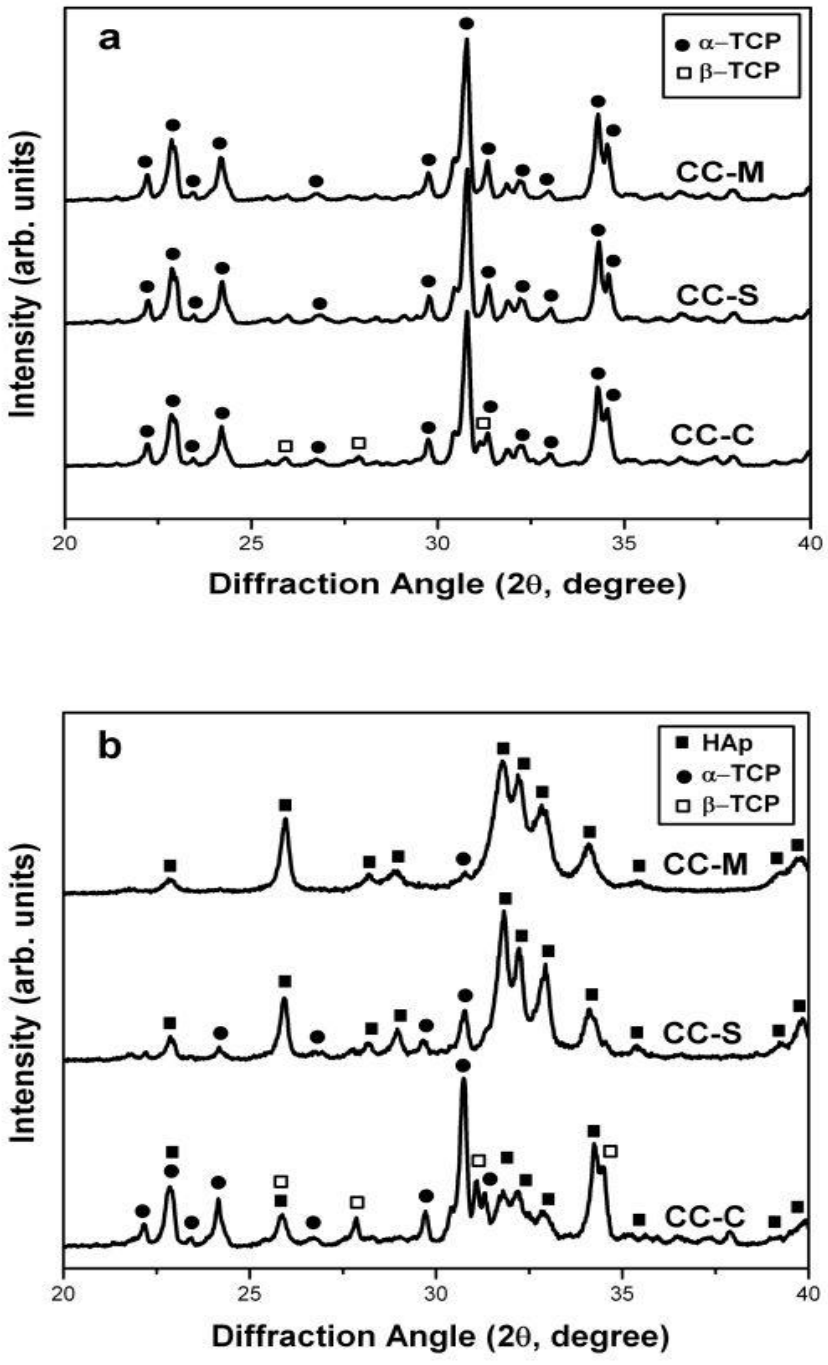

Figure 2.3 XRD diffractograms of α-TCP powders synthesized from different $CaCO_3$ sources (*CC-M, CC-S* and *CC-C)* by firing at 1200°C for 2 h. **(a)** α-TCP powders and **(b)** their hydration products.

In order to have more definite conclusion about the effect of firing operation on reactivity of α-TCP powders, longer firing treatments extending to 24 h were performed on all samples which were obtained from different sources and the hydraulic reactivities of their products were evaluated. The results are summarized by the XRD data shown in Figure 2.4. This figure illustrates the XRD diffractograms of the α-TCP powders (obtained from different $CaCO_3$ sources)–as synthesized (Figure 2.4a) and after hydration (Figure 2.4b). Extending the firing operation does not lead to any apparent change in the chemical nature and phase identity of α-TCP in as-synthesized condition. The 24 h-fired and 2 h-fired α-TCPs were almost identical, as revealed by the similarity of the XRD data presented in Figure 2.4a and Figure 2.3a. Meanwhile, similar trends in hydraulic reactivity were observed for the α-TCPs obtained after prolonged firing operations. Again, α-TCP of *CC-M* exhibited the highest reactivity while α-TCP of *CC-C* had the least. Besides these general observations one important finding associated with the prolonged firing is the recognition of a marginal decrease in the overall hydraulic reactivities of all α-TCP products. In all cases relatively more α-TCP remained in the hydrated product as shown by the XRD data in Figure 2.4b. This change is valid both for α-TCP of *CC-M* and of *CC-S,* however more obvious for the latter. This observation is related with the microstructural coarsening simply due to excessively long firing operation, as also discussed earlier in firing temperature studies. In this case, time factor becomes dominant instead of temperature leading to coarsening. This microstructural change impedes dissolution of α-TCP, which is essential for the cement-type hydraulic reactivity.

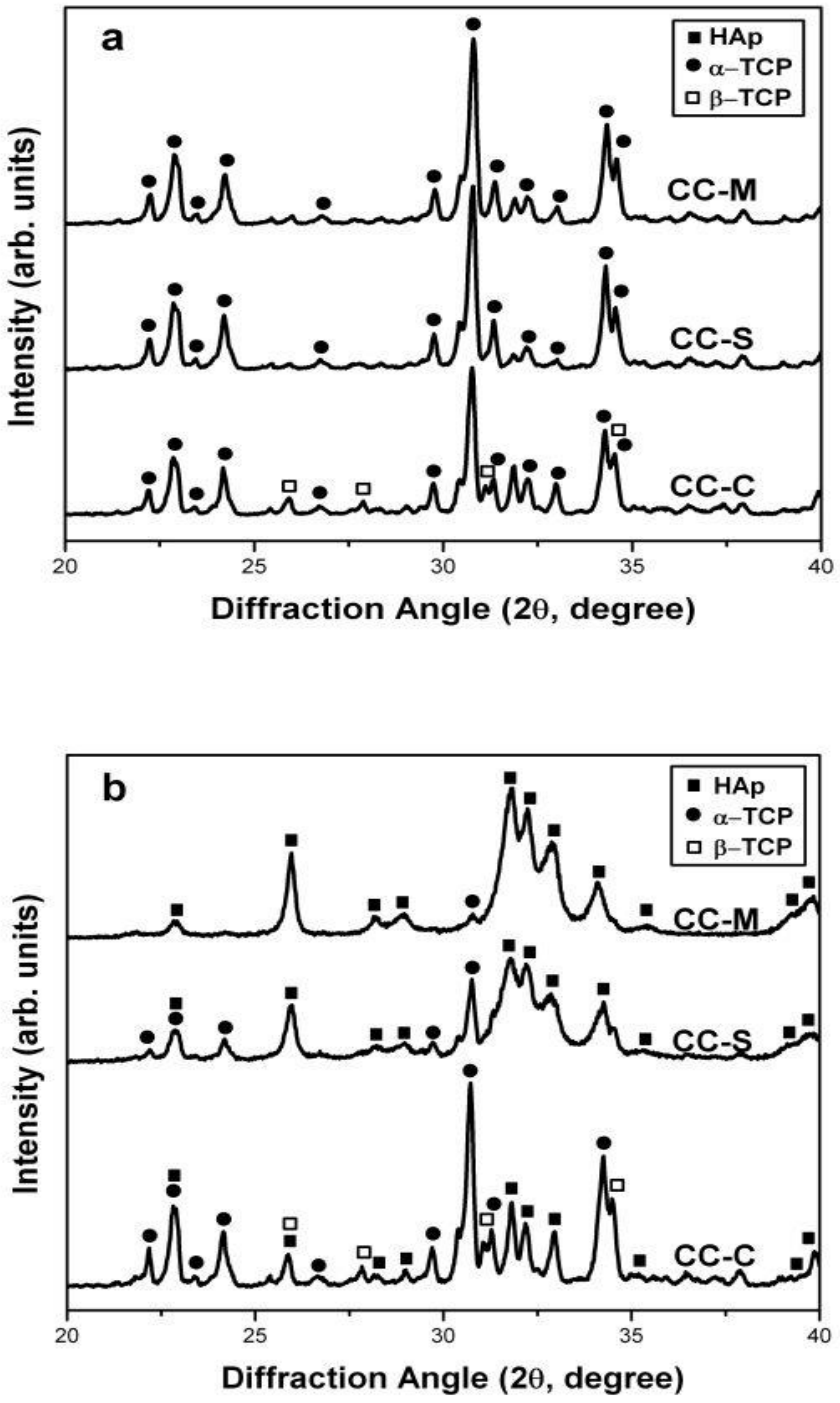

Figure 2.4 XRD diffractograms of α-TCP powders synthesized from different $CaCO_3$ sources (*CC-M, CC-S* and *CC-C*) by firing at 1200°C for 24 h. **(a)** α-TCP powders and **(b)** their hydration products.

2.2.3 Microstructural Investigations

The SEM micrographs of the $CaCO_3$ sources**,** α-TCP powders synthesized from these sources (fired at 1200°C for 2 h) and the cement-type products obtained by hydration of respective α-TCPs are given in Figure 2.5. The $CaCO_3$ sources of *CC-M* and *CC-S* exhibit prismatic/cubic crystal morphology typical to highly crystalline $CaCO_3$ mineral, as shown by the micrographs in Figure 2.5 (a-b). The average particle sizes were determined as approximately 5 μm and 8 μm, for *CC-M* and *CC-S*, respectively. The morphological appearance of *CC-C* is distinctly different, exhibiting irregularly shaped submicron-crystals (Figure 2.5c).

The morphologies of the α-TCP powders, as shown in Figure 2.5 (d-f), are identical with slightly distorted and equiaxed-like shape without any sharp discontinuities or features. This morphology is common for the ceramic powders obtained by high temperature solid state reactions at conditions approaching to sintering temperatures. The average particle size of the α-TCP powders produced from *CC-M, CC-S* and *CC-C* sources had comparable particle sizes at around 2-3 μm. This data revealing that the particle size does not directly correlate with the observed overall hydraulic activity, as all α-TCPs were almost identical particle size but still, the hydraulic reactivities of *CC-S* and *CC-M* were obviously different from *CC-C*.

SEM micrographs showing the morphologies of the cement-type products, i.e. the HAp crystals, obtained by hydration of respective α-TCP samples are given in Figure 2.5 (g-i). For the hydration products of α-TCP obtained from *CC-M* and *CC-S* (which were shown to be completely converted to HAp by the XRD analyses) the morphologies resemble the typical equiaxed-like shape of α-TCP powders. However, the surfaces of the α-TCP particles are completely covered with newly formed small

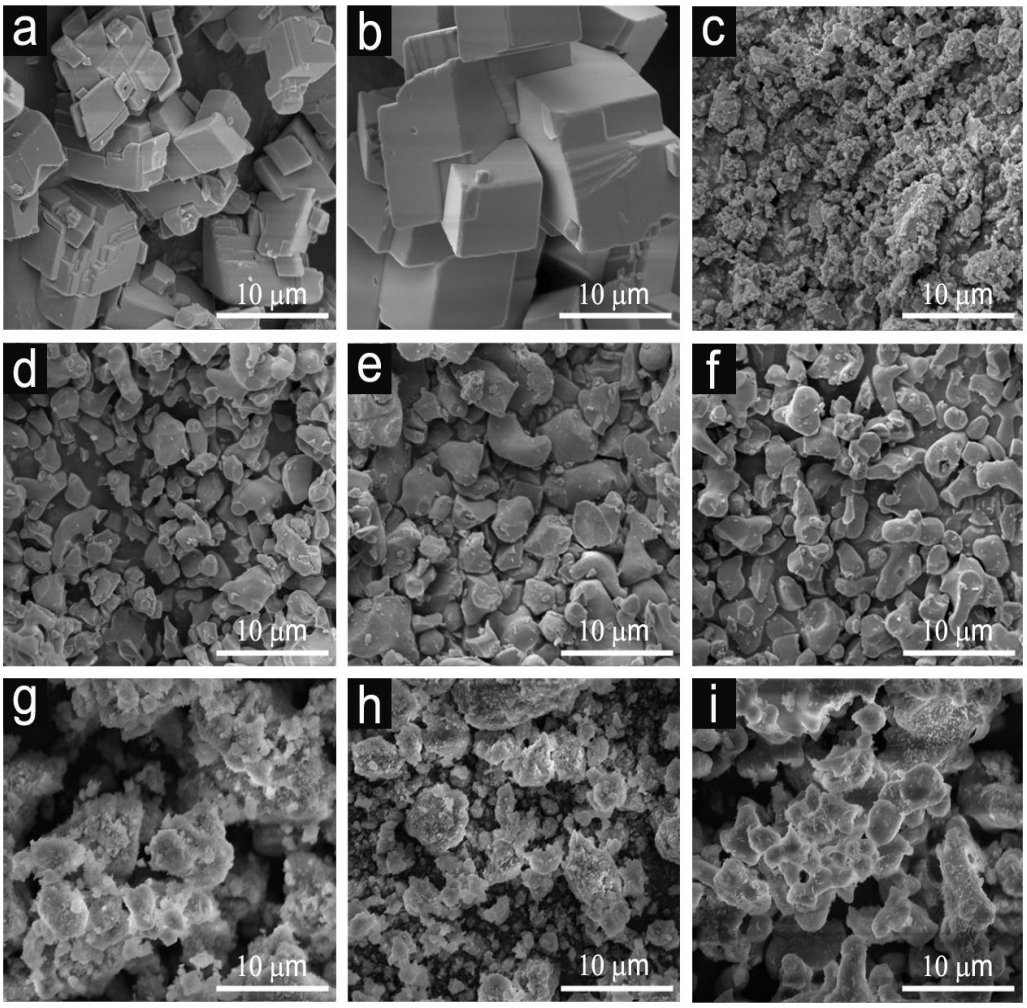

Figure 2.5 SEM micrographs of $CaCO_3$ precursors **(a)** *CC-M*, **(b)** *CC-S*, **(c)** *CC-C*; α-TCP powders synthesized at 1200°C for 2 h from **(d)** *CC-M*, **(e)** *CC-S*, **(f)** *CC-C*; and HAp products obtained by hydration of these α-TCP powders **(g–i).**

sub-micron size reticulated needle-like HAp crystals. On the other hand, the morphology of the α-TCP of *CC-C* seems to be relatively unchanged upon hydration. There are some very small need-like HAp crystals partially covering the α-TCP particle surfaces, but distinctly at a much smaller extent compared to those of α-TCP of *CC-M* and of *CC-S*. The SEM findings in general correlate with the XRD analyses, suggesting relatively poor hydraulic reactivity for α-TCP of *CC-C*. It is worth to emphasize that, no significant morphology and particle size differences were observed

for the α-TCPs synthesized from different $CaCO_3$ sources (*CC-M, CC-S* and *CC-C*). Therefore, it is reasonable to suggest that the differences in the hydraulic reactivities of α-TCPs are not directly related with physical factors, but most likely with chemical characteristics, initiating from the differences in impurity content of starting mineral precursor of $CaCO_3$.

2.2.4 The Impurity Effect on Hydraulic Reactivity of α-TCP

The amounts of some impurities for the $CaCO_3$ precursors obtained by ICP-MS analyses are given in Table 2.1. The total amounts of the impurities are different for each $CaCO_3$ source. The highest amount of impurity was detected for *CC-C*, which turned out to α-TCP product with the poorest hydraulic reactivity. In fact, the morphological investigations of the $CaCO_3$ precursors with SEM provided some foresee for such chemical differences. The crystals of *CC-C* were submicron in size, much smaller compared to crystals of the other $CaCO_3$. On the other hand, *CC-M* and *CC-S* crystals were in the form of large planar facets with cubical resemblance as shown in Figure 2.5a and 2.5b. This difference is most likely due to the ionic impurities, which can effectively change the crystal growth mechanism during mineral formation, leading to differences in the shape and size of the $CaCO_3$ crystal deposits.

As shown in Table 2.1, the contents of sodium (Na), potassium (K), strontium (Sr), barium (Ba), lead (Pb) and cadmium (Cd) impurity are different, however are at comparable levels for all three $CaCO_3$ sources. Meanwhile, magnesium (Mg) content is significantly different in all $CaCO_3$ sources. For *CC-C,* Mg content was detected as 1054.8 μg g^{-1}, order of magnitude higher than Mg content of *CC-M* (30.4 μg g^{-1}) and *CC-S* (93.5 μg g^{-1}). Most probably this is the main reason for the poor reactivity of *CC-C,* since it is known that Mg doping changes the crystal structure of TCP [79].

Table 2.1 ICP-MS analysis results for the $CaCO_3$ sources; *CC-M*, *CC-S* and *CC-C*

Element	*CC-M**	*CC-S**	*CC-C**
Na	33.0 ± 2.8	20.3 ± 3.7	38.7 ± 2.3
K	<<9.3	51.7 ± 3.4	25.0 ± 3.8
Mg	30.4 ± 0.5	93.5 ± 1.4	1054.8 ± 12.0
Sr	92.1 ± 1.1	87.4 ± 1.9	73.6 ± 0.6
Ba	0.8 ± 0.03	1.61 ± 0.12	1.51 ± 0.1
Fe	<<5.5	<<5.5	75.1 ± 1.2
Al	<<3.0	<<3.0	73.3 ± 4.9
Pb	<<0.075	<<0.075	1 ± 0.1
Cd	<<0.075	<<0.075	1± 0.1

*The values are in μg g^{-1}.

The substitution of Ca^{2+} by smaller sized Mg^{2+} ions in the TCP crystal, leads to a more relaxed geometry for the crystal lattice. Due to the higher electronegativity of Mg^{2+} compared to Ca^{2+} a stronger interaction forms between Mg and O weakening the Ca-O bonding [79]. Therefore, presence of Mg^{2+} results in an enhancement in the chemical stability and consequently decreases the solubility of TCP [80, 82, 152] limiting its cement-type conversion by hydration. This was the case for the α-TCP synthesized from *CC-C* source containing high level Mg which exhibited no hydraulic reactivity and poor setting characteristic. In addition, high Mg content of *CC-C* also becomes a determining factor for the crystal nature of fired α-TCP product thereof synthesized by high temperature solid state reaction. It has been shown that the Mg ion doping stabilizes the low temperature β-polymorph of TCP and increases the β to α-TCP phase transformation temperature (1125°C) to higher values [80, 81, 84, 153, 154]. In this respect, the formation of β-TCP phase from *CC-C* reactant after firing at 1200°C is quite reasonable, again attributed to its considerable high Mg impurity content.

Another compositional difference between $CaCO_3$ sources (*CC-M* and *CC-S)* leading to highly reactive α-TCP, and *CC-C* source that yields to poorly reactive α-TCP, is in the amount of Fe impurity. The amount of Fe was found much less than 5 μg g^{-1} both for *CC-M* and *CC-S,* and at around 75 μg g^{-1} for *CC-C*. Fernandez et al. investigated the effect of iron citrate modification on setting characteristics of α-TCP and they reported shorter initial and final setting times with Fe modification [78]. In this regard, the poorest reactivity of α-TCP of *CC-C* suggests that the inhibitory effect of Mg seems to be more dominant than synergetic effect of Fe.

The amount of Al was also much higher for *CC-C* (73.3 μg g^{-1}) compared to that for *CC-M* and *CC-S* which was much less than 3.0 μg g^{-1}. It is not possible to propose an educated guess about the direct effect of Al on hydraulic reactivity from the data of the present study. However, if Al had an effect on reactivity this should be inhibitory, as it is the highest in *CC-C*. However, this conclusion is just vague, as there is no data for the effect of Al on reactivity of α-TCP in the literature for the best of our knowledge.

The effect of Sr, which is a common impurity for the all calcium precursors employed in this study, on hydraulic reactivity of α-TCP has been also reported in literature. It is given that, a decrease in hydraulic reactivity was observed for α-TCP samples containing more than 1 mol% Sr substitution [76]. Similarly, decrease in α-TCP reactivity was observed when Sr ion was present in the hydration media [75]. The Sr impurity content of the $CaCO_3$ precursors used in present study was found to be almost identical; in the order of 70-90 μg g^{-1}. This Sr amount is much lower than the amount of Sr-substitution (1 to 10 mol %) achieved in the previous reports [76]. The sufficiently high reactivity of α-TCPs, obtained from *CC-M* and *CC-S* containing trace amounts of Sr impurity suggest that there at least a critical content of Sr is required to cause an obvious decrease in the reactivity and at this concentration, Sr does not have a negative effect on the reactivity of α-TCP.

As a summary, in this part of the study, the effects of α-TCP synthesis parameters such as firing temperature and firing time, and the impurity content of the starting calcium sources on hydration reactivity were investigated. For this purpose, the samples of α-TCPs were synthesized by using different firing temperatures between 1150-1350°C by applying firing time of 2 h or 24 h. Three commercial $CaCO_3$ sources with different impurity contents (*CC-M*, *CC-S*, *CC-C)* were used as primary calcium precursors. It is concluded that, the phase pure α-TCP powder synthesized from *CC-M* by firing at 1200°C for 2 h exhibited the highest reactivity among most of other α-TCP products and was completely set to HAp after hydration process. The main difference behind this is the differences in trace amount of impurities that are present in $CaCO_3$ sources. The results indicated that presence of magnesium impurity leads to a significant and adverse effect on the hydraulic reactivity of α-TCP.

It is worthy of note that, the first step of this thesis was to obtain a pure α-TCP powder with high hydraulic reactivity. In order to reach this goal, a number of different synthesis routes were tried with two different phosphate precursors as monetite and pyrophosphate. In an attempt to contribute to the fund of knowledge on CaP synthesis, the main body of α-TCP synthesis experiments and their results were given in Appendix A.

CHAPTER 3

INJECTABLE CALCIUM DEFICIENT HYDROXYAPATITE-CHITOSAN FIBER COMPOSITES

It is well known that, new bone tissue formation towards the CDHAp is very slow and restricted in comparison with bone healing process. Therefore, providing porosity to CDHAp structure to enable cell penetration and tissue ingrowth towards the material is necessary to accelerate the resorption and induce bone tissue replacement of the implant. Chitosan is a natural originated biodegradable and osteoinductive polymer that commonly used in hard tissue applications. In this study, α-TCP and chitosan were combined to prepare injectable bone cement systems which are designed to degrade gradually in time to be replaced by the natural bone tissue. For this purpose, composites were prepared from chitosan fibers (CFs) and α-TCP as bone graft materials which may accelerate the bone healing process. α-TCP/CF composites were prepared in different compositions and the effect of CF addition on cement properties were examined by mechanical and injectability tests as well as microstructural and phase analysis studies.

3.1 Experimental

3.1.1 Materials

Low-viscous chitosan (>78% deacetylation degree, Fluka, catalog no. 50494, Switzerland), glacial acetic acid (99-100% J.T. Baker, Netherlands), sodium sulphate (Na_2SO_4, Merck, catalog no.106643, Germany) and sodium hydroxide (NaOH, J.T. Baker, catalog no. 0402, Netherlands) and methanol (CH_3OH, Sigma-Aldrich, catalog no. 24229, Germany) were used to prepare chitosan fibers. Sodium alginate (Sigma-Aldrich, catalog no. 2033, Germany), Ringer's tablets (Merck, catalog no. 115525, Germany) were used for composite studies.

3.1.2 Methods

3.1.2.1 Preparation of the Stock α-TCP Powder

The optimum synthesis procedure of α-TCP was determined in the light of the previous studies given in Chapter 1. Depending on the prior results, *CC-M* was used as the calcium precursor and the 1200°C – 2 h of firing operation was chosen as the optimum solid state parameters in terms of hydration reactivity of the end product, α-TCP. The powder synthesis procedure was described in detail in Chapter 1. Briefly, the solid state synthesis of α-TCP was achieved by firing of pre-synthesized $CaHPO_4$ and $CaCO_3$ mixture (2:1 molar ratio) at 1200°C for 2 h. The powder product was ball milled and sieved through -200 mesh. The produced α-TCP stock was stored in a vacuum desiccator to be used in the rest of the study.

3.1.2.2 Preparation of Chitosan Fibers by Wet Spinning

Wet-spun CFs were produced according to the procedure used by Tuzlakoglu et al. in 2004 [111]. In order to obtain a chitosan dope, 4% (wt/v) chitosan was dissolved in 2% (v/v) aqueous solution of acetic acid. In the mean time, the coagulation bath was prepared as an aqueous mixture (v/v) of 10% NaOH solution (1M), 30% Na_2SO_4 solution (0.5 M) and 60% distilled (DI) water. Following this, the chitosan dope was placed in a plastic syringe with a needle diameter of 0.5 mm and injected into a beaker containing the coagulation bath (100 mL) at a rate of 5 mL/h by using a syringe pump (New, Era Inc. model no. NE-300, USA). After CFs were formed, they were kept in coagulation bath overnight and then washed five times with DI water. For the purpose of dehydration, fibers were suspended in 50% methanol (1 h) and 100% methanol (3 h). Finally, fibers were cut into filaments at an average length of 3 mm with the help of scalpel and dried at room temperature.

3.1.2.3 Composite Formation

Totally, four groups of cement specimens were studied and α-TCP cement without fiber defined as the control group. The other three groups were prepared as α-TCP/CF composites with 1.5%, 3% and 6% (w/w) fiber content. The liquid phase was an aqueous solution of sodium alginate 1% (w/v) for all specimens. For all four formulations, the cement liquid was added dropwise to the α-TCP at a liquid to powder ratio of 0.6 (v/w) and manually mixed with spatula to obtain a cement paste of workable consistency. Previously prepared CFs were introduced subsequently and the total system was mixed for 1 min. The compositions of these composites are given in Table 3.1.

Table 3.1 Compositions of α-TCP/CF composites

Composite	α-TCP (g)	Sodium alginate 1 wt% (mL)	CF (g)
C-0 (control)	2	1.2	-
C-1.5	2	1.2	0.03
C-3	2	1.2	0.06
C-6	2	1.2	0.12

In order to perform mechanical tests, microstructural investigations and phase analysis studies, each paste was placed into a cylindrical teflon mold of 6 mm diameter and 12 mm height. Molds were immersed into Ringer solution (simulated body fluid, the composition is given in Appendix C) at 37°C for 24 h to actualize the cement-type setting of α-TCP based products. Afterwards, set cement samples were removed from molds and tests were carried out.

3.1.2.4 Composite Characterization Methods

3.1.2.4.1 Injectability Tests

Injectability characteristics were evaluated by using a Lloyd LRX 5K Mechanical Tester and an apparatus designed in our laboratory. The system consists of a stainless steel syringe with 11.3 mL-volume and a hole diameter of 2 mm and the syringe is vertically fixed on top of a table-like holder (Figure 3.1).

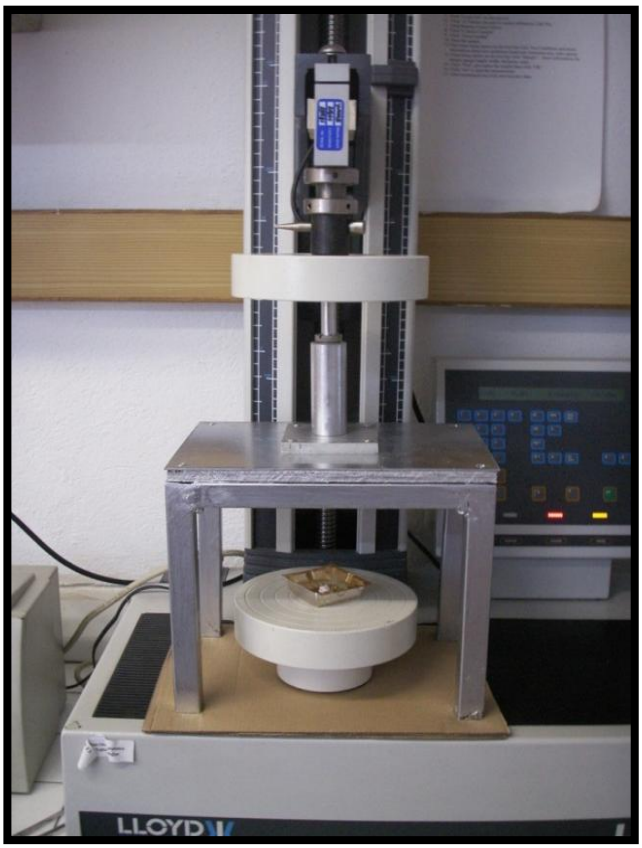

Figure 3.1 The injectability apparatus and the injectability test system.

Each cement paste (~3 g) was filled into the syringe by means of a metallic spatula. In order to perform the test, the syringe system was placed between the compression plates of the mechanical tester. The maximum load that can be applied manually on an injection device is in the range of 250 - 300 N [155, 156]. For this reason, 250 N was selected as the maximum load and this load was exerted on the syringe at a constant crosshead speed of 10 mm/min to extrude the cement paste. The extrusions were initiated 3 min after mixing of cement composition and continued until a maximum load of 250 N was reached.

The injectability was calculated according to Equation 1, where M1 is the initial weight of the paste inside the syringe and M2 is the weight of the cement paste extruded from the syringe.

$$\text{Injectability (\%)} = \frac{M2}{M1} \text{ x } 100 \quad (1)$$

Injectability tests were repeated four times for each specimen and the average values were calculated.

3.1.2.4.2 Contact Angle Measurements

Water contact angle measurements were carried out with the object of clarifying the possible interactions between CFs, α-TCP particles and water during the injection process.

A chitosan film was prepared by adaptation of the wet spinning procedure. One side of a lamella was covered with a 1 mL of chitosan dope solution, the system was immersed into the coagulation bath and incubated over a night at room temperature. The following washing and drying steps as described in the wet spinning procedure were applied to the chitosan films formed on lamellas.

For the purpose of evaluating the water interactions of the α-TCP cement phase during the injection process, a film consisting of α-TCP and cement liquid was prepared. The cement mixture was pressed in between two lamellas and dried for 1 h at 50°C in an open atmosphere furnace.

Contact angle measurements were performed by a goniometer (CAM 200, Finland) at room temperature. In order to determine the contact angle, at least five DI water

drops (5 μL) were placed on the chitosan and α-TCP cement films and the average values were calculated for each.

3.1.2.4.3 Mechanical Tests

Mechanical properties of wet α-TCP/CF composite samples were examined by a mechanical testing machine (Lloyd LRX 5K Mechanical Tester). The specimens (cylindrical, r = 6 mm, h = 12 mm) were removed from Ringer solution, demoulded and urgently submitted to compression tests. Each self-hardened and wet cylindrical sample was vertically placed into the mechanical tester. Load application was performed at a speed of 10 mm/min. The maximum load applied before the failure of the sample was recorded and put in the Equation 2 to calculate the compressive strength value.

$$\sigma_p = P/\Pi r^2 \qquad (2)$$

where σ_p is the compressive strength (MPa), P is the maximum load applied (N) before failure, Π is pi constant and r is the radius of the cylindrical sample (mm).

At least six samples were tested for each subgroup and the average values of compressive strengths were calculated.

3.1.2.4.4 Phase Conversion Analysis

The qualitative phase analysis of hydration products of the control group and composites of 3 wt% and 6 wt% fiber content were performed by XRD (Rigaku/Ultima-IV). CuKa radiation was used at 40 kV voltage and 40 mA current. The scanning range of the samples was 20–40° with a speed of 2°/min.

3.1.2.4.5 Morphological Investigations

The microstructure and morphology of all hydration products of 3 wt% and 6 wt% fiber containing α-TCP/CF composites were examined with a FEI QUANTA 400F SEM. The samples were coated with Au–Pd thin films by a Hummle VII sputter prior to SEM investigations.

3.2 Results and Discussions

3.2.1 Injectability Test Results

The filter-pressing (phase separation of liquid and solid phase) is one of the major limiting factor on the injectability of the CPCs. Incorporation of cohesion promoters such as sodium alginate into the cement liquid is a well accepted common technique to decrease the filter pressing effect which is also used in the present study [91, 92, 157]. In a few words, the presence of alginate increases the water retention capacity of the system and the adsorption of alginate on to the CaP particles reduces the friction between solid granules while decreasing the flow shear stress [111].

A number of methods have been introduced to improve the poor injectability of the CaP phases such as changing the liquid/powder ratio, decreasing the particle size and modification of liquid phase viscosity by using various additives. Nevertheless, to date no approaches have focused on the effect of polymeric fiber addition on the cement injectability.

The influence of CF content on the injectability of α-TCP cement is illustrated in Figure 3.2. The graph shows a clear trend of increase in the amount of cement extrusion with the increase in fiber content. The injectability of the cement without

fiber (82%) was remarkably lower than the composite systems containing 1.5 wt%, 3 wt% and 6 wt% CF, which were exhibited an injectability of 88%, 90% and 93%, respectively.

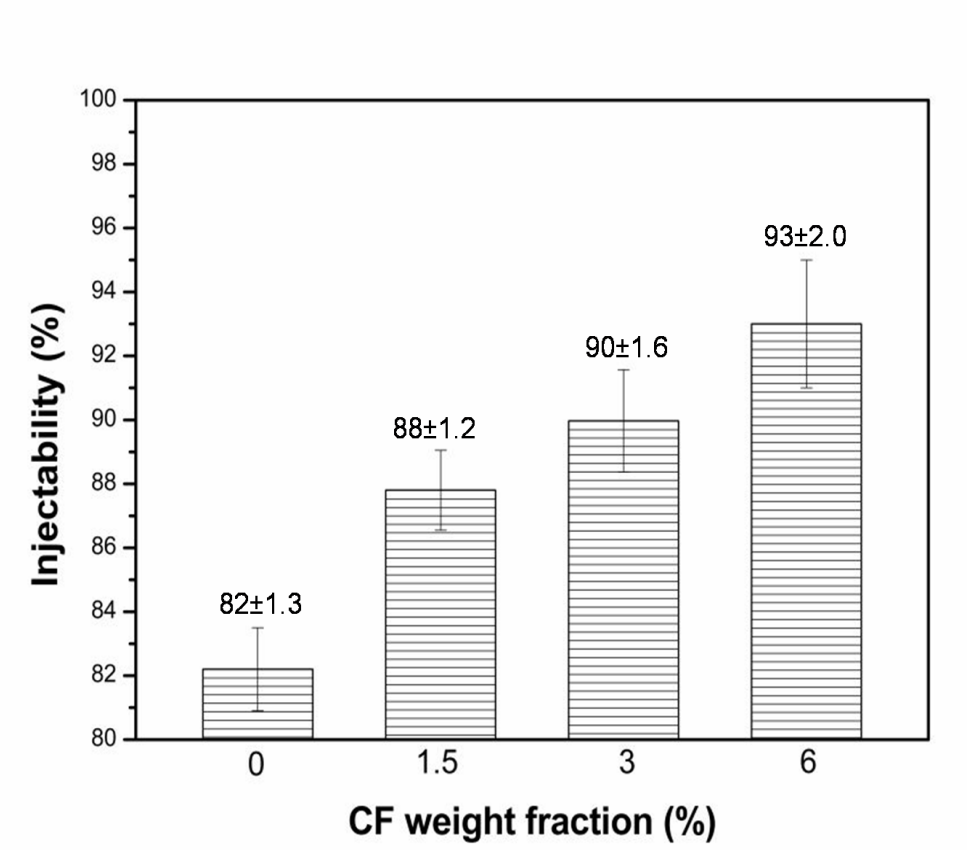

Figure 3.2 The influence of CF content on the injectability of α-TCP cement.

This significant positive correlation between cement injectability and CF amount could be attributed to the chemical nature of the fiber-cement interfaces. In order to understand the possible interactions between cement particles and fiber surfaces during the injection process, water contact angle measurements were performed. The apparent difference between the contact angle value of CF surface (64°) and the CaP system (13°) indicates the distinction in water interaction tendency of each component. Water molecules are strongly attracted and adsorbed onto hydrophilic

alginate-CaP particle system whereas the attraction between water and CFs were not as stronger as CaP. In the overall perspective, when the total system is moving towards the direction of the applied load, CFs act as slippage layers for water-adsorbed calcium phosphate particles during the injection process. This is the basic phenomena behind the injectability promoter capacity of CFs.

Despite the known advantages of chitosan on bone tissue healing, the usage of polymer in the injectable CaP based systems is restricted. In the previous studies, chitosan was directly added into the cement liquid and the destructive effect on injectability was reported in consequence of chitosan adsorption on crystal surface and agglomeration of cement particles [73]. At this point, the superiority of the CFs for the improvement of the injectability of CPC comes into play since; there is a minimized charge attraction between CaP particles and chitosan in fibrillar form. During the fiber formation, interaction between individual chitosan macromolecules leads to a reduction in the number of free charged groups on chitosan. Therefore, the total number of charged groups on CF surface is much lower than the dissolved form of chitosan as mentioned in literature [73].

3.2.2 Compressive Properties

Figure 3.3 is related to the average compressive strength of four specimens with different fiber weight fractions of 0, 1.5, 3 and 6%. Compressive strength of the control group (9.54 MPa) was slightly changed to the values of 9.65 MPa and 9.77 MPa with the 1.5 and 3 wt% fiber addition, respectively. These negligible differences reveal that incorporation of CFs up to a certain amount (3 wt%) has almost no influence on compressive strength of the composite structures. The incorporation of 6 wt% fiber caused a significant decrease on mechanical properties; the strength of this group of samples was found as 6.95 MPa. (Representative load-deformation and stress-strain curves of composites are given in Appendix B)

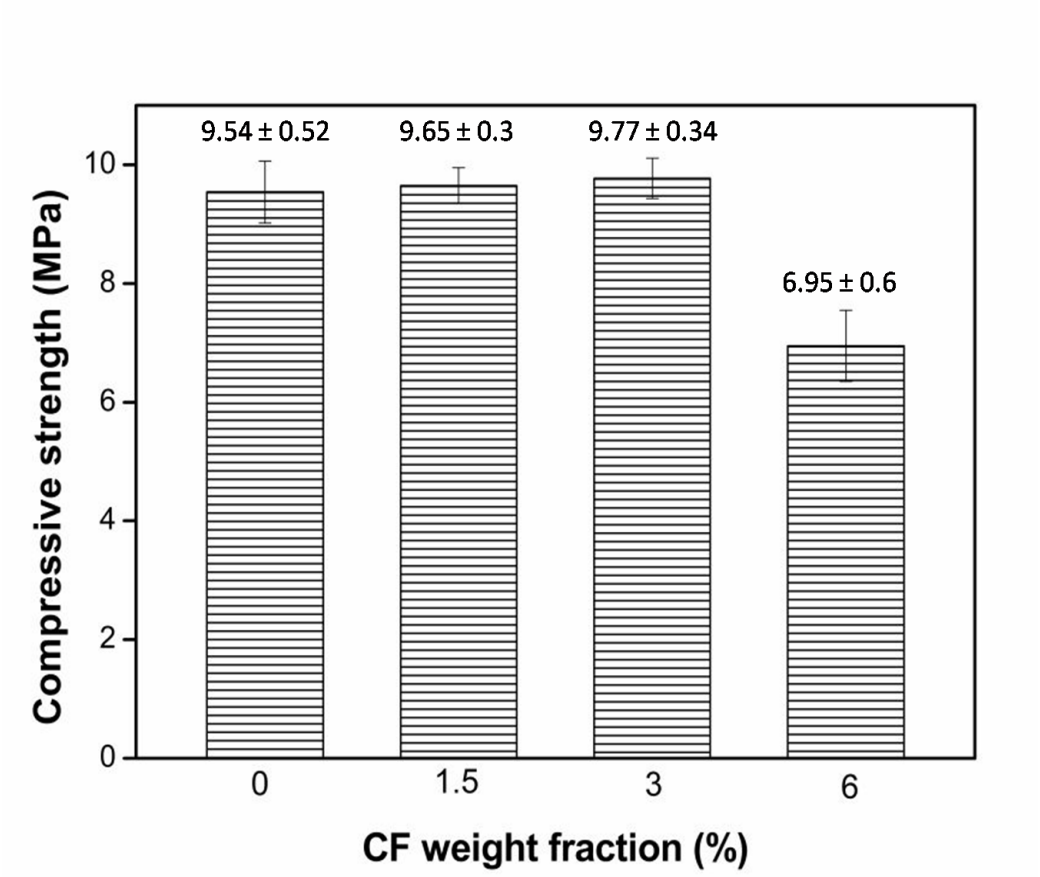

Figure 3.3 Influence of CF content on the compressive strength of the cylindrical composites.

Generally, the presence of fibers reduces the stress concentration and helps to suppress crack propagation in composites. The existence of fibers introduces interfacial layers to the cement matrix which can absorb some energy from crack tips and relieve stress zones to prevent crack growth. Besides, the elastic wet fibers have a potential to deflect the direction of applied load which also cause to relieve the systemic stress. In this regard, the higher CF content could be expected to show higher efficiency to prevent crack propagation and improve the strength of the system. However, another important factor should also be considered; fiber/cement interfaces have a very low bonding strength and tend to nucleation of voids during

the composite formation. The number of voids which is effective on reducing the strength of the composite reverses the reinforcement effect of fibers. Consequentially, on account of these contrary influences, addition of CFs up to a certain limit did not cause a change in mechanical properties of the CPC systems in the present study. A similar result was reported by a previous work showed that the incorporation of non-modified CFs had no influence on compressive characteristics of a CPC system [117]. On the other hand, a further increase in CF content (up to 6 wt%) caused a negative effect on compressive strength. At a fiber amount of 6 wt%, the well distribution of fibers are disrupted and small fibrillar flogs are started to form which constitute weak regions in the system and causing a decrease in mechanical properties of the composite.

It is also worth to mention that, fibers provide noteworthy crack bridging property which is also important on reinforcement mechanism and failure behavior of the cement systems. In this study, macro images of failed cement specimens just after the compressive tests indicated the remarkable difference in physical appearance of fiber involving and fiber-free composites (Figure 3.4). Despite of the excessive vertical crack formation and failure, the pieces of 3 wt% (Figure 3.4b) and 6 wt% (Figure 3.4c) fiber containing composites was still intact, whereas the specimens without CF are broken into pieces (Figure 3.4a) upon application of 250 N load. This extensive crack bridging potential of fibers allows composites to undergo numerous microcracks instead of one large detrimental crack and prevents the catastrophic failure of the cement structure.

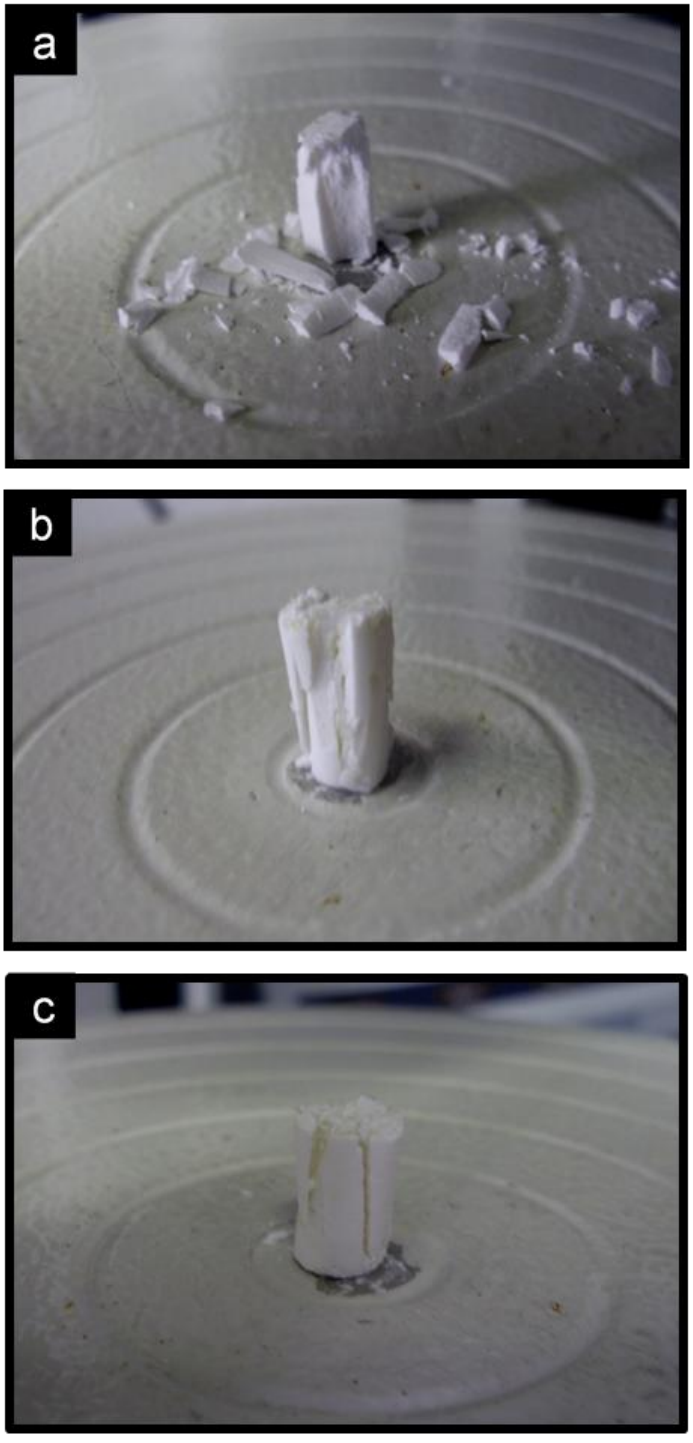

Figure 3.4 Macro images of failed CPC samples after the compression test. **(a)** Fiber-free, **(b)** 3 wt% and **(c)** 6 wt% CF containing CPCs.

3.2.3 Phase Analysis Results

XRD diffractograms of 24 h hydrated CPC composites with different CF contents are given in Figure 3.5. The XRD spectra of all samples displayed the characteristic peaks of HAp (JCPDS card no. 9-432) which is an indicator of a full phase transformation by means of completed setting reaction. These results reveal that CFs do not have a destructive influence on the setting characteristics of the CaP system and the full hydration was achieved regardless of the fiber weight fractions. Although dissolved chitosan is known to hamper α-TCP hydration efficiency, fiber form of the polymer demonstrated to have no negative effect on cement setting due to the decreased surface charge and suppressed ionic interaction with α-TCP particles.

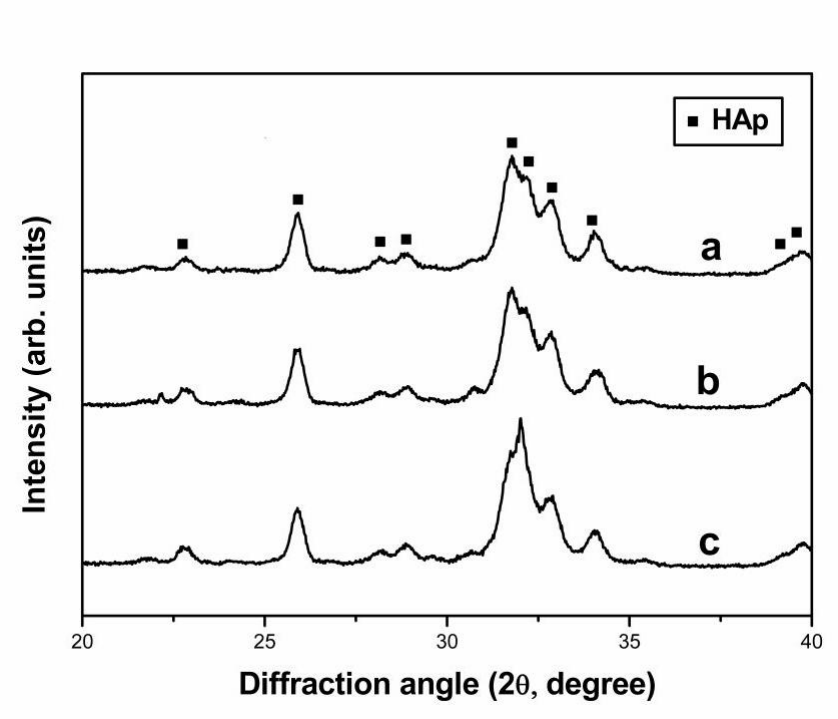

Figure 3.5 XRD diffractograms of 24 h hydration products of CPC composite specimens. **(a)** 0 wt%, **(b)** 3 wt% and **(c)** 6 wt% CF containing CPCs.

3.2.4 Morphological Analyses Results

SEM images of CPC composites with the fiber weight fractions of 3 wt% and 6 wt% are shown in Figures 3.6a and 3.6b, respectively. As apparently seen from the figure, CFs created channel-like pores with a diameter about 150 μm which is higher than the minimum necessary pore size (100 μm) to achieve bone tissue in growth [158]. Therefore, it is easy to suggest that after the degradation of CFs, the incorporation of bone tissue into CPC implants potentially occur. The major disadvantage of using short fibers is the lack of interconnectivity between the pores but still, the presence of these pores introduces extra domains for newly generated bone tissue to move along and accelerate the degradation process of CPC in comparison with fiber-free cements.

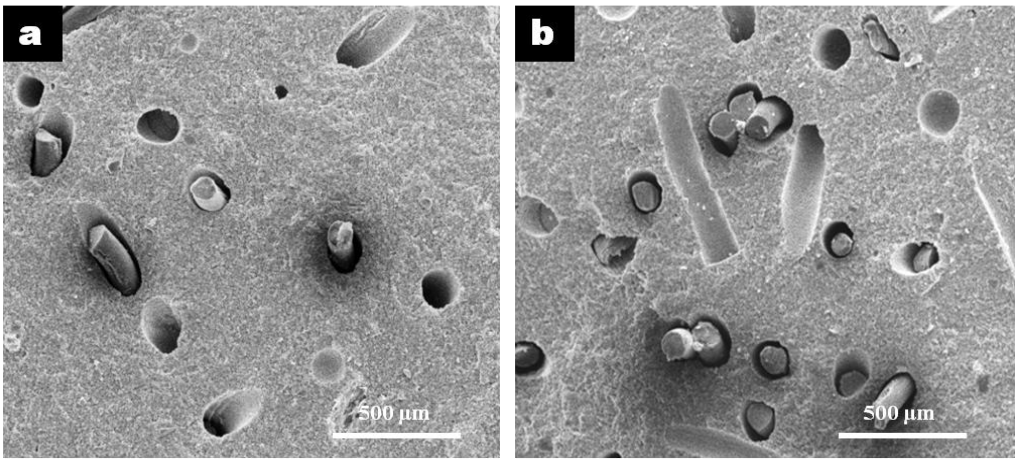

Figure 3.6 SEM micrographs of CF/CaP composite cement specimens. **(a)** 3 wt% and **(b)** 6 wt% fiber containing composites.

The micrographs (Figure 3.6) indicated that the composites with the fiber weight fraction of 3 wt% (a) exhibited relatively more homogenous structure than 6 wt% fiber containing composites (b). The spots of fiber agglomerates can be clearly seen in CPC specimens of 6wt% fibers which were previously reported as the main reason of the decrease in mechanical properties of the system. The isotropy of the composite systems is established by the observed random orientation of CFs (Figure 3.6). This nondirectional behavior of short fibers result in a uniform mechanical performance of the composites in all directions which is an important phenomena for bone implant materials.

As a summary, in this part of the study, an injectable α-TCP/CF composite bone cement system which has a potential to enhance bone regeneration and replacement was developed. α-TCP/CF composites were prepared by using different amounts of CFs and the effect of CF addition on cement properties was investigated. CFs promoted the injectability of the system by introducing interface layers for CaP particles to slip. Existence of CFs was shown not to be effective on compressive strength up to a certain limit (3 wt%) whereas at a fiber amount of 6 wt%, a significant decrease was observed in mechanical properties. In addition, presence of CFs enhanced the failure behavior of cement samples by providing a noteworthy crack bridging property and preventing the catastrophic failure. Presence of CFs in the cement composition demonstrated to have no influence on hydration reactivity of α-TCP.

CHAPTER 4

ZINC CONTAINING CHITOSAN FIBER SCAFFOLDS FOR HARD TISSUE APPLICATIONS

Zinc is an essential mineral having several critical functions on osteogenesis and increased amounts of zinc are found at the sites of bone repair. Adequate levels of zinc are needed on the elevation of calcium and collagen levels, osteoblastic cell function and new bone tissue formation where as zinc deficiency results in bone loss that is closely related to osteoporosis and impair bone healing. However, the inductive effect of zinc on osteogenesis was shown to be concentration dependent; above a certain level, presence of zinc lead to side effects on bone metabolism. On this basis, it is required to have site specific administration and controlled release of zinc for bone treatment to observe a positive effect on bone mineralization and to avoid toxic effects in surrounding tissues. Despite of being a biocompatible, biodegradable and conventional biopolymer, non-usage of chitosan in essential trace metal delivery for tissue healing purposes is a gap in the field of biomaterial research. It is reported that wet-spun CFs have been efficiently used in metal chelating and these fibers were able to chelate up to 6.2% zinc of their own weight [122]. It is quite apparent that the metal chelating property of CFs could potentially be used on development of controlled zinc release systems and can be applied in local zinc deficiency therapies of bone tissue to avoid systemic side effects. For this purpose, wet spun CF scaffolds were prepared and appropriate amount of zinc was loaded on these scaffolds in regard to the zinc content of healthy human bone tissue. Zinc release studies were performed on CaP covered (CF+CaP) and uncovered (CF) scaffolds and zinc ion concentrations of the release solutions were determined by ICP-MS analysis.

4.1 Experimental

4.1.1 Materials

Low-viscous chitosan (>78% deacetylation degree, Fluka, catalog no. 50494, Switzerland), glacial acetic acid (99-100% J.T. Baker, Netherlands), sodium sulphate (Na_2SO_4, Merck, catalog no.106643, Germany), sodium hydroxide (NaOH, J.T. Baker, catalog no. 0402, Netherlands) and methanol (CH_3OH, Sigma-Aldrich, catalog no. 24229, Germany) were used to prepare chitosan fibers. Zinc absorption was performed by using zinc sulphate ($ZnSO_4 \cdot 7H_2O$, Fischer, catalog no. 287558, USA) compound. 10 mM, pH 7.4 phosphate buffered saline (PBS) solution which was prepared by dissolving 0.05 mole K_2HPO_4, 0.045 mole KH_2PO_4 in deionized water was used in zinc release studies.

4.1.2 Methods

4.1.2.1 Absorption of Zinc into Chitosan Scaffolds

Chitosan fibers in the form of fibrous scaffolds were prepared according to the method described in Chapter 3. Wet-spun fibers were placed in cylindrical teflon molds (r = 1 cm, h = 1 cm) and dried at 50°C after the methanol treatment. Zinc absorption was carried out by using an aqueous stock solution of zinc sulphate in a concentration of 656 mg/L for all samples (confirmed by ICP-MS). Under vacuum pressure cycle, 35 μL stock solution was imposed on each 45 mg scaffold which are placed in tissue culture well plates. The dose of zinc to be loaded for a certain weight of chitosan scaffold was defined in regard to the information of zinc content of human bone tissue (0.0126-0.0217 wt%) [159].

4.1.2.2 Preparation of CaP-Covered Scaffolds

CaP coating was performed on previously zinc loaded chitosan scaffolds which are placed in a tissue culture well plate. For this purpose, ~ 30 μL α-TCP cement paste (water to particle ratio:2 (w/w)) was added dropwise on each scaffold under vacuum pressure cycle and the total system was incubated in 37°C for 24 h.

4.1.2.3 Zinc Release Studies

Zinc release studies were carried out on α-TCP covered (CF+CaP) and non-covered (CF) chitosan scaffolds, separately. To perform the zinc release experiments, scaffolds were immersed in 2 mL PBS (10 mM, pH 7.4) and conditioned at 37°C. After certain incubation times (24 h and 1, 2, 3, 4 weeks) scaffolds were taken out from the buffer solution and immersed into fresh PBS solution (2 mL). Taken buffer solutions were tested for zinc ion concentration by ICP-MS analysis.

4.1.2.4 Microstructural Investigations

The microstructure and morphology of CaP covered and uncovered CF scaffolds were examined with a FEI QUANTA 400F SEM. The samples were coated with Au–Pd thin films by a Hummle VII sputter prior to SEM investigations.

4.2 Results and Discussion

4.2.1 Zinc Release Results

The time dependent zinc release profiles of CaP covered and uncovered chitosan scaffolds are given in Table 4.1 and Figure 4.1. First of all, it is worth to note that no zinc release could be detected at the end of 24 h incubation period representing non-existence of weakly bonded zinc ions on the surface of chitosan fibers. This data also indicate the successful chelation of introduced zinc ions into the chitosan structure.

Table 4. 1 The time dependent zinc release profiles of CaP covered (CF+CaP) and uncovered (CF) chitosan scaffolds.

Release Period	**Amount of Zinc in Release Medium**			
	CF		**CF + CaP**	
	(mg/L)	**(%)**	**(mg/L)**	**(%)**
24 h	<<0.003	-	<<0.003	-
1 week	0.097 ± 0.0048	0.87 ± 0.04	0.055 ± 0.0027	0.49 ± 0.02
2 weeks	0.226 ± 0.0113	2.02 ± 0.10	0.131 ± 0.0065	1.17 ± 0.06
3 weeks	0.286 ± 0.0143	2.56 ± 0.13	0.163 ± 0.0081	1.46 ± 0.07
4 weeks	0.399 ± 0.0169	3.57 ± 0.18	0.219 ± 0.0109	1.96 ± 0.10

For chitosan scaffolds, after 4 weeks of incubation period, the total amount of released-zinc was determined as ~0.4 mg/L (Table 4.1) which is only 3.6 wt% of the loaded dose (11.15 mg/L). (Cumulative zinc release percentages of chitosan

scaffolds are given in Appendix D) It is possible to hypothesize that this circumstance is less likely to occur in vivo conditions since, all release studies were carried out in an enzyme-free buffer release medium and the release of zinc was independent from the degradation of chitosan. This striking data revealed the requirement of chitosan degradation to fulfill the zinc release, which is an ideal strategy to manage the biocontrolled release of zinc. The result also denotes the correlation between zinc release from chitosan scaffold and the bioactivity of the host tissue which possibly occur in balance with the tissue healing process in the presently designed system. However, further investigations are needed to understand the association of these factors in vitro and vivo environment.

As shown in Figure 4.1, at the end of the 4 weeks, zinc release from CaP covered specimens (~0.22 mg/L) was significantly lower than uncovered ones (~0.40 mg/L). The observed difference could be attributed to the extra barrier formed by CaP particles present on fiber surfaces. Because of charge attraction between zinc ions and CaP particles, existence of CaP particles hampered the release of zinc ions and prolonged the zinc release period.

Because of the weak surface attraction between CaP crystals and CFs, CaP particles were inclined to detach from the surface of chitosan fibers in the PBS solution. Consequently, a remarkable amount of CaP particles slided down from the CF surfaces and precipitated in the release medium after each time period of incubation. At this point, a weakness of the study about incompetent CaP covering onto the chitosan fibers become apparent and more specific techniques should be developed to activate the surface of chitosan fibers and achieve a more stable CF-CaP interfaces.

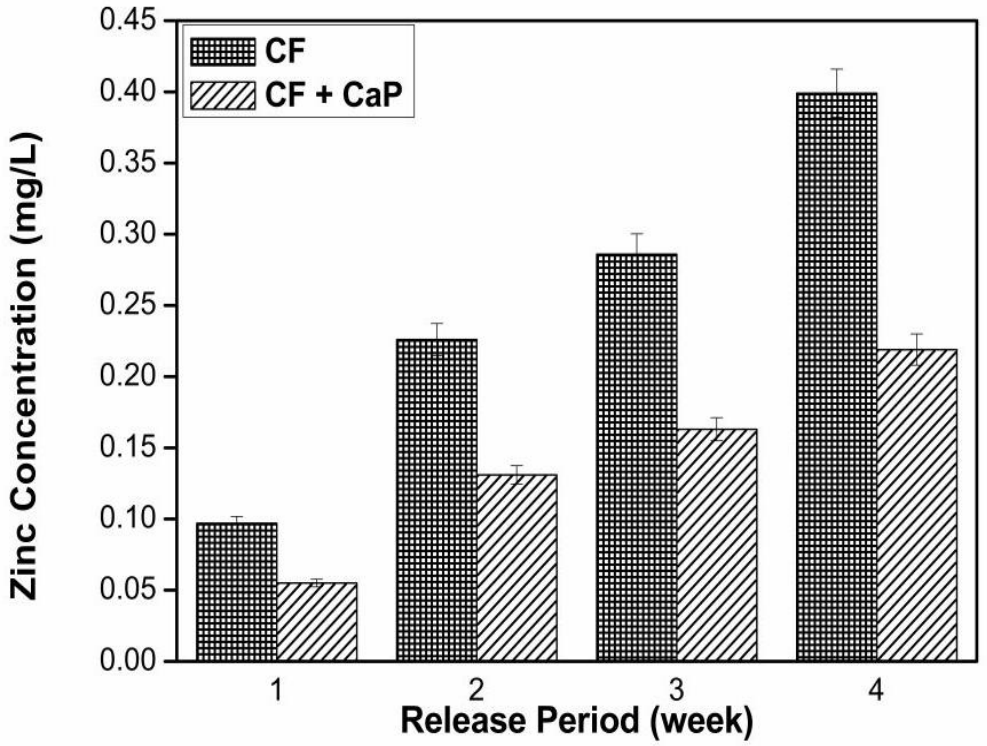

Figure 4.1 The time dependent zinc release profiles of CaP covered (CF+CaP) and uncovered (CF) chitosan scaffolds.

4.2.2 Microstructural Investigation Results

SEM micrographs showing the morphologies of the CaP covered and uncovered chitosan scaffolds are given in Figure 4.2a and Figure 4.2b, respectively. As apparently seen from the Figure 4.2a, small CaP particles covers CFs and forms a rough characteristic to fiber surfaces. Surface topography is known to be important on bone-biomaterial interaction and roughness is a favorable property which induces bioactivity of osteoblasts, improves mineralization and bone anchorage [160, 161]. Therefore, the presence of CaP particles on CF surfaces is expected to enhance bone

tissue-CF scaffold interaction and osteointegration of the implant system. However, this assumption should be confirmed by further in vitro and in vivo studies.

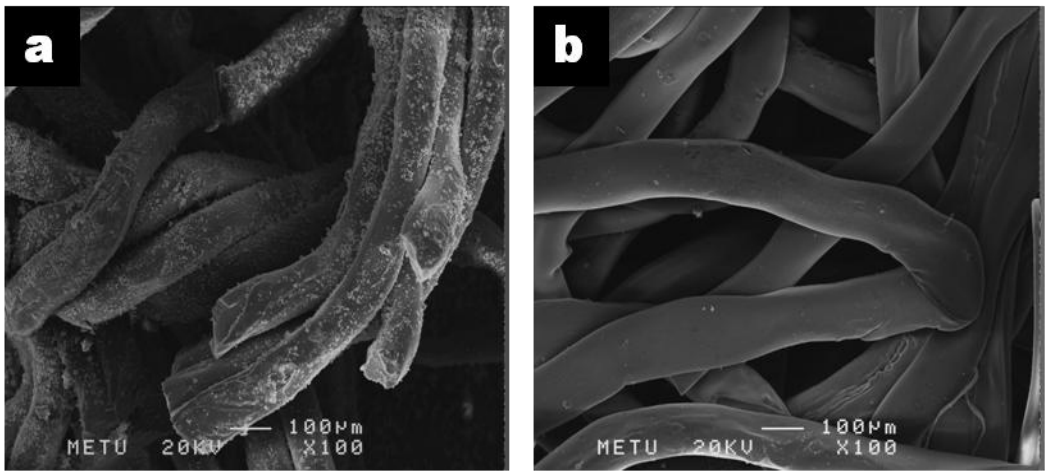

Figure 4.2 SEM micrographs of zinc containing CF scaffolds. **(a)** CaP covered (CF+CaP) and **(b)** CaP uncovered (CF).

Porosity is an important requirement for an ideal osteoconductive bone substitute and CF scaffolds display a porous nature as clearly seen from the Figure 4.2b. Owing to the macro porous structure of the scaffolds (Figure 4.2b), CF network could enable cell penetration and tissue ingrowth towards the pores of the implant and act as a constructive support material for new bone tissue.

Zinc is an essential mineral having several critical functions on osteogenesis and zinc deficiency results in bone loss that is closely related to osteoporosis and impair bone healing. However, the inductive effect of zinc on osteogenesis was shown to be concentration dependent; above a certain level, presence of zinc lead to side effects on bone metabolism. In this study, a novel zinc chelated CF scaffold system was developed in order to manage the controlled release of zinc for hard tissue applications. The presently developed CF based bone supporting system is a good candidate for local zinc supply in zinc deficiency therapies while avoiding toxic effects in surrounding tissues. Despite of being a conventional and extensively studied biopolymer, chitosan was not used for essential trace metal ion delivery for tissue healing purposes up to now. It is quite apparent that presently developed system can also be used in delivery of other essential trace metal ions in various applications. However, further investigations are needed to understand the physiological effect of metal release from CF scaffolds in vitro and vivo environment.

CHAPTER 5

CONCLUSIONS

The overall conclusions of the thesis can be given as follows;

In chapter 1, general information related to the structure of natural bone, bioceramics as bone graft materials, the concept of α-TCP bone cement, chitosan as a biomaterial, chelating capacity of chitosan and physiological effect of zinc are given.

In chapter 2, the hydraulic reactivity of α-TCP was found to be controlled by combination of several interrelated synthesis parameters, but predominantly by the chemical composition of the primary calcium precursor. The experimental approach in making reactive α-TCP by solid state reaction relies on a simple systematic optimization in regard to choosing proper firing temperature and time. The present study highlights some general findings in regard to determination of these parameters for the $CaCO_3$–$CaHPO_4$ solid reactant system. It has been found that both the firing temperature higher than 1200°C and prolonged firing reduce the hydraulic reactivity. These two factors are most likely valid for any solid reactants co-fired for obtaining α-TCP. However, system specific assessments on hydraulic reactivity of α-TCP require precise information about the chemical identity of the precursors. Some impurities conveyed from the calcium precursor completely annihilate the setting of α-TCP. The results obtained in this study indicated that magnesium impurity content, leading to a significant and adverse effect on the hydration of α-TCP, is one of the primary concerns for the selection of proper calcium precursor. This part of the study was published with the title of ‘Alpha-tricalcium phosphate (α-TCP): solid state synthesis from different calcium precursors and the hydraulic reactivity’ [162].

In chapter 3, an injectable α-TCP/CF composite bone cement system which has a potential to enhance bone regeneration and replacement was developed. A clear trend of increase in the cement injectability with the increase in fiber content was observed. This significant positive correlation between cement injectability and CF amount is attributed to the chemical nature of the fiber-cement interfaces. CFs act as slippage layers for water-adsorbed calcium phosphate particles during the injection process and take role as an injectability promoter agent in the total system. Existence of CFs was shown not to be effective on compressive strength up to a certain limit (3 wt%) whereas at a fiber amount of 6 wt%, small fibrillar flogs are started to form which constitute weak regions in the system and causing a decrease in mechanical properties. In addition, short CFs provide noteworthy crack bridging property which is also important on reinforcement mechanism and failure behavior of the cement systems. Presence of CFs in the cement composition demonstrated to have no influence on hydration reactivity of α-TCP. SEM micrographs revealed the extremely nonuniform nature of 6 wt% fiber containing composite which is responsible for the decrease in mechanical properties.

In chapter 4, a zinc chelated CF scaffold system was developed in order to manage the controlled release of zinc for hard tissue applications. As a result of release studies, no zinc release could be detected at the end of 24 h incubation period representing non-existence of weakly bonded zinc ions on the surface of CFs. This data also indicate the successful chelation of introduced zinc ions into the chitosan structure. After 4 weeks of incubation in enzyme-free phosphate buffer environment, only ~3.6 wt% of the loaded dose was released. This striking data revealed the requirement of chitosan degradation to fulfill the zinc release, which is an ideal strategy to manage the local application and biocontrolled release of zinc. At the end of the 4 weeks, zinc release from CaP covered specimens was significantly lower than uncovered ones. However, further investigations are needed to understand the association of these factors and the effect of zinc release in vitro and vivo environment.

As an overall summary, in the first part of the studies, the proper α-TCP synthesis parameters (firing temperature and time) and calcium precursors to obtain highly reactive α-TCP end product was defined. It is concluded that, the phase pure α-TCP powder synthesized from *CC-M* by firing at 1200°C for 2 h exhibited the highest reactivity among most of other α-TCP products and was completely set to HAp after hydration process. Therefore, this synthesis route was chosen and applied for production of α-TCP stock for further studies (for production of α-TCP based bone supporting composites and for covering the zinc containing scaffolds). In the second part, an injectable α-TCP and CF composite bone cement system which is designed to degrade gradually in time to be replaced by the natural bone tissue was prepared and the effect of CF addition on cement properties were examined and compared. Addition of 3 wt% CFs increased injectability of the system and did not cause a negative effect on compressive strength of the composite structures. In the third part, a biodegradable bone supporting material was attempted to develop by using zinc chelated chitosan scaffolds which potentially achieve site specific administration and controlled release of zinc. However, more specific techniques should be developed to observe the effect of chitosan degradation on zinc release and to achieve more stable CF-CaP interfaces. In addition, further investigations should be carried out in order to understand the effect of zinc release in *in vitro* and *in vivo* environment.

REFERENCES

[1] Fung YC. Mechanical Properties of Living Tissues. Biomechanics. New York: Springer-Verlag Inc; 1993. p. 500.

[2] Weiner S, Wagner HD. The material bone: Structure-mechanical function relations. Annu Rev Mater Sci. 1998;28:271–279.

[3] Olszta JM, Cheng X, Jee SS, Kumar R, Kim YY, Kaufman MJ, Elliot PD, Gower BG. Bone structure and formation: a new perspective. Mater Sci En. 2007;77–116.

[4] Hellmich C, Ulm FJ. Are mineralized tissues open crystal foams reinforced by crosslinked collagen?—some energy arguments. J Biomech. 2002;35:1199-1212.

[5] Landis WJ, Hodgens KJ, Arena J, Song MJ, McEven BF. Structural relations between collagen and mineral in bone as determined by high voltage electron microscopic tomography. Microsc Res Tech. 1996;33:192-202.

[6] Glimcher MJ, Muir H. Recent studies of the mineral phase in bone and its possible linkage to the organic matrix by protein-bound phosphate bonds [and discussion]. Phil Trans R Soc Lond B. 1984;304:479-508.

[7] Elliott JC. Space group and lattice constants of $Ca_{10}(PO_4)_6CO_3$. J Appl Cryst. 1980;13:618-621.

[8] Rey C, Shimizu M, Collins B, Glimcher MJ. Resolution-enhanced fourier transform infrared spectroscopy study of the environment of phosphate ion in the early deposits of a solid phase of calcium phosphate in bone and enamel and their evolution with age: 2. Investigations in the v3 PO_4 domain. Calcif Tissue Int. 1991;49:383-388.

[9] Rho JY, Spearing LK, Zioupo P. Mechanical properties and the hierarchical structure of bone. Med Eng Phys. 1998;20:92–102.

[10] Nyman JS, Royc A, Shenb X, Acunaa RL, Tylera JH, Wanga X. The influence of water removal on the strength and toughness of cortical bone. J Biomech. 2006;39:931-938.

[11] Wilson EE, Awonusi A, Morris MD, Kohn DH, Tecklenburg MMJ, Beck LW. Three structural roles for water in bone observed by solid-state NMR. Biophys J. 2006;90:3722-3731.

[12] Marks SC, Popoff SN. Bone cell biology: The regulation of development, structure, and function in the skeleton. Am J Anat. 1988;183:1-44.

[13] Kwun IS, Cho YE, Lomeda RAR, Shin HI, Choi JY, Kang YH, Beattie JH. Zinc deficiency suppresses matrix mineralization and retards osteogenesis transiently with catch-up possibly through Runx 2 modulation. Bone. 2010;46:732-741.

[14] Vallet Regí M. Ceramics for medical applications. J Chem Soc, Dalton Trans. 2001:97-108.

[15] Vallet Regí M. Revisiting ceramics for medical application. Dalton Trans. 2006;44:5211-5220.

[16] Hench LL. Bioceramics. J Am Ceram Soc. 1998;81:1705–1728.

[17] Wolff KD, Swaid S, Nolte D, Böckmann RA, Hölzle F, Müller Mai C. Degradable injectable bone cement in maxillofacial surgery: Indications and clinical experience in 27 patients. J Craniomaxillofac Surg. 2004;32:71-79.

[18] Maestretti G, Cremer C, Otten P, Jakob RP. Prospective study of standalone balloon kyphoplasty with calcium phosphate cement augmentation in traumatic fractures. Eur Spine J. 2007;16:601-610.

[19] Constanz BR, Ison IC, Fulmer MT, Poser RD, Smith ST, VanWagoner M, Ross J, Goldstein SA, Jupiter JB, Rosenthal DI. Skeletal repair by in situ formation of the mineral phase of bone. Science. 1995;267:1706-1799.

[20] Heini PF, Berlemann UJ. Bone substitutes in vertebroplasty. Eur Spine J. 2001;10:205-213.

[21] Jimbo R, Coelho PG, Vandeweghe S, Schwartz Filho HO, Hayashi M, Ono D, Andersson M, Wennerberg A. Histological and three-dimensional evaluation of osseointegration to nanostructured calcium phosphate-coated implants. Acta Biomater. 2011;7:4229-4234.

[22] Wennerberg A, Albrektsson T. Structural influence from calcium phosphate coatings and its possible effect on enhanced bone integration. Acta Odontol Scand. 2009;67:333-340.

[23] Ohtsuki C, Kamitakahara M, Miyazaki T. Bioactive ceramic-based materials with designed reactivity for bone tissue regeneration. J R Soc Interface. 2009;6:349-360.

[24] Hing KA, Wilson LF, Buckland T. Comparative performance of three ceramic bone graft substitutes. Spine J. 2007;7:475-490.

[25] Subbaiah R, Thomas B. Efficacy of a bioactive alloplast, in the treatment of human periodontal osseous defects-a clinical study. Med Oral Patol Oral Cir Bucal. 2011;2:239-244.

[26] von Doernberg MC, von Rechenberg B, Bohner M, Grünenfelder S, van Lenthe GH, Müller R, Gasser B, Auer J. In vivo behavior of calcium phosphate scaffolds with four different pore sizes. Biomaterials. 2006;27:5186-5198.

[27] Karageorgiou V, Kaplan D. Porosity of 3D biomaterial scaffolds and osteogenesis. Biomaterials. 2005;26:5474-5491.

[28] Liu DM. Influence of porosity and pore size on the compressive strength of porous hydroxyapatite ceramic. Ceram Int. 1997;23:135-139.

[29] Dudek A. Microstructure and properties of the composites: hydroxyapatite with addition of zirconia phase. J Eng Mater Tech. 2011;133:1-5.

[30] Choi JW, Kong YM, Kim HE, Lee IS. Reinforcement of hydroxyapatite bioceramic by addition of Ni_3Al and Al_2O_3. J Am Ceram Soc. 1998;81:1743-1748.

[31] Fernandez E, Vlad MD, Hamcerencu M, Darie A, Torres R, Lopez J. Effect of iron on the setting properties of α-TCP bone cements. J Mater Sci. 2005;40:3677-3682.

[32] Bandyopadhyay A, Bernard S, Xue W, Böse S. Calcium phosphate-based resorbable ceramics: Influence of MgO, ZnO, and SiO_2 dopants. J Am Ceram Soc. 2006;89:2675-2688.

[33] Dos Santos LA, De Oliveira LC, Rigo ECS, Carrodeguas RG, Boschi AO, De Arruda ACF. Influence of polymeric additives on the mechanical properties of α-tricalcium phosphate cement. Bone. 1999;25:99-102.

[34] Xu HHK, Quinn JB. Calcium phosphate cement containing resorbable fibers for short-term reinforcement and macroporosity. Biomaterials. 2002;23:193-202.

[35] Xu HHK, Simon Jr. CG. Fast setting calcium phosphate-chitosan scaffold: Mechanical properties and biocompatibility. Biomaterials. 2005;26:1337-1348.

[36] Dorozhkin SV, Epple M. Biological and medical significance of calcium phosphates. Angew Chem Int Ed. 2002;41:3130-3146.

[37] Yuan H, Li Y, De Bruijn J, De Groot K, Zhang X. Tissue responses of calcium phosphate cement: A study in dogs. Biomaterials. 2000;21:1283-1290.

[38] Ooms EM, Wolke JGC, van der Waerden JP, Jansen JA. Trabecular bone response to injectable calcium phosphate (Ca-P) cement. J Biomed Mater Res. 2002;61:9-18.

[39] Yuasa T, Miyamoto Y, Ishikawa K, Takechi M, Momota Y, Tatehara S, Nagayama M. Effects of apatite cements on proliferation and differentiation of human osteoblasts in vitro. Biomaterials. 2004;25:1159-1166.

[40] Koutsoukos P, Amjad Z, Tomson MB, Nancollas GH. Crystallization of calcium phosphates. A constant composition study. J Am Chem Soc. 1980;102:1553-1557.

[41] Ray RD, Ward Jr. AA. A preliminary report on studies of basic calcium phosphate in bone replacement. Surg Forum. 1951:429-434.

[42] Costantino PD, Friedman CD. Synthetic bone graft substitutes. Otolaryngol Clin N Am. 1994;27:1037-1074.

[43] Tripathi G, Basu B. A porous hydroxyapatite scaffold for bone tissue engineering: Physico-mechanical and biological evaluations. Ceram Int. 2012;38:341-349.

[44] Chang BS, Lee KK, Hong KS, Youn HJ, Ryu HS, Chung SS, Park KW. Osteoconduction at porous hydroxyapatite with various pore configurations. Biomaterials. 2000;21:1291-1298.

[45] Tamai N, Myoui A, Tomita T, Nakase T, Tanaka J, Ochi T, Yoshikawa H. Novel hydroxyapatite ceramics with an interconnective porous structure exhibit superior osteoconduction in vivo. J Biomed Mater Res. 2001;59:110-117.

[46] Pramanik S, Agarwal AK, Rai KN, Garg A. Development of high strength hydroxyapatite by solid-state-sintering process. Ceram Int. 2007;33:419-426.

[47] Mobasherpour I, Heshajin MS, Kazemzadeh A, Zakeri M. Synthesis of nanocrystalline hydroxyapatite by using precipitation method. J Alloy Compd. 2007;430:330-333.

[48] Yoshimura M, Suda H, Okamoto K, Ioku K. Hydrothermal synthesis of biocompatible whiskers. J Mater Sci. 1994;29:3399-3402.

[49] Durucan C, Brown PW. Reactivity of α-tricalcium phosphate. J Mater Sci. 2002;37:963-969.

[50] Brown WE, Chow LC. A new calcium phosphate setting cement. J Dent Res. 1983;62:672.

[51] Ginebra MP, Traykova T, Planell JA. Calcium phosphate cements as bone drug delivery systems: A review. J Control Release. 2006;113:102-110.

[52] Wang X, Ye J, Wang Y, Wu X, Bai B. Control of crystallinity of hydrated products in a calcium phosphate bone cement. J Biomed Mater Res A. 2007;81:781-790.

[53] Murayama JK, Nakai S, Kato M, Kumazawa M. A dense polymorph of $Ca_3(PO_4)_2$: A high pressure phase of apatite decomposition and its geochemical significance. Phys Earth Planet Inter. 1986;44:293-303.

[54] Nurse RW, Welch JH, Gutt W. A new form of tricalcium phosphate. Nature. 1958;182:1230-1230.

[55] Albee FH. Studies in bone growth: Triple calcium phosphate as a stimulus to osteogenesis. Ann Surg. 1920;71:32-39.

[56] Perera FH, Martínez-Vázquez FJ, Miranda P, Ortiz AL, Pajares A. Clarifying the effect of sintering conditions on the microstructure and mechanical properties of β-tricalcium phosphate. Ceram Int. 2010;36:1929-1935.

[57] Welch JH, Gutt W. High-temperature studies of the system calcium oxide-phosphorus pentoxide. J Chem Soc. 1961:4442-4444.

[58] Tenhuisen KS, Clark BA, Klimkiewicz M, Brown PW. A microstructural investigation of calcium hydroxyapatites synthesized from $CaHPO_4.2H_2O$ and $Ca_4(PO_4)_2O$. Cells Mater. 1996;6:251-267.

[59] Brown PW, Hocker N, Hoyle S. Variations in solution chemistry during the low-temperature formation of hydroxyapatite. J Am Ceram Soc. 1991;74:1848-1854.

[60] Yamada M, Shiota M, Yamashita Y, Kasugai S. Histological and histomorphometrical comparative study of the degradation and osteoconductive characteristics of α- and β-tricalcium phosphate in block grafts. J Biomed Mater Res part B: Appl Biomater. 2007;82B:139-148.

[61] Seebach C, Schultheiss J, Wilhelm K, Frank J, Henrich D. Comparison of six bone-graft substitutes regarding to cell seeding efficiency, metabolism and growth behaviour of human mesenchymal stem cells (MSC) in vitro. Injury. 2010;41:914-921.

[62] Dorozhkin SV, Epple M. Biological and medical significance of calcium phosphates. Angew Chem Int Ed. 2002;41:3130-3146.

[63] Carrodeguas RG, De Aza S. α-Tricalcium phosphate: Synthesis, properties and biomedical applications. Acta Biomaterialia. 2011;7:3536-3546.

[64] Ginebra MP, Fernández E, Driessens FCM, Planell JA. Modeling of the hydrolysis of α-tricalcium phosphate. J Am Ceram Soc. 1999;82:2808–2812.

[65] Durucan C, Brown PW. Kinetic model for α-tricalcium phosphate hydrolysis. J Am Ceram Soc. 2002;85:2013-2018.

[66] Brunner TJ, Bohner M, Dora C, Gerber C, Stark WJ. Comparison of amorphous TCP nanoparticles to micron-sized α-TCP as starting materials for calcium phosphate cements. J Biomed Mater Res Part B: Appl Biomater. 2007;83B:400-407.

[67] Camire CL, Gbureck U, Hirsiger W, Bohner M. Correlating crystallinity and reactivity in an α-tricalcium phosphate. Biomaterials. 2005;26:2787–2794.

[68] Brunner TJ, Grass RN, Bohner M, Stark WJ. Effect of particle size, crystal phase and crystallinity on the reactivity of tricalcium phosphate cements for bone reconstruction. J Mater Chem. 2007;17:4072–4078.

[69] Bohner M, Brunner TJ, Stark WJ. Controlling the reactivity of calcium phosphate cements. J Mater Chem. 2008;18:5669-5675.

[70] Ginebra MP, Driessens FCM, Planell JA. Effect of particle size on the micro and nanostructural features of a calcium phosphate cement: a kinetic analysis. Biomaterials. 2004;25:3453-3462.

[71] Bigi A, Bracci B, Panzavolta S. Effect of added gelatin on the properties of calcium phosphate cement. Biomaterials. 2004;25:2893-2899.

[72] Rau JV, Generosi A, Smirnov VV, Ferro D, Rossi Albertini V, Barinov SM. Energy dispersive X-ray diffraction study of phase development during hardening of calcium phosphate bone cements with addition of chitosan. Acta Biomater. 2008;4:1089-1094.

[73] Leroux L, Hatim Z, Frèche M, Lacout JL. Effects of various adjuvants (lactic acid, glycerol, and chitosan) on the injectability of a calcium phosphate cement. Bone. 1999;25:31-34.

[74] Pina S, Torres PM, Goetz Neunhoeffer F, Neubauer J, Ferreira JMF. Newly developed Sr-substituted α-TCP bone cements. Acta Biomater. 2010;6:936-942.

[75] Boanini E, Panzavolta S, Rubini K, Gandolfi M, Bigi A. Effect of strontium and gelatin on the reactivity of α-tricalcium phosphate. Acta Biomater. 2010;6:936–942.

[76] Saint Jean SJ, Camire CL, Nevsten P, Hansen S, Ginebra MP. Study of the reactivity and in vitro bioactivity of Sr-substituted α-TCP cements. J Mater Sci: Mater Med. 2005;16:993–1001.

[77] Yashima M, Kawaike Y. Crystal structure and site preference of Ba-doped α-tricalcium phosphate. Chem Mater. 2007;19:3973-3979.

[78] Fernández E, Vlad MD, Hamcerencu M, Darie A, Torres R, López J. Effect of iron on the setting properties of α-TCP bone cements. J Mater Sci. 2005;40:3677-3682.

[79] Yin X, Calderin L, Stott MJ, Sayer M. Density functional study of structural, electronic and vibrational properties of Mg- and Zn-doped tricalcium phosphate biomaterials. Biomaterials. 2002; 23: 4155-4163.

[80] Lin FH, Liao CJ, Chen KS, Sun JS, Lin CP. Petal-like apatite formed on the surface of tricalcium phosphate ceramic after soaking in distilled water. Biomaterials. 2001;22:2981-2992.

[81] Enderle R, Gotz Neunhoeffer F, Gobbels M, Muller FA, Greil P. Influence of magnesium doping on the phase transformation temperature of β-TCP ceramics examined by Rietveld refinement. Biomaterials. 2005;26:3379–3384.

[82] Pina S, Torres PMC, Ferreira JMF. Injectability of brushite-forming Mg-substituted and Sr-substituted α-TCP bone cements. J Mater Sci: Mater Med 2010;21:431-438.

[83] Kannan S, Ventura JMG, Lemos AF, Barba A, Ferreira JMF. Effect of sodium addition on the preparation of hydroxyapatites and biphasic ceramics. Ceram Int. 2008;34:7-13.

[84] Matsumoto N, Yoshida K, Hashimoto K, Toda Y. Thermal stability of β-tricalcium phosphate doped with monovalent metal ions. Mater Res Bull. 2009;44:1889-1894.

[85] Yubao L, Xingdong Z, de Groot K. Hydrolysis and phase transition of alpha-tricalcium phosphate. Biomaterials. 1997;18:737-741.

[86] Durucan C, Brown PW. Low temperature formation of calcium-deficient hydroxyapatite-PLA/PLGA composites. J Biomed Mater Res. 2000;51:717-725.

[87] Durucan C, Brown PW. Biodegradable hydroxyapatite–polymer composites. Adv Eng Mater. 2001;3:227-231.

[88] Bigi A, Bracci B, Panzavolta S. Effect of added gelatin on the properties of calcium phosphate cement. Biomaterials. 2004;25:2893-2899.

[89] Bigi A, Torricelli P, Fini M, Bracci B, Panzavolta S, Sturba L, Giardino R. A biomimetic gelatin-calcium phosphate bone cement. Int J Artif Organs. 2004;27:664-673.

[90] Touny A, Laurencin C, Nair L, Allcock H, Brown PW. Formation of composites comprised of calcium deficient HAp and cross-linked gelatin. J Mater Sci: Mater Med. 2008;19:3193-3201.

[91] Khairoun I, Driessens FCM, Boltong MG, Planell JA, Wenz R. Addition of cohesion promotors to calcium phosphate cements. Biomaterials. 1999;20:393-398.

[92] Alves RLH, dos Santos LA, Bergmann CP. Injectability evaluation of tricalcium phosphate bone cement. J Mater Sci: Mater Med. 2008;19:2241-2246.

[93] Ilium L. Chitosan and its use as a pharmaceutical excipient. Pharm Res. 1998;15:1326-1331.

[94] Di Martino A, Sittinger M, Risbud MV. Chitosan: A versatile biopolymer for orthopaedic tissue-engineering. Biomaterials. 2005;26:5983-5990.

[95] VandeVord PJ, Matthew HWT, DeSilva SP, Mayton L, Wu B, Wooley PH. Evaluation of the biocompatibility of a chitosan scaffold in mice. J Biomed Mater Res. 2002;59:585-590.

[96] Madihally SV, Matthew HWT. Porous chitosan scaffolds for tissue engineering. Biomaterials. 1999;20:1133-1142.

[97] Aoyagi S, Onishi H, Machida Y. Novel chitosan wound dressing loaded with minocycline for the treatment of severe burn wounds. Int J Pharm. 2007;330:138-145.

[98] Tchemtchoua VT, Atanasova G, Aqil A, Filée P, Garbacki N, Vanhooteghem O, Deroanne C, Noel A, Jérome C, Nusgens B, Poumay Y, Colige A. Development of a chitosan nanofibrillar scaffold for skin repair and regeneration. Biomacromolecules. 2011;12:3194-3204.

[99] Burkatovskaya M, Tegos GP, Swietlik E, Demidova TN, P Castano A, Hamblin MR. Use of chitosan bandage to prevent fatal infections developing from highly contaminated wounds in mice. Biomaterials. 2006;27:4157-4164.

[100] Li D, Diao J, Zhang J, Liu J. Fabrication of new chitosan-based composite sponge containing silver nanoparticles and its antibacterial properties for wound dressing. J Nanosci Nanotech. 2011;11:4733-4738.

[101] Leedy M, Martin H, Norowski P, Jennings J, Haggard W, Bumgardner J. Use of chitosan as a bioactive implant coating for bone-implant application. Adv Polym Sci. 2011;244:129-165

[102] Datta P, Dhara S, Chatterjee J. Hydrogels and electrospun nanofibrous scaffolds of N-methylene phosphonic chitosan as bioinspired osteoconductive materials for bone grafting. Carbohyd Polym. 2012;87:1354-1362.

[103] Klokkevold PR, Vandemark L, Kenney EB, Bernard GW. Osteogenesis enhanced by chitosan (poly-N-acetyl glucosaminoglycan) in vitro. J Periodontol. 1996;67:1170-1175.

[104] Fakhry A, Schneider GB, Zaharias R, Senel S. Chitosan supports the initial attachment and spreading of osteoblasts preferentially over fibroblasts. Biomaterials. 2004;25:2075-2079.

[105] Seol YJ, Lee JY, Park YJ, Lee YM, Ku Y, Rhyu IC, Lee SJ, Han SB, Chung CP. Chitosan sponges as tissue engineering scaffolds for bone formation. Biotech Lett. 2004;26:1037-1041.

[106] Tanase CE, Popa MI, Verestiuc L. Biomimetic bone scaffolds based on chitosan and calcium phosphates. Mater Lett. 2011;65:1681-1683.

[107] Xia W, Liu W, Cui L, Liu Y, Zhong W, Liu D, Wu J, Chua K, Cao Y. Tissue engineering of cartilage with the use of chitosan-gelatin complex scaffolds. J Biomed Mater Res B: Appl Biomater. 2004;71B:373-380.

[108] Wei W, Soichiro I, Tomoyasu A, Atsushi O, Katsuyoshi S, Tsuneo O, Makoto D. Development of an injectable chitosan/marine collagen composite gel. Biomed Mater. 2010;5:65-79

[109] Chenite A, Chaput C, Wang D, Combes C, Buschmann MD, Hoemann CD, Leroux JC, Atkinson BL, Binette F, Selmani A. Novel injectable neutral solutions of chitosan form biodegradable gels in situ. Biomaterials. 2000;21:2155-2161.

[110] Ko JA, Kim BK, Park HJ. Preparation of acetylated chitosan sponges (chitin sponges). J Appl Polym Sci. 2010;117:1618-1623.

[111] Tuzlakoglu K, Alves CM, Mano JF, Reis RL. Production and characterization of chitosan fibers and 3-D fiber mesh scaffolds for tissue engineering applications. Macromol Biosc. 2004;4:811-819.

[112] Liu H, Xu W, Zou H, Ke G, Li W, Ouyang C. Feasibility of wet spinning of silk-inspired polyurethane elastic biofiber. Mater Lett. 2008;62:1949-1952.

[113] Cronin EM, Thurmond FA, Bassel Duby R, Williams RS, Wright WE, Nelson KD, Garner HR. Protein-coated poly(L-lactic acid) fibers provide a substrate for differentiation of human skeletal muscle cells. J Biomed Mater Res A. 2004;69A:373-381.

[114] Knaul JZ, Hudson SM, Creber KAM. Improved mechanical properties of chitosan fibers. J Appl Polym Sci. 1999;72:1721-1732.

[115] Knaul J, Hooper M, Chanyi C, Creber KAM. Improvements in the drying process for wet-spun chitosan fibers. J Appl Polym Sci. 1998;69:1435-1444.

[116] Matsuda A, Ikoma T, Kobayashi H, Tanaka J. Preparation and mechanical property of core-shell type chitosan/calcium phosphate composite fiber. Mater Sci Eng C. 2004;24:723-728.

[117] Lian Q, Li DC, He JK, Wang Z. Mechanical properties and in-vivo performance of calcium phosphate cement-chitosan fibre composite. Proc Inst Mech Eng H. 2007;222:347-353.

[118] Pan Z, Jiang P, Fan Q, Ma B, Cai H. Mechanical and biocompatible influences of chitosan fiber and gelatin on calcium phosphate cement. J Biomed Mater Res B: Appl Biomater. 2006;82B:246-252.

[119] Li D, Lian Q, Jin Z, Wang J, Li A, Wang Z. Fabrication and in vitro evaluation of calcium phosphate combined with chitosan fibers for scaffold structures. J Bioact Compat Polym. 2009;24:113-124.

[120] Juang RS, Shao HJ. A simplified equilibrium model for sorption of heavy metal ions from aqueous solutions on chitosan. Water Res. 2002;36:2999-3008.

[121] Ding P, Huang KL, Li GY, Zeng WW. Mechanisms and kinetics of chelating reaction between novel chitosan derivatives and Zn(II). J Hazard Mater. 2007;146:58-64.

[122] Qin Y. The chelating properties of chitosan fibers. J Appl Polym Sci. 1993;49:727-731.

[123] Qin Y, Shi B, Liu J. Application of chitosan and alginate in treating waste water containing heavy metal ions. Indian J Chem Tech. 2006;13:464-469.

[124] Momenzadeh H, Tehrani Bagha AR, Khosravi A, Gharanjig K, Holmberg K. Reactive dye removal from wastewater using a chitosan nanodispersion. Desalination. 2011;271:225-230.

[125] Onsosyen E, Skaugrud O. Metal recovery using chitosan. J Chem Tech Biotech. 1990;49:395-404.

[126] Brzonova I, Steiner W, Zankel A, Nyanhongo GS, Guebitz GM. Enzymatic synthesis of catechol and hydroxyl-carboxic acid functionalized chitosan microspheres for iron overload therapy. Eur J Pharm Biopharm. 2011;79:294-303.

[127] Burke A, Yilmaz E, Hasirci N. Evaluation of chitosan as a potential medical iron (III) ion adsorbent. Turk J Med Sci. 2000;30:341-348.

[128] Agrawal P, Strijkers GJ, Nicolay K. Chitosan-based systems for molecular imaging. Adv Drug Delivery Rev. 2010;62:42-58.

[129] Kumar A, Jena PK, Behera S, Lockey RF, Mohapatra S, Mohapatra S. Multifunctional magnetic nanoparticles for targeted delivery. Nanomed: Nanotech Biol Med. 2010;6:64-69.

[130] Andreini C, Banci L, Bertini I, Rosato A. Counting the zinc-proteins encoded in the human genome. J Proteome Res. 2005;5:196-201.

[131] Coleman JE. Zinc proteins: enzymes, storage proteins, transcription factors, and replication proteins. Annu Rev Biochem. 1992;61:897-946.

[132] Todd WR, Elvehjem CA, Hart EB. Zinc in the nutrition of the rat. Nutr Rev. 1980;38:151-154.

[133] Yamaguchi M. Role of nutritional zinc in the prevention of osteoporosis. Mol Cell Biochem. 2010;338:241-254.

[134] Sun JY, Wang JF, Zi NT, Jing MY, Weng XY. Effects of zinc supplementation and deficiency on bone metabolism and related gene expression in rat. Biol Trace Elem Res. 2011;143:394-402.

[135] Oner G, Bhaumick B, Bala RM. Effect of zinc deficiency on serum somatomedin levels and skeletal growth in young rats. Endocrinology. 1984;114:1860-1863.

[136] Hadley KB, Newman SM, Hunt JR. Dietary zinc reduces osteoclast resorption activities and increases markers of osteoblast differentiation, matrix maturation, and mineralization in the long bones of growing rats. J Nutr Biochem. 2010;21:297-303.

[137] Yamaguchi M, Yamaguchi R. Action of zinc on bone metabolism in rats: Increases in alkaline phosphatase activity and DNA content. Biochem Pharmacol. 1986;35:773-777.

[138] Yamaguchi M, Oishi H, Suketa Y. Stimulatory effect of zinc on bone formation in tissue culture. Biochem Pharmacol. 1987;36:4007-4012.

[139] Yamaguchi M, Oishi H, Suketa Y. Zinc stimulation of bone protein synthesis in tissue culture: Activation of aminoacyl-tRNA synthetase. Biochem Pharmacol. 1988;37:4075-4080.

[140] Hashizume M, Yamaguchi M. Stimulatory effect of β-alanyl-L-histidinato zinc on cell proliferation is dependent on protein synthesis in osteoblastic MC3T3-E1 cells. Mol Cell Biochem. 1993;122:59-64.

[141] Hashizume M, Yamaguchi M. Effect of β-alanyl-L-histidinato zinc on differentiation of osteoblastic MC3T3-El cells: Increases in alkaline phosphatase activity and protein concentration. Mol Cell Biochem. 1994;131:19-24.

[142] Cerovic A, Miletic I, Sobajic S, Blagojevic D, Radusinovic M, El Sohemy A. Effects of zinc on the mineralization of bone nodules from human osteoblast-like cells. Biol Trace Elem Res. 2007;116:61-71.

[143] Yamaguchi M, Hashizume M. Effect of β-alanyl-L-histidinato zinc on protein components in osteoblastic MC3T3-El cells: Increase in osteocalcin, insulin-like growth factor-I and transforming growth factor-β. Mol Cell Biochem. 1994;136:163-169.

[144] Yamaguchi M, Goto M, Uchiyama S, Nakagawa T. Effect of zinc on gene expression in osteoblastic MC3T3-E1 cells: enhancement of Runx2, OPG, and regucalcin mRNA expressions. Mol Cell Biochem. 2008;312:157-166.

[145] Yamaguchi M, Segawa Y, Shimokawa N, Tsuzuike N, Tagashira E. Inhibitory effect of β-Alanyl-L-Histidinato zinc on bone resorption in tissue culture. Pharmacology. 1992;45:292-300.

[146] Moonga BS, Dempster DW. Zinc is a potent inhibitor of osteoclastic bone resorption in vitro. J Bone Miner Res. 1995;10:453-457.

[147] Hie M, Tsukamoto I. Administration of zinc inhibits osteoclastogenesis through the suppression of RANK expression in bone. Eur J Pharmacol. 2011;668:140-146.

[148] Kishi S, Yamaguchi M. Inhibitory effect of zinc compounds on osteoclast-like cell formation in mouse marrow cultures. Biochem Pharmacol. 1994;48:1225-1230.

[149] Kreidler ER, Hummel FA. Phase relationships in the system $SrO-P_2O_5$ and the influence of water vapor on the formation of $Sr_4P_2O_9$. Inorg Chem. 1967;6:884-891.

[150] Kingery WD, Bowen HK, Uhlman DR. Introduction to Ceramics. 2 ed. New York: John Wiley & Sons; 1960. p. 343.

[151] Durucan C, Brown PW. Reactivity of α-tricalcium phosphate. J Mater Sci 2002;37:963-969.

[152] Xue W, Dahlquist K, Banerjee A, Bandyopadhyay A, Bose S. Synthesis and characterization of tricalcium phosphate with Zn and Mg based dopants. J Mater Sci: Mater Med. 2008;19:2669-2677.

[153] Dickens B, Schroeder LW, Brown WE. Crystallographic studies of the role of Mg as a stabilizing impurity in β-$Ca_3(PO_4)_2$. The crystal structure of pure β-$Ca_3(PO_4)_2$. J Solid State Chem. 1974;10:232-248.

[154] Schroeder LW, Dickens B, Brown WE. Crystallographic studies of the role of Mg as a stabilizing impurity in β-$Ca_3(PO_4)_2$. II. Refinement of Mg-containing β-$Ca_3(PO_4)_2$. J Solid State Chem. 1977;22:253-262.

[155] Bohner M, Baroud G. Injectability of calcium phosphate pastes. Biomaterials. 2005;26:1553-1563.

[156] Gbureck U, Barralet JE, Spatz K, Grover LM, Thull R. Ionic modification of calcium phosphate cement viscosity. Part I: hypodermic injection and strength improvement of apatite cement. Biomaterials. 2004;25:2187-2195.

[157] Wang X, Chen L, Xiang H, Ye J. Influence of anti-washout agents on the rheological properties and injectability of a calcium phosphate cement. J Biomed Mat Res B: App Biomater. 2007;81B:410-418.

[158] Klawitter JJ, Bagwell JG, Weinstein AM, Sauer BW, Pruitt JR. An evaluation of bone growth into porous high density polyethylene. J Biomed Mat Res. 1976;10:311-323.

[159] Underwood EJ. Trace Elements in Human and Animal Nutrition. 4 ed. London: Academic Press; 1977. p. 196.

[160] Wong M, Eulenberger J, Schenk R, Hunziker E. Effect of surface topology on the osseointegration of implant materials in trabecular bone. J Biomed Mater Res. 1995;29:1567-1575.

[161] Schneider GB, Perinpanayagam H, Clegg M, Zaharias R, Seabold D, Keller J, Stanford C. Implant surface roughness affects osteoblast gene expression. J Dent Res. 2003;82:372-376.

[162] Cicek G, Aksoy EA, Durucan C, Hasirci N. Alpha-tricalcium phosphate (α-TCP): solid state synthesis from different calcium precursors and the hydraulic reactivity. J Mater Sci Mater Med. 2011;22:809-817.

APPENDIX A

SYNTHESIS METHODS OF SOME CaP POWDERS AND EXPERIMENTAL METHOS ON α-TCP SYNTHESIS

The first step of this thesis was to obtain a pure α-TCP powder with high hydraulic reactivity. In order to reach this goal, a number of different synthesis routes were tried with two different phosphate precursors as monetite and pyrophosphate. It is worthy of note that, a β-TCP synthesis procedure was also established during this experimental research period. In an attempt to contribute to the fund of knowledge on CaP synthesis, the main body of α-TCP synthesis experiments and their results, pyrophosphate and β-TCP synthesis procedures were given in this appendix.

A.1 Materials and Characterizations

Three different $CaCO_3$ precursors were used to prepare α-TCP. They were the commercial grade products of Merck (Germany, Catalog no. 102066), and Carlo Erba (Italy, Catalog no.327059) and Sigma (Germany, Catalog no. C4830) which will be referred as *CC-M*, *CC-C* and *CC-S*, respectively hereafter. H_3PO_4 (85 wt%) was received from Merck (Germany, Catalog no. 100573).

Phase analyses of all products were performed using XRD (Rigaku, Ultima D/MAX 2200/PC, Japan). CuKα radiation was used at 40 kV voltage and 40 mA current. The scanning range of the samples was 20-40° and the scanning speed was 2°/min.

A.2 Pyrophosphate Synthesis

For the preparation of pyrophosphate ($Ca_2P_2O_7$), the pre-synthesized $CaHPO_4$ (the synthesis route was described in Chapter 1) was fired in an alumina crucible in an open atmosphere furnace at 500°C for 2 h. The schematic illustration of synthesis protocol of $Ca_2P_2O_7$ was given in Figure A.1. XRD analyses were performed for phase analysis of the monetite (Figure A.2) and pyrophosphate (Figure A.3) samples.

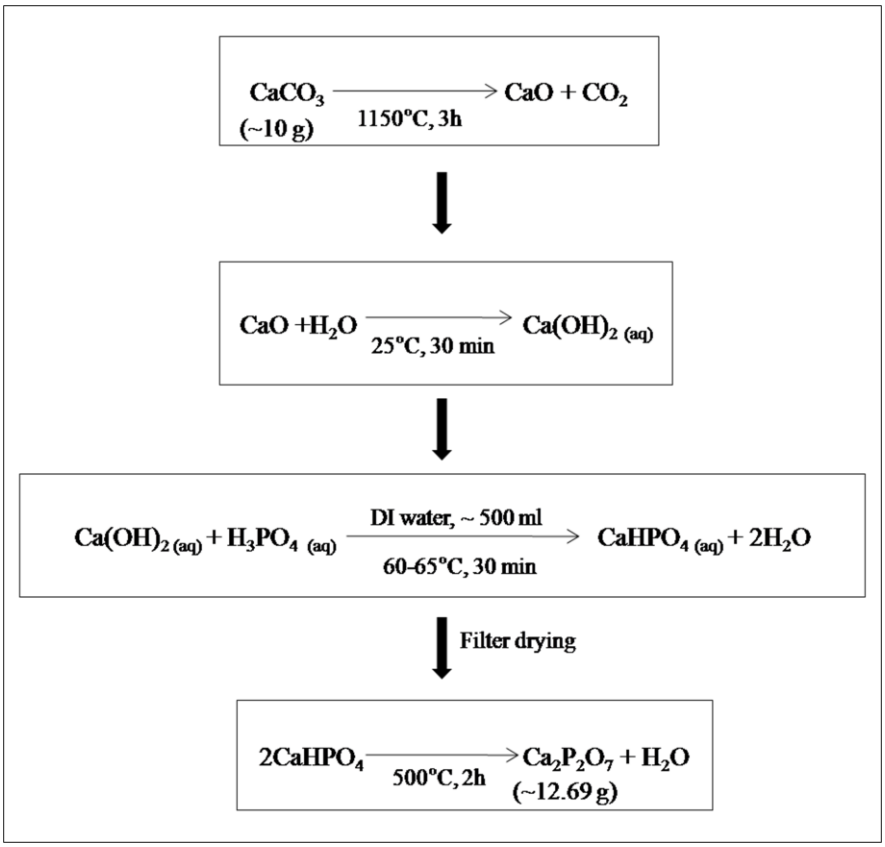

Figure A.1 Schematic illustration of the synthesis procedure of pyrophosphate.

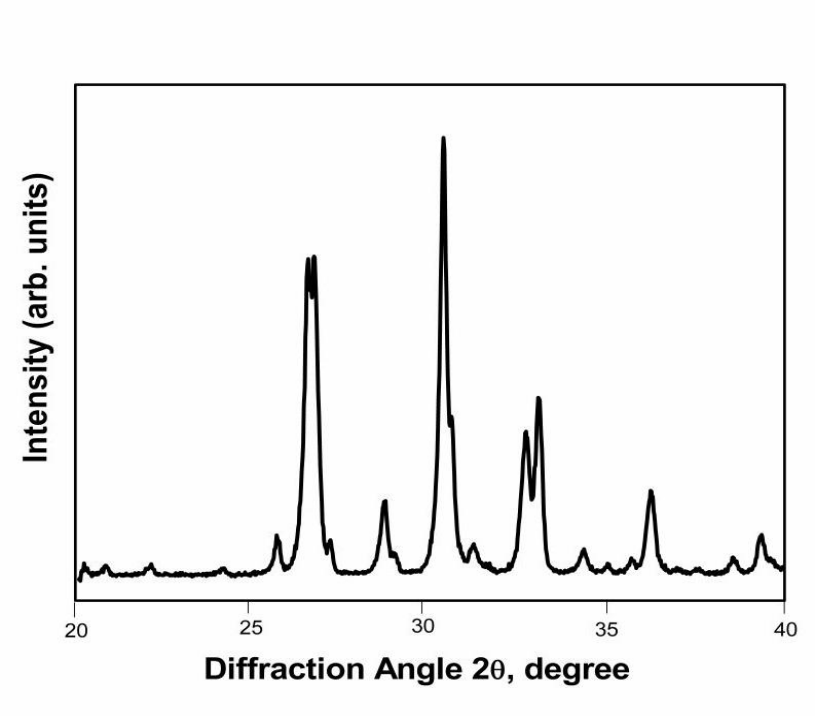

Figure A.2 XRD diffractogram of monetite.

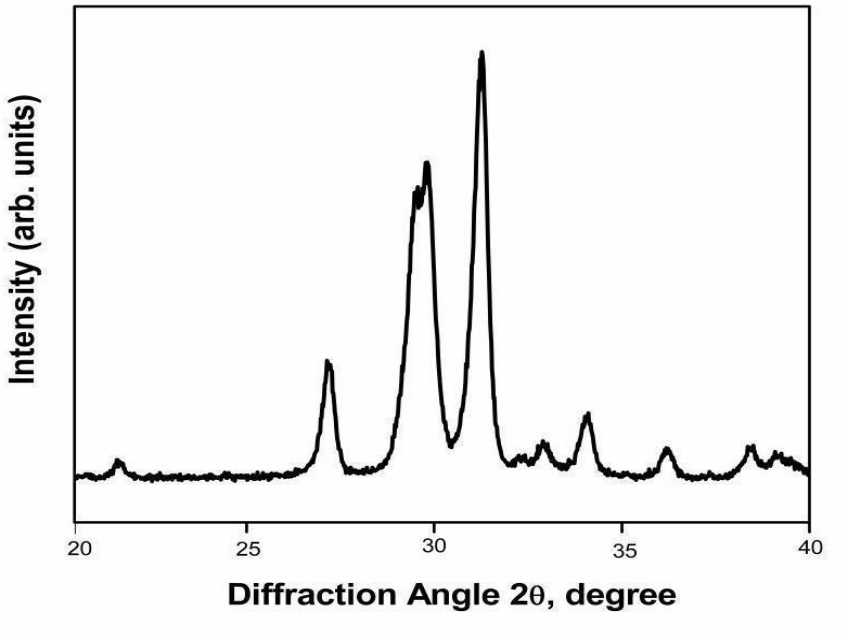

Figure A.3 XRD diffractogram of pyrophosphate.

A.3 β-TCP Synthesis

β-TCP was synthesized by solid state reaction between $CaCO_3$ and pre-synthesized $Ca_2P_2O_7$ according to the following reaction.

$$CaCO_3\,(s) + Ca_2P_2O_7\,(s) \rightarrow Ca_3(PO_4)_2\,(s) + CO_2\,(g)$$

For the preparation of β-TCP, the pre-synthesized $Ca_2P_2O_7$ (~10 g) was mixed with $CaCO_3$ (~3.94g) in 1:1 molar ratio using Turbula T2F mixer (WAB, Switzerland). After 1 h mixing, the solid powder blend was fired in an alumina crucible in an open atmosphere furnace at 900°C for 1 h. Following this, the product was fired at 1150°C for 1.5 h and cooled to room temperature in the furnace. XRD diffractogram of the synthesized β-TCP powder is given in Figure A.4.

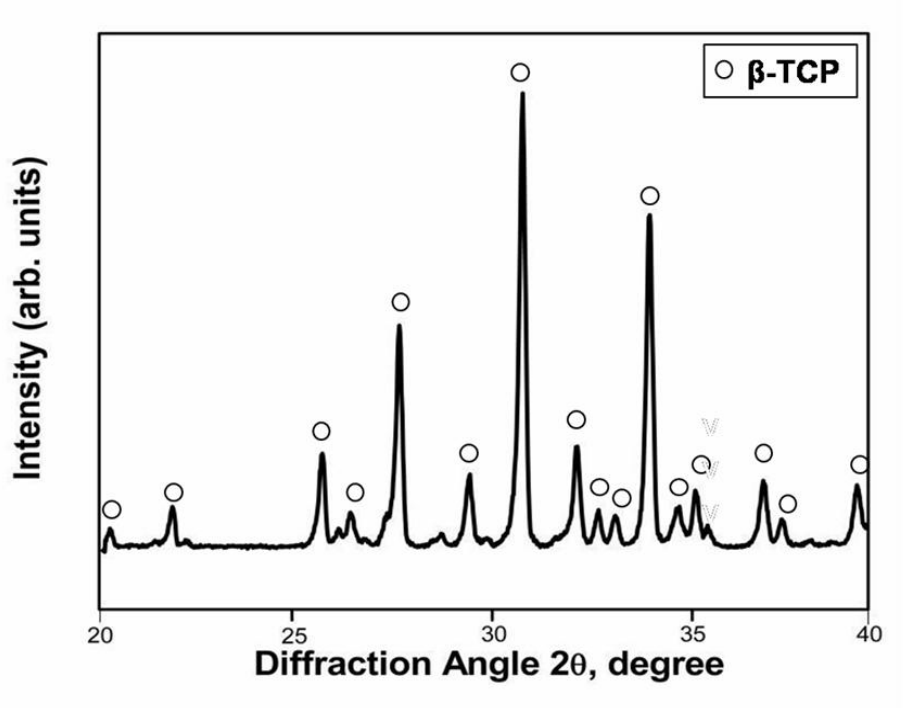

Figure A.4 XRD diffractogram of β-TCP.

A.4 α-Tricalcium Phosphate Synthesis Experiments and Results

In order to provide a reproducible and well-detailed α-TCP powder synthesis protocol, a number of different experimental synthesis routes have been tried using different commercially available $CaCO_3$ sources with different chemical grades, i.e. different amounts of impurities. Some of these synthesis experiments are given in this section.

A.4.1 Synthesis Experiment 1

The pre-synthesized $Ca_2P_2O_7$ was mixed with $CaCO_3$ (*CC*-*C*) in 1:1 molar ratio (5 g /1.97 g) and vibratory milled in ethanol (10 mL) for 24 h (or 48 h) using a turbula mixer. Following this step, the samples were dried at 80ºC for 5 h in order to remove the ethanol. The solid powder blend was fired in an alumina crucible in an open atmosphere furnace at 1150°C for 2 h. At the end of the firing period, the chunky product was discharged on a borosilicate glass plate and air quenched to room temperature. XRD diffractograms of the synthesized products are given in Figure A.5. The resulting powders were three-phasic CaP mixtures of HAp, α-TCP and β-TCP with HAp as a dominant phase.

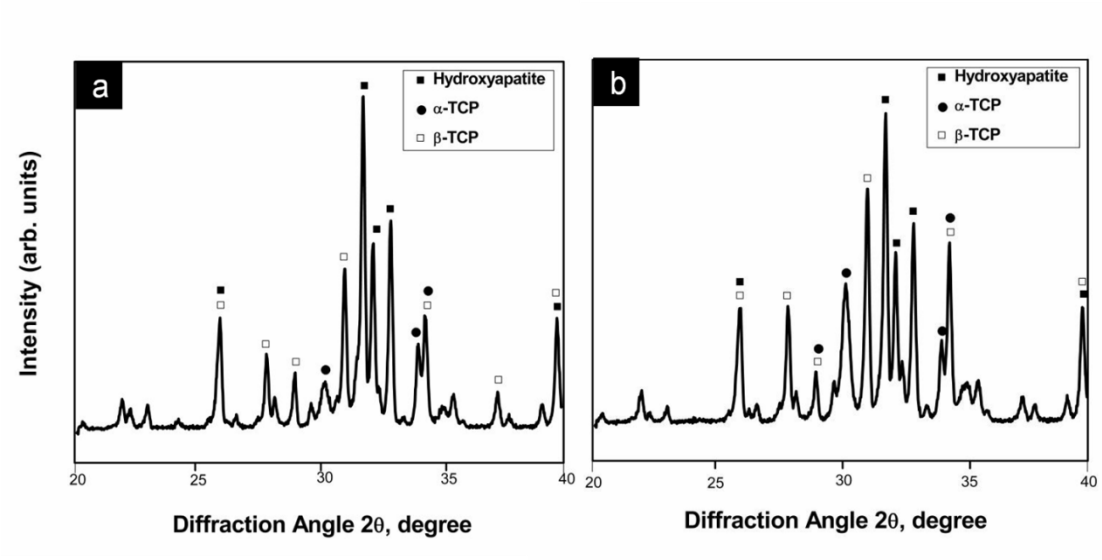

Figure A.5 XRD diffractograms of CaP powders synthesized from $Ca_2P_2O_7$ and $CaCO_3$ (*CC*-*C*) blend which was vibratory milled for different periods. **(a)** 48 h and **(b)** 24 h milled. The same firing operation (at 1150°C for 2 h) was applied to both samples.

A.4.2 Synthesis Experiment 2

The pre-synthesized $Ca_2P_2O_7$ was mixed with $CaCO_3$ (*CC*-*C*) in 1:1 molar ratio (5 g /1.97 g) using turbula mixer. After 1 h mixing, the solid powder blend was fired in an alumina crucible in an open atmosphere furnace at 1150°C for 2 h. At the end of the firing period, the chunky product was discharged on a borosilicate glass plate and air quenched to room temperature. XRD diffractogram of the synthesized product is given in Figure A.6. The resulting powder was a three-phasic CaP mixture of HAp, α-TCP and β-TCP with α-TCP as a dominant phase.

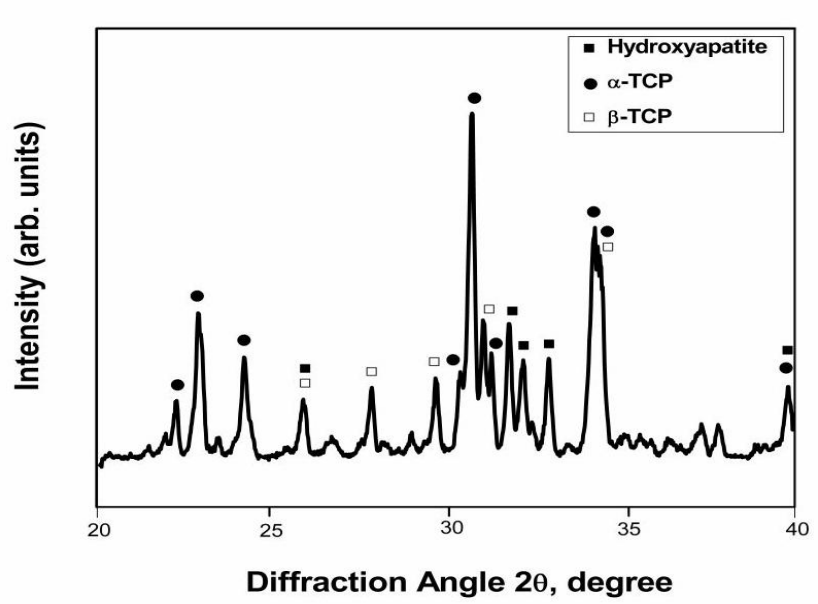

Figure A.6 XRD diffractogram of CaP powder synthesized from $Ca_2P_2O_7$ and $CaCO_3$ (*CC-C*) blend by firing at 1150°C for 2 h.

A.4.3 Synthesis Experiment 3

The pre-synthesized $Ca_2P_2O_7$ was mixed with $CaCO_3$ (*CC-C*) in 1:1 molar ratio (5 g /1.97 g) using turbula mixer. After 1 h mixing, two steps firing operation was applied. The solid powder blend was fired in an alumina crucible in an open atmosphere furnace at 900°C for 1 h, and then cooled down to room temperature. Following this, the product was fired at 1150°C for 2 h. At the end of the firing period, the chunky product was discharged on a borosilicate glass plate and air quenched to room temperature. XRD diffractogram of the synthesized product is given in Figure A.7. The resulting powder was mainly HAp with β-TCP as a second phase.

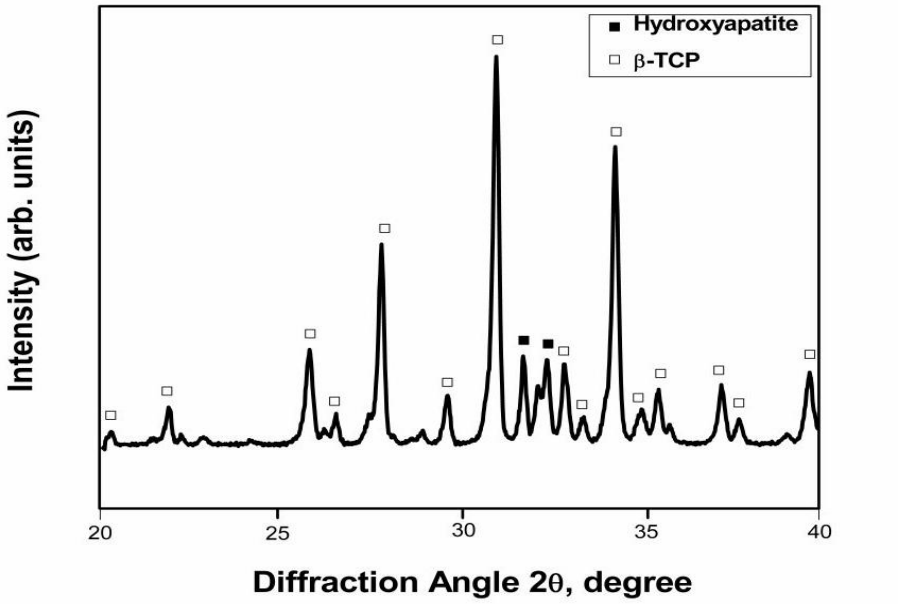

Figure A.7 XRD diffractogram of CaP powder synthesized from $Ca_2P_2O_7$ and $CaCO_3$ (*CC-C*) blend by applying pre-heat treatment at 900°C for 1 h and a firing operation at 1150°C for 2 h.

A.4.4 Synthesis Experiment 4

The pre-synthesized $CaHPO_4$ was mixed with $CaCO_3$ (*CC-M*) in 1:2 molar ratio (4 g/2.94 g) using turbula mixer. After 1 h mixing, two steps firing operation was applied. The solid powder blend was fired in an alumina crucible in an open atmosphere furnace at 900°C for 1 h, and then cooled down to room temperature. Following this step, the product was fired at 1350°C for 24 h. At the end of the firing period, the chunky product was discharged on a borosilicate glass plate and air quenched to room temperature.

The cement-type setting of α-TCP products was performed by exposing powders to DI water. The hydration was achieved at 37°C for 24 h, at a solid to liquid weight

ratio of 1:2. At the end of 24 h, the solid reaction products were washed with acetone and dried by air blowing to finalize hydration. XRD diffractograms of the synthesized powder and the hydration product are given in Figure A.8. The resulting α-TCP product was containing a small amount of HAp as a second phase (Figure A.8a). The remaining α-TCP peak in the hydration product reveals the limited hydraulic reactivity of the powder (Figure A.8b).

A.4.5 Synthesis Experiment 5

The pre-synthesized $CaHPO_4$ was mixed with $CaCO_3$ (*CC-M*) in 1:2 molar ratio (4 g/2.94 g) using turbula mixer. After 1 h mixing, two steps firing operation was applied. The solid powder blend was fired in an alumina crucible in an open atmosphere furnace at 900°C for 1 h then, cooled down to room temperature. Following this step, the product was fired at 1200°C for 2 h. At the end of the firing period, the chunky product was discharged on a borosilicate glass plate and air quenched to room temperature.

The cement-type setting of α-TCP products was performed by exposing powders to DI water. The hydration was achieved at 37°C for 24 h, at a solid to liquid weight ratio of 1:2. At the end of 24 h, the solid reaction products were washed with acetone and dried by air blowing to finalize hydration. XRD diffractograms of the synthesized powder and the hydration product are given in Figure A.9. The resulting α-TCP was containing a small amount of HAp as a second phase (Figure A.9a). The hydration product was almost a phase pure HAp with a negligible peak of remaining α-TCP (Figure A.9b).

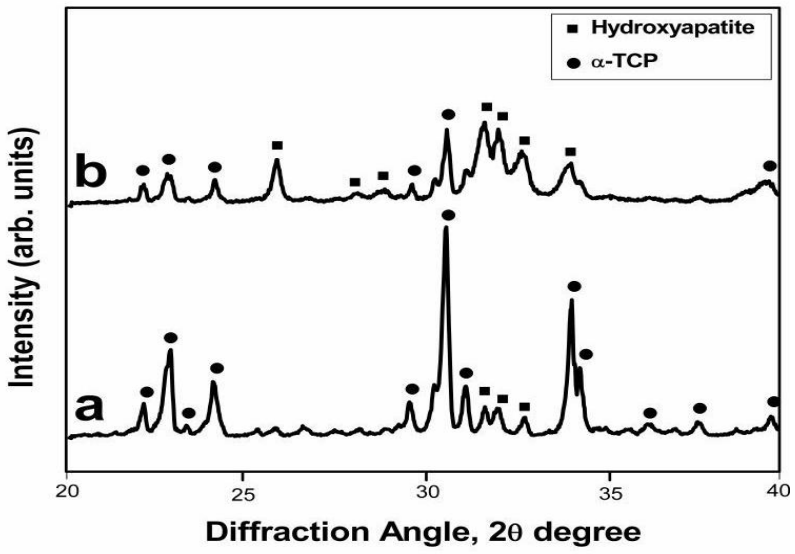

Figure A.8 XRD diffractogram of **(a)** α-TCP powder synthesized from $CaHPO_4$ and $CaCO_3$ blend by applying pre-heat treatment at 900°C for 1h and a firing operation at 1350°C for 24 h and **(b)** the hydration product.

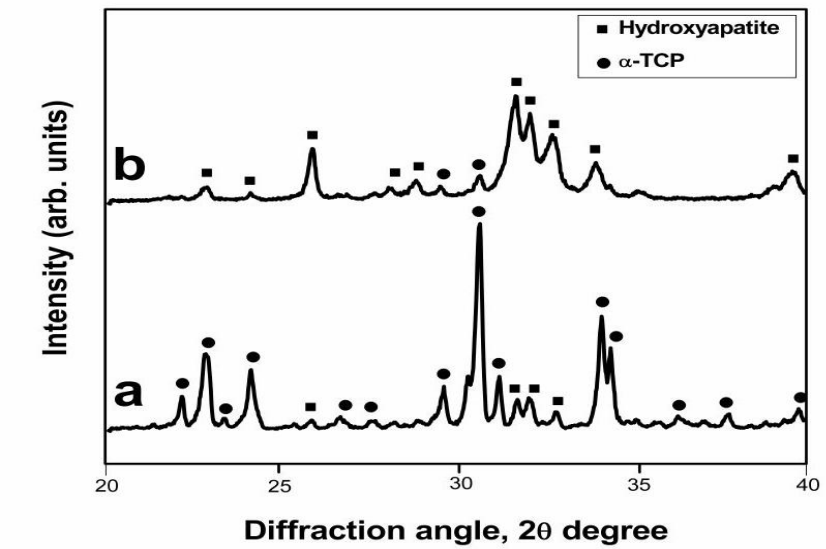

Figure A.9 XRD diffractograms of **(a)** α-TCP powder synthesized from $CaHPO_4$ and $CaCO_3$ (*CC-M*) blend by applying pre-heat treatment at 900°C for 1 h and a firing operation at 1200°C for 2 h and **(b)** the hydration product.

APPENDIX B

LOAD-DEFORMATION AND STRESS-STRAIN CURVES OF α-TCP/CHITOSAN FIBER COMPOSITES

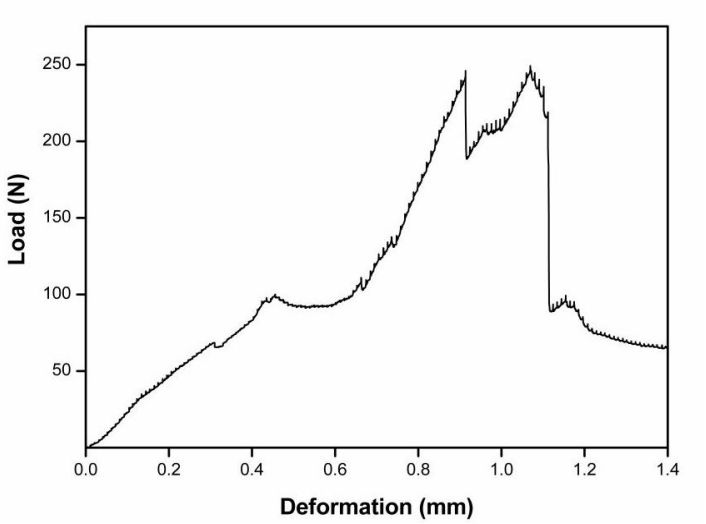

Figure B.1 Representative load-deformation curve of CPC after 24 h hydration.

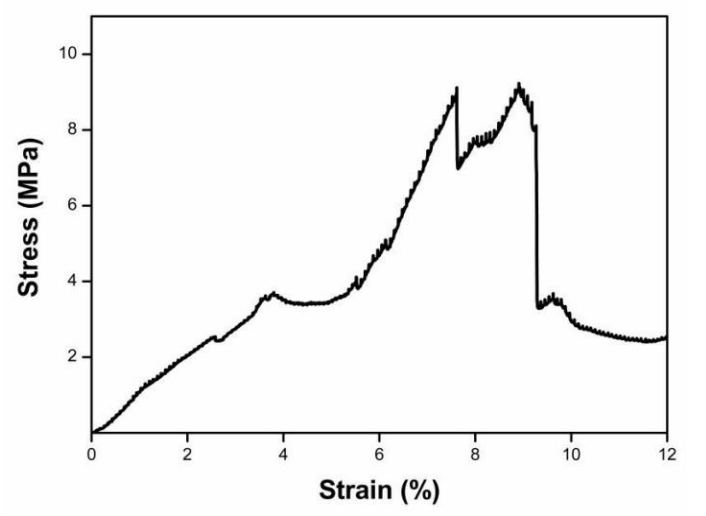

Figure B.2 Representative stress-strain curve of CPC after 24 h hydration.

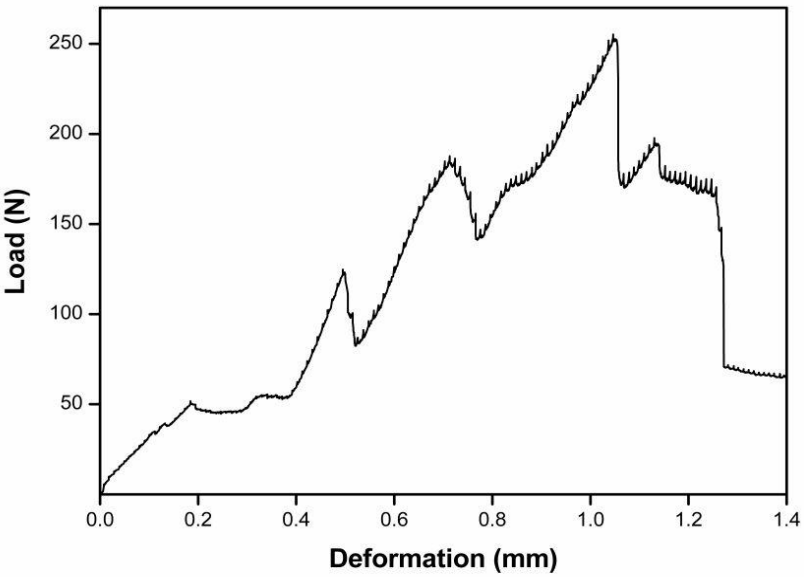

Figure B.3 Representative load-deformation curve of 24 h hydration product of CPC with 1.5 wt% chitosan fiber content.

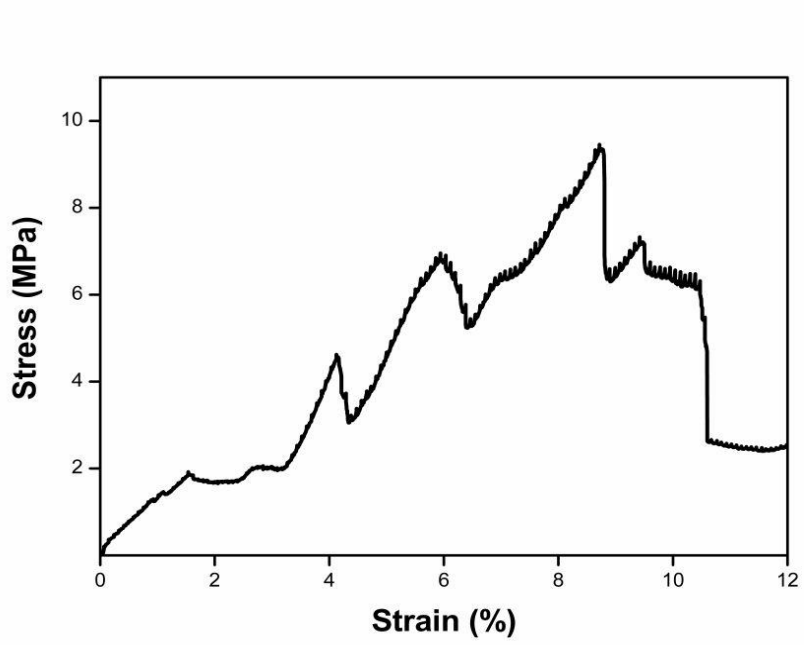

Figure B.4 Representative stress-strain curve of 24 h hydration product of CPC with 1.5 wt% chitosan fiber content.

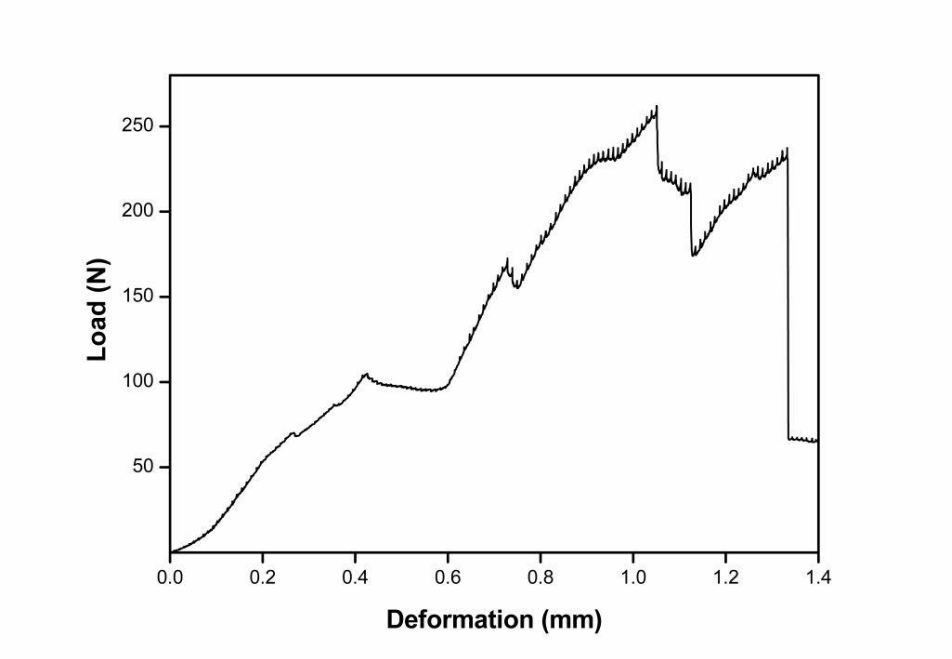

Figure B.5 Representative load-deformation curve of 24 h hydration product of CPC with 3 wt% chitosan fiber content.

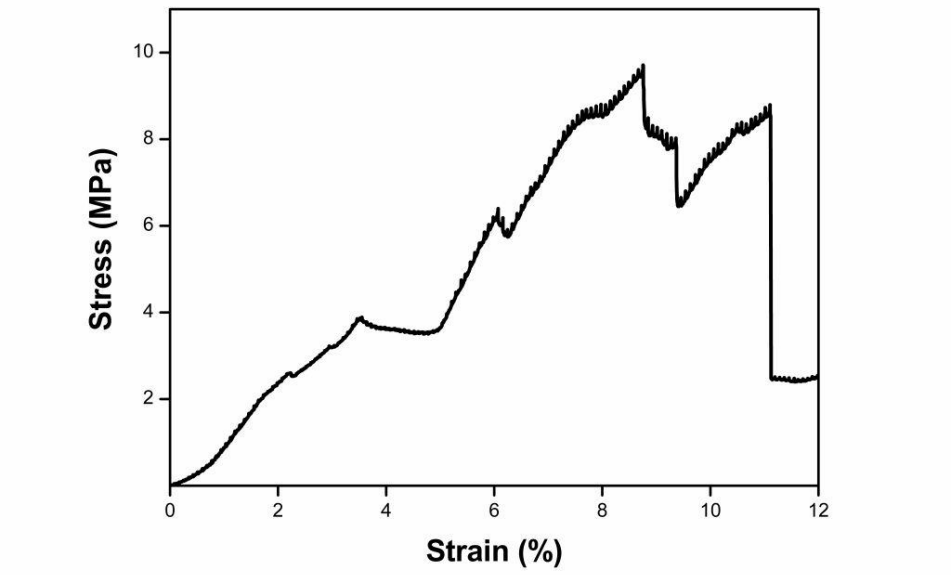

Figure B.6 Representative stress-strain curve of 24 h hydration product of CPC with 3 wt% chitosan fiber content.

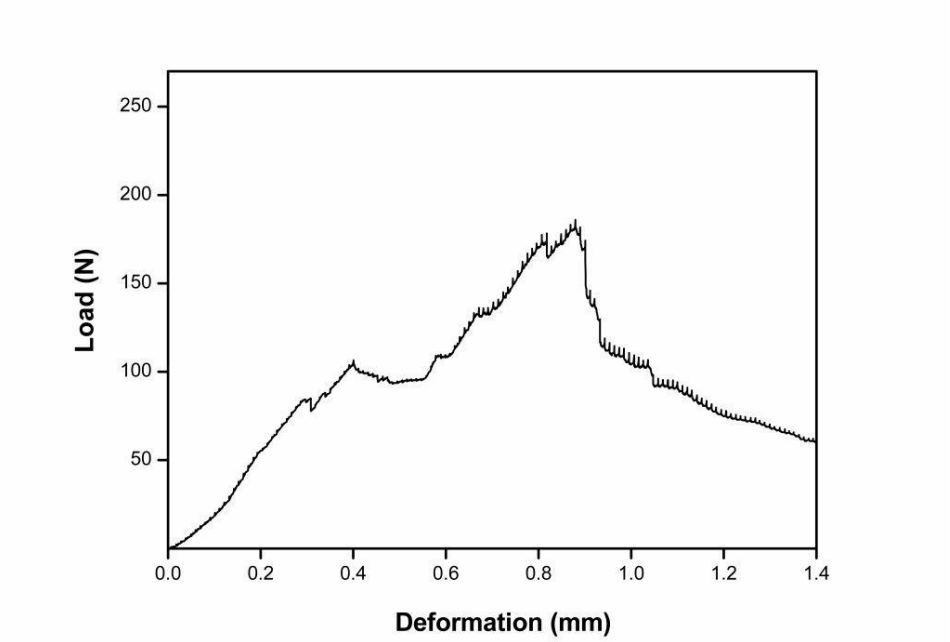

Figure B.7 Representative load-deformation curve of 24 h hydration product of CPC with 6 wt% chitosan fiber content.

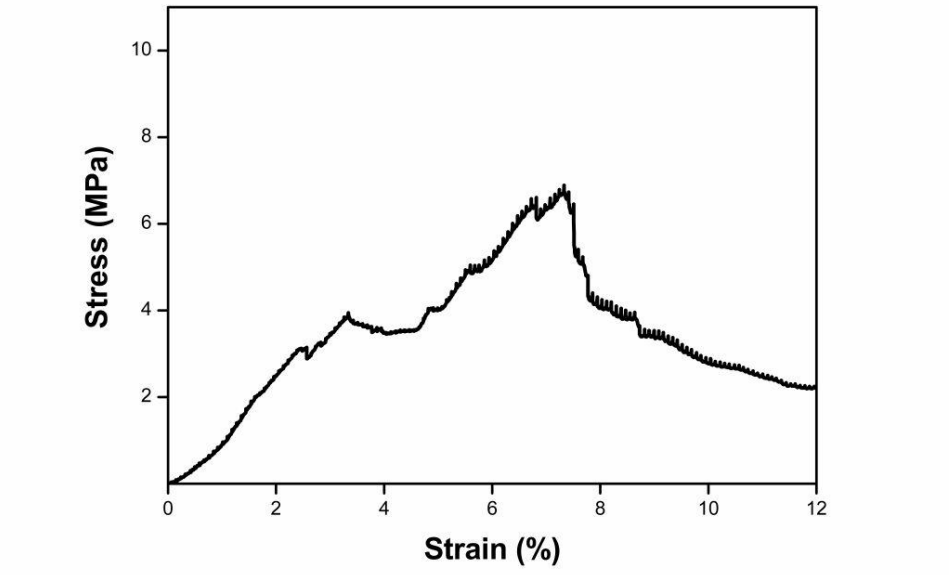

Figure B.8 Representative stress-strain curve of 24 h hydration product of CPC with 6 wt% chitosan fiber content.

APPENDIX C

COMPOSITION OF RINGER SOLUTION

Ringer solution is prepared by dissolving 1 tablet in 500 ml deionized water. The composition of Ringer's tablets is given in Table C.1.

Table C.1 The composition of Ringer's tablets.

Ingredient	**Amount (g/tablet)**
Ammonium chloride	0.00525
Sodium hydrogen carbonate	0.005
Calcium chloride-2-hydrate	0.04
Potassium chloride	0.00525
Sodium chloride	1.125

APPENDIX D

CUMULATIVE ZINC RELEASE PERCENTAGES OF CHITOSAN SCAFFOLDS

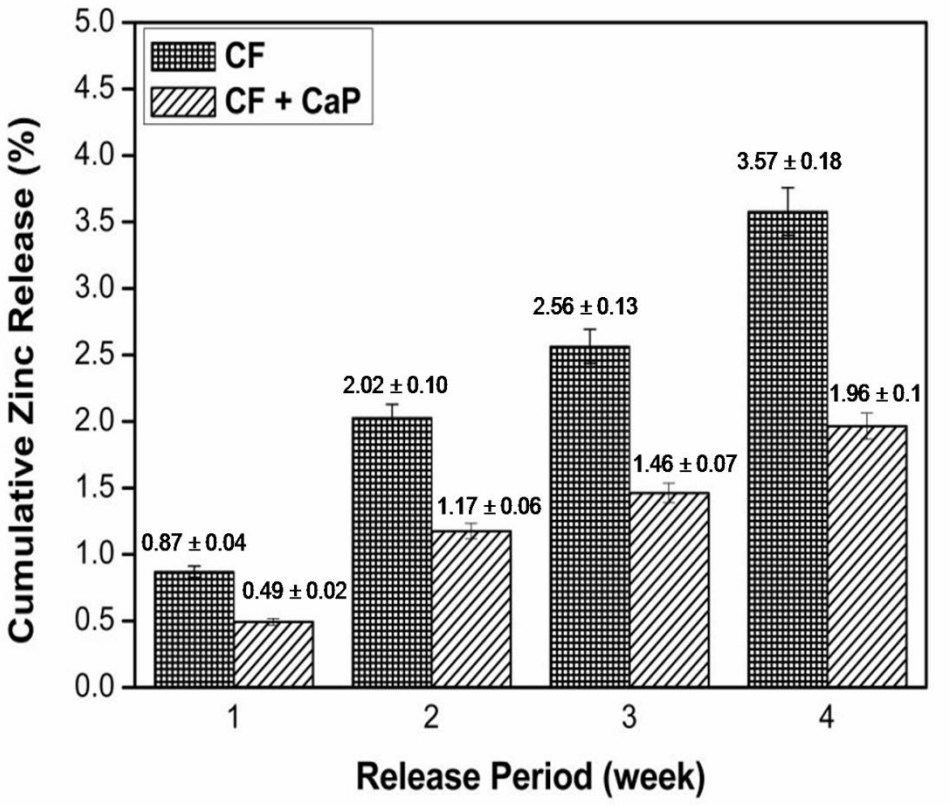

Figure D.1 The time dependent cumulative zinc release percentages of CaP covered (CF+CaP) and uncovered (CF) chitosan scaffolds.